

# **TRACE ELEMENT-MINERAL ASSOCIATIONS IN THE REGOLITH, SCUDDLES MASSIVE Cu-Zn SULPHIDE DEPOSIT, WESTERN AUSTRALIA**

*Maité Le Gleuher*

**CRC LEME OPEN FILE REPORT 197**

**February 2008**

CRCLEME

(CRC LEME Restricted Report 195R 2003  
2nd Impression 2008)

# **TRACE ELEMENT-MINERAL ASSOCIATIONS IN THE REGOLITH, SCUDDLES MASSIVE Cu-Zn SULPHIDE DEPOSIT, WESTERN AUSTRALIA**

*Maité Le Gleuher*

**CRC LEME OPEN FILE REPORT 197**

February 2008

(CRC LEME Restricted Report 195R 2003  
2nd Impression 2008)

© CRC LEME 2008

Open File Report 197 is a second impression (second printing) of CRC LEME Restricted Report 195R. It was produced in July 2003 for Newmont Australia, as part of the CRC LEME Mineral Hosts Project. The period of Confidentiality has now expired. Thanks and acknowledgements are extended to Newmont Australia

Electronic copies of this publication in PDF format can be downloaded from the CRC LEME website: <http://crlceme.org.au/Pubs/OFRSindex.html>. Information on this and other LEME publications can be obtained from <http://crlceme.org.au>.

Hard copies will be retained in the Australian National Library, the Western Australian State Reference Library, and Libraries at The Australian National University and Geoscience Australia, Canberra, The University of Adelaide and the CSIRO Library at the Australian Resources Research Centre, Kensington, Western Australia.

**Reference:**

Le Gleuher M. 2008. Trace element-mineral associations in the regolith, Scuddles Massive Cu-Zn sulphide deposit, Western Australia. *CRC LEME Open File Report 197*. 68pp.

**Keywords:**

1. Regolith. 2. Trace elements. 3. Mineral hosts 4. Weathering. 5. Geochemistry.  
6. Mineralogy. 7. VMS. 8. Scuddles (Golden Gove), Western Australia

ISSB 1329-4768

ISBN 1 921039 34 5

**Address and affiliation of author**

Dr Maïté Le Gleuher  
formerly CRC LEME, and  
The Australian National University

**Published by:**

CRC LEME, c/o CSIRO Exploration and Mining  
PO Box 1130  
Bentley, Western Australia 6102

**Disclaimer**

The user accepts all risks and responsibility for losses, damages, costs and other consequences resulting directly or indirectly from using any information or material contained in this report. To the maximum permitted by law, CRC LEME excludes all liability to any person arising directly or indirectly from using any information or material contained in this report.

© **This report is Copyright of the** Cooperative Research Centre for Landscape Environments and Mineral Exploration, from the date of the original publication, which resides with its Core Participants: CSIRO Exploration and Mining and Land and Water, The Australian National University, Curtin University of Technology, The University of Adelaide, Geoscience Australia, Primary Industry and Resources SA, NSW Department of Primary Industries and Minerals Council of Australia.

Apart from any fair dealing for the purposes of private study, research, criticism or review, as permitted under Copyright Act, no part may be reproduced or reused by any process whatsoever, without prior written approval from the Core Participants mentioned above.

## ABSTRACT

The association between trace elements and regolith minerals has been studied at the Scuddles Cu-Zn sulphide deposit, Golden Grove, Western Australia. The mineralogy and the trace element abundance were characterised using a combination of bulk and *in situ* micro-analytical techniques. The determination of low abundance elements in the minerals was carried out with *in situ* Laser Ablation Inductively Coupled Plasma Mass Spectrometry (LA-ICP-MS).

The Scuddles deposit occurs in a sequence dominated by felsic and intermediate volcanoclastic sediments and lavas. The mineralised horizon is up to 80 m thick. The hanging wall lavas are deeply weathered to a depth exceeding 100 m in places. The regolith consists of a lower saprolite, 10 to > 60 m thick, which roughly coincides with the modern water-table, a 10 to 50 m thick upper saprolite, a mottled zone and a 1 to 2 m thick silicified hardpanised colluvium.

The samples selected for this study are from 2 drill holes located directly above the mineralisation and 4 drill holes intersecting the weathered hanging-wall rocks. Data from Normandy Mining Ltd. indicate anomalies of Sb, In, Bi as well as Cu, Pb and Zn in some samples, directly up dip from mineralisation. In contrast, samples located further west into the hanging wall lavas are enriched in Cu, Pb and Zn, but not in Sb, Bi and In.

### *Mineralogy*

#### Hanging wall

The lower saprolite consists of quartz, muscovite, kaolinite, corrensites (high and low-charge) and accessory ilmenite, goethite, coronadite and plumbogummite. The upper saprolite is characterized by a decrease in abundance of Mg-rich clays.

#### Over mineralisation

The saprolite is thin and comprises quartz, chlorite, kaolinite, muscovite and accessory high-charge corrensite, rutile, Mn-oxides (coronadite, coronadite-hollandite and lithiophorite) and plumbogummite. Relicts of mineralised material pseudomorphed by colloform goethite and hematite, and quartz crystals containing inclusions of euhedral pyrite, are widespread in the lower saprolite. The upper saprolite is intensively silicified and locally displays banded concretions of microcrystalline kaolinite and goethite.

### *Mineral-trace elements associations*

The mineralogical and geochemical investigations of the Scuddles regolith have provided new information about the location of trace elements and have improved the understanding of the geochemical dispersion observed in this area.

#### Hanging wall

Lead, Cu, Mn, Zn and Co are concentrated in the lower saprolite but decrease towards the surface. Manganese is concentrated in coronadite and lithiophorite and Pb in coronadite and plumbogummite. Copper and Zn are hosted in corrensites, smectites, coronadite and goethite. Zinc and Mn are also contained in ilmenite-eandrewsite. Cobalt and Ni are immobilized in lithiophorite and marginally in corrensites and smectites. Bismuth, Sb, In and Mo are not significantly concentrated. However Mo is locally scavenged by coronadite and iron oxides, and Sb is present in weathered ilmenite and goethite.

#### Over mineralisation

There is an overall concentration of Sb, Bi, In and Mo immediately above the orebody. Antimony, Mo and In occur predominantly in iron oxides whereas Bi is contained in Pb-Bi phases and rutile. Antimony, Mo and Bi are abundant in rutile present in the bleached and Fe-rich upper saprolite. Fresh sphalerite inclusions in quartz crystals contain In. Copper and Zn are moderately concentrated in Fe and Mn oxides (coronadite and lithiophorite) and in rare corrensite in the lower saprolite. Iron oxides contain abundant Cu and Zn in the upper saprolite reddish mottles. In the lower saprolite, Pb is concentrated in iron oxides -with an affinity for hematite- and in Mn oxides (coronadite and hollandite). It is relatively

less depleted than Cu and Zn in the upper saprolite where it is retained in Fe-oxides, plumbogummite, Pb-Bi phases, and sphalerite inclusions.

At Scuddles, trace element dispersion is strongly controlled by the mineralogy of the regolith. Above the mineralisation, potential mineral hosts corrensites and smectites are not abundant enough to immobilise, and as a result Cu, Zn and Pb released from the dissolution of sulphides. Instead, the Mg-clays and Mn oxides concentrate Cu and Zn further west. Bismuth, Mo, Sb and In anomalies are considered residual, with local variations associated with Fe oxides.

It has been shown that Bi, Mo and Sb anomalies are either directly related to the mineralisation or result from the relative accumulation of rutile towards the surface of the regolith. Kaolinite is a barren clay and does not give any base metals signature. For base metal exploration in Scuddles area, Fe-stained kaolinite is the preferred sampling medium instead of bleached kaolinite.

## TABLE OF CONTENTS

<b>ABSTRACT .....</b>	<b>i</b>
<b>TABLE OF CONTENTS.....</b>	<b>iii</b>
<b>PREFACE AND SUMMARY .....</b>	<b>v</b>
<b>1. INTRODUCTION.....</b>	<b>1</b>
<b>2. METHODS OF INVESTIGATION .....</b>	<b>2</b>
2. 1. Analytical methods .....	2
2. 1. 1. Bulk samples analysis .....	2
2. 1. 2. In situ analysis .....	2
2. 2. Laser Ablation Inductively Coupled Plasma Mass Spectrometry analysis of regolith material .....	2
2. 2. 1. Description of the technique and equipment.....	2
2. 2. 2. Samples .....	3
2. 2. 3. Data acquisition and sampling protocol.....	4
2. 2. 4. Data reduction .....	4
2. 3. LA-ICP-MS analysis of regolith materials .....	6
2. 3. 1. Introduction.....	6
2. 3. 2. Homogeneous and heterogeneous regolith materials.....	6
2. 3. 3. Nature of the ablated material .....	7
2. 3. 4. Data acquisition.....	7
2. 3. 5. Data processing .....	7
2. 3. 6. Interferences and contamination .....	8
<b>3. GEOLOGICAL SETTING OF THE SCUDDLES Zn-Cu DEPOSIT .....</b>	<b>10</b>
3. 1. Regional geology .....	10
3. 2. Mineralized horizon.....	10
<b>4. THE REGOLITH.....</b>	<b>13</b>
4. 1. Introduction .....	13
4. 2. Description of the regolith units .....	13
4. 3. Sampling, bulk mineralogical and chemical composition of the regolith units.....	13
<b>5. MINERALOGY AND CHEMISTRY OF THE REGOLITH UNITS .....</b>	<b>16</b>
5. 1. Lower saprolite .....	16
5. 1. 1. Hanging wall.....	16
5. 1. 2. Over the mineralisation .....	21
5. 2. The upper Saprolite .....	24
5. 2. 1. Hanging wall.....	24
5. 2. 2. Over mineralisation .....	25
5. 3. Silicified horizon and laterite .....	32
5. 3. 1. Hanging wall.....	32
5. 3. 2. Over mineralisation .....	32

<b>6. DETERMINATION OF TRACE ELEMENTS IN REGOLITH MATERIAL BY LASER ABLATION-INDUCTIVELY COUPLED PLASMA-MASS SPECTROMETRY (LA-ICP-MS)...</b>	<b>35</b>
6. 1. Introduction .....	35
6. 2. Lower saprolite .....	35
6. 2. 1. <i>Hanging-wall</i> .....	35
6. 2. 2. <i>Over mineralisation</i> .....	37
6. 3. Upper saprolite .....	39
6. 3. 1. <i>Hanging-wall</i> .....	39
6. 3. 2. <i>Over mineralisation</i> .....	40
<b>7. MINERALOGY AND CHEMISTRY OF SIZE FRACTIONS .....</b>	<b>54</b>
7. 1. Introduction .....	54
7. 2. Distribution of the trace elements in the size fractions.....	54
7. 2. 1. <i>Hanging wall: samples SCRB103, SCRB102 and SCRB07</i> .....	54
7. 2. 2. <i>Over mineralisation: samples SCRB09 (14-15 m) and SCRB10 (9-10)</i> .....	55
7. 3. Effectiveness of the method .....	55
<b>8. DISCUSSION AND CONCLUSIONS ON ELEMENT-MINERAL ASSOCIATIONS IN THE SCUDDLES ZN-CU-DEPOSIT .....</b>	<b>58</b>
8. 1. Element-mineral associations .....	58
8. 1. 1. <i>Hanging wall</i> .....	58
8. 1. 2. <i>Over mineralisation</i> .....	59
8. 1. 3. <i>Conclusions</i> .....	59
8. 2. Implications for exploration .....	60
<b>9. ACKNOWLEDGEMENTS.....</b>	<b>63</b>
<b>10. REFERENCES.....</b>	<b>64</b>
<b>11. APPENDICES .....</b>	<b>66</b>

## PREFACE

CRC LEME-Normandy Mining Limited (now Newmont Australia) Project has its principal objective to establish case-by-case relationships between mineral and trace element abundance and to develop new exploration methods based on mineral host for significant elements. This is part of the larger research theme which integrates the hydromorphic, mechanical and biogenic processes that control the distribution and dispersion of elements within the regolith in order to make exploration geochemistry more predictive, particularly in areas of cover. The project has investigated the element-mineral associations at three deposits in a variety of geological and geomorphological environments. The Scuddles Cu-Zn deposit is located in the Golden Grove district, about 400 km north-northeast of Perth, in the Murchison province of the Archaean Yilgarn Craton. A combination of mineralogical and chemical microanalyses, with emphasis on in situ analyses, has been performed to locate trace elements in regolith material. Laser Ablation Inductively Coupled Plasma Mass Spectrometry has been intensively used, and has been shown to be valuable tool for the determination of trace elements in clays, Fe and Mn oxides and resistates.

At Scuddles, trace element dispersion is strongly controlled by the mineralogy of the regolith. Above the mineralisation, potential captors such as corrensite and smectites are not abundant, and as a result, Cu, Zn and Pb mobilised by the dissolution of sulphides, are not retained. They have been captured further west by abundant receptors such as corrensite and Mn oxides. Copper and Zn are preferentially captured by high charge corrensite (chlorite-vermiculite interstratified mineral), indicating that vermiculite has a higher ability to integrate these cations than smectite layers. Bismuth, Mo, Sb and In anomalies are considered residual with local variations associated with goethite. Bismuth, Mo and Sb anomalies detected by analysing the bulk samples have two origins. They are directly related to the mineralisation and are retained in Fe oxides, minor phases (Bi-Pb phases) and sulphide inclusions. They can also result from the relative accumulation of resistates such as rutile towards the surface of the regolith. Kaolinite is a barren clay and does not incorporate any base metals.

The mineralogical and geochemical investigation of the Scuddles regolith has provided new information about the location of trace elements. The selection of the material containing the trace element hosts for chemical analysis will greatly improve anomalies and reveal some anomalies undetected in bulk samples. For example, Fe-stained kaolinite is the preferred sampling medium instead of bleached kaolinite. Iron oxides are choice sampling material able to retain In, Sb, Bi and Mo.

This work also demonstrates the important role played by smectites, vermiculites and interstratified minerals, in the dispersion of base metals in the regolith. In addition to geochemical anomalies, much information is provided by a basic mineralogical investigation of the regolith material. There are numerous reliable mineralogical indicators of mineralisation and associated hydrothermal activity at Scuddles: sphalerite inclusions in quartz and gossan chips.

R. R. Anand and R. A. Eggleton  
Project Leaders



## 1. INTRODUCTION

The overall objective of this project was to investigate the association between regolith minerals and trace elements. Apart from a few resistates, most minerals are destabilised under surface conditions. As a result, minor and trace elements may be released into the environment and trapped in various secondary mineral phases. Understanding the secondary hosts is of particular importance as the geochemical dispersion of gold, base elements and their pathfinders is partly controlled by the availability of these receptors in the regolith. Once the location of trace elements has been established, directions for exploration sampling and geochemical prospecting can be suggested.

Three sites were selected to investigate the mineralogy and geochemistry of various regolith materials. The element-mineral associations observed in the lateritic profiles in the Scuddles Cu-Zn sulphide deposit are discussed in this report, and a companion report investigates the regolith at the Boddington and Mt Percy gold deposits (Le Gleuher, 2003).

The associations between trace elements and minerals can be partially derived using statistical analyses of bulk geochemical data, backed up with a relatively simple qualitative study of the mineralogy of the regolith. Selective sampling such as size-fractionation or chemical selective extraction improves the result. In this study the physical location of the trace elements in the regolith minerals was directly determined using *in situ* optical and electron optical techniques. A combination of conventional bulk and micro-analytical techniques covering a wide range of observation scales (X-ray diffraction, Scanning and Transmission Electron Microscopy) were employed to characterize the mineralogy and trace element distribution. As most trace element concentrations lie beyond the detection capability of the electron microprobe, *in situ* Laser Ablation Inductively Coupled Plasma Mass Spectrometry (LA-ICP-MS) analyses have been performed on the regolith materials. The application of this technique to the study of regolith samples, including processing and interpretation of the data has been assessed and developed.

## **2. METHODS OF INVESTIGATION**

### **2. 1. Analytical methods**

#### **2. 1. 1. Bulk samples analysis**

X-ray diffraction analyses of crushed and unoriented bulk samples were performed on a Siemens 5005D diffractometer operating at 40 mA and 40 kV using Co K $\alpha$  radiation, with a counting time of 1 second per 0.02° 2 $\theta$ . Slower scans were run on handpicked or micro-drilled microsamples mounted on a low-background quartz plate. The clay fraction was prepared and analysed following the procedures described by Moore and Reynolds (1997). Three scans were collected from each sample after treatment with MgCl<sub>2</sub>, ethylene glycol saturation and heating to 350°C.

Selected samples were separated into size fractions and the fractions analysed by ICP-MS after acid digestion, to compare with the results of the mineralogical study. The protocol is described in Appendix 1. In some cases, sufficient material was obtained for chemical and X-ray diffraction analyses.

The bulk samples have been analysed for Al, Fe, Mg, Ca, K, Na, Mn, Co, Cu, Pb, Zn, Ni, Bi, In, Mo and Sb (Normandy Mining Ltd data).

#### **2. 1. 2. In situ analysis**

Thin sections of selected samples were investigated by optical microscopy. Electron microprobe analyses were performed on polished thin sections and single grains mounted in an epoxy resin using a JEOL 64000 SEM equipped with a LINK analytical EDAX system (Energy Dispersive X-ray analysis). Observations in backscattered electron imaging mode (BSE) provide additional information about the microfabric of the rock fragment, clay and accessory mineral mineralogy and distribution of the phases. Transmission electron microscopy (TEM) and analytical electron microscopy (AEM) were used to refine the mineralogy and the chemical composition of individual microcrystals. Images and chemical analyses were obtained with a Philips EM430 TEM and a Philips CM300 TEMs operating at 300 KV, both equipped with an energy dispersive X-ray (EDS) detector.

The *in situ* determination of trace elements was carried out with a quadrupole inductively coupled plasma spectrometer instrument (Plasmaquad PQ2) coupled to an excimer laser (Argon Fluoride 193nm). The following section is dedicated to the analysis of regolith samples with this relatively new technique.

### **2. 2. Laser Ablation Inductively Coupled Plasma Mass Spectrometry analysis of regolith material**

Laser ablation inductively coupled plasma spectrometry is an extremely powerful analytical technique for *in situ* analysis of solids. It has the potential to determine almost all the elements at the part-per million level in 1 minute, with a spatial resolution of around 20  $\mu$ m.

#### **2. 2. 1. Description of the technique and equipment**

The technique can be summarized into three steps:

1. Ablation of solid samples using pulses from a laser and formation of microparticles;
2. Transport of the released material by a gas flow to the plasma where the atoms are ionized.
3. The ions are sorted by mass and detected in the mass spectrometer.

The analyses were performed using a quadrupole inductively coupled plasma spectrometer instrument (Plasmaquad PQ2) coupled to an excimer laser (Argon Fluoride 193nm; supplied by Resonetics and based on a Lambda Physik LPX120i laser). The instrumental set up is as shown in Figure 1. The laser is

deflected on to the sample cell by a mirror. The sample sits in a “Perspex” ablation cell on a holder which can be moved in the X and Y directions. Ablation occurs under a controlled atmosphere of argon and helium, and the ablated material is then carried out the cell in an argon gas stream to the ICP via a pulse-smoothing manifold.

The size of the probe — *i.e.* the diameter of the ablation pit — is controlled by inserting an aperture in the light path. The sample can be observed on a screen at a range of low magnifications.

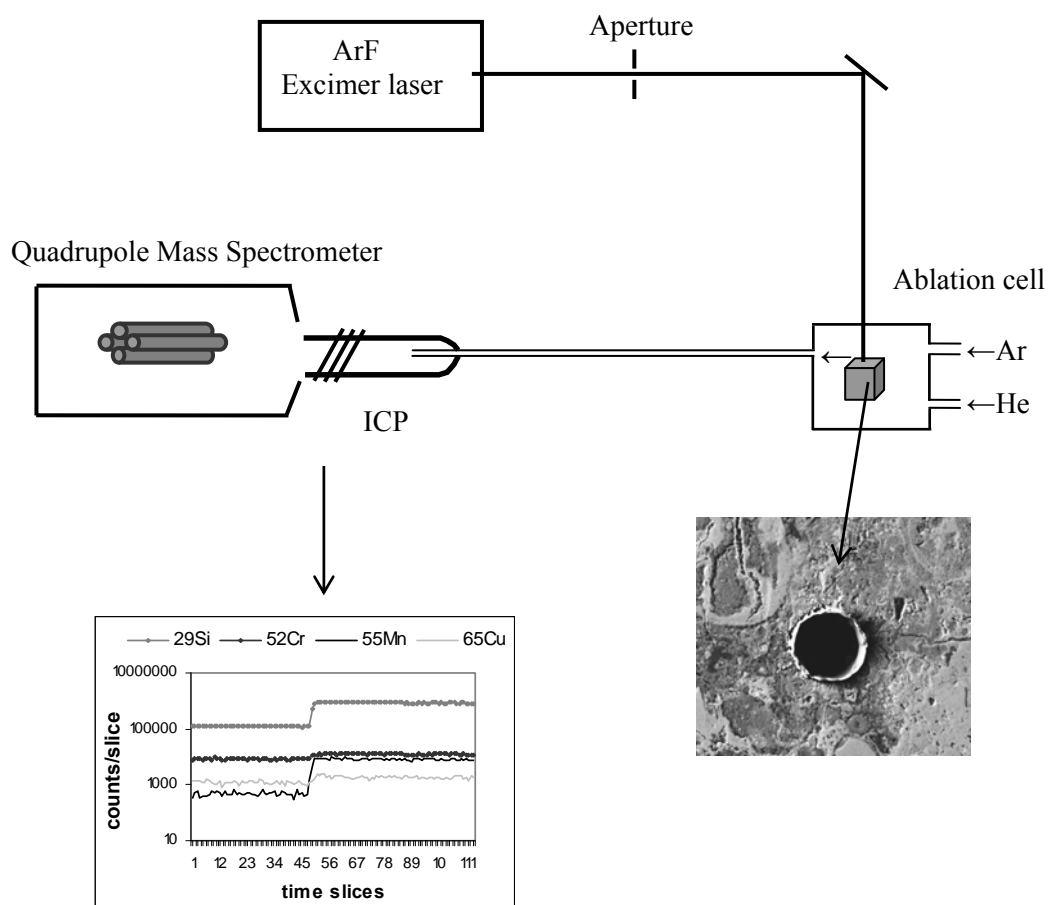


Figure 1. Laser ablation inductively coupled mass spectrometry analytical set up. Inserts show the ablated sample and the ICP-MS responses of selected isotopes in the NIST SRM 612.

### 2. 2. 2. Samples

The *in situ* LA-ICP-MS analyses were carried out on conventional polished thin sections, and polished stubs containing single grains or chips mounted in epoxy resin. Thin sections with a thickness greater than 30  $\mu\text{m}$  have also been prepared to avoid ablating the glass. Polished surfaces are required for the preliminary mineralogical and chemical characterisation and “mapping” of the samples (light optical microscopy, SEM). These samples were directly fitted in a custom-built ablation cell where they could be ablated without any further preparation.

### 2. 2. 3. Data acquisition and sampling protocol

Standards and samples were ablated using pulse rates of 5 Hz and beam energies of 100 mJ/pulse. In these conditions the average drill rate is about 0.5  $\mu\text{m/s}$ . Pits with a surface diameter of 29  $\mu\text{m}$  were ablated during 60 s incorporating 74 to 114 mass spectrum sweeps during routine analyses. In order to increase the response a 50  $\mu\text{m}$  probe was used when analysing for gold and silver, and the total analysis time was also 60 s with 97 sweeps. In some cases pre-ablation of the surface with a larger probe (65 or 200  $\mu\text{m}$ ) was carried out to clean up the site.

A typical analytical sequence comprises:

- Acquisition of a “blank” signal (*i.e.* laser off) to obtain the background intensity;
- Analysis of 2 calibration standards;
- Ten analyses of samples;
- Analysis of 2 calibration standards;
- Acquisition of a “blank” signal.

Alternatively the plasma gas blank was acquired at the beginning of each sample analysis during 60 s. Data were collected in time-resolved mode to monitor possible inter-element fractionation and compositional heterogeneity. Figure 2A shows an example of LA-ICP-MS responses obtained on the NIST SRM 612 for a selection of trace elements. Backgrounds were counted for about 60 s prior to ablation and the laser was switched off after 120 s. The analyses were conducted in two modes: the samples were either scanned along a transect or ablated in depth (depth profiling).

### 2. 2. 4. Data reduction

The data reduction method is based on Longerich *et al* (1996).

All data reduction is carried out off-line using spreadsheet programs and involves, for each isotope:

- Calculation of the background intensity mean;
- Calculation of the analyte intensity mean;
- Subtraction of the background and
- Concentration calculation (developed below).

#### Concentration calculation

In ICP-MS analysis it is not possible to calibrate results directly by comparing the raw count data for an analyte (sample) between standards and samples. The number of ions arriving to the detector depends partially on the amount of material removed during ablation. The behavior of minerals with respect to ablation varies greatly. Under similar analytical conditions it depends mainly on the nature of the sample. The only two ways to get quantitative analyses are to normalise the intensities of the observed peaks to the weight of the sample or alternatively to an internal standard. The second option is routinely used as the first option is not easily feasible as not all the ablated material reaches the plasma or collector. When the ratio of the analyte peak relative to that of an internal standard  $I_{\text{unknown}} / I_{\text{Int STD}}$  is calculated, the concentration of the analyte can be calculated from the same ratio obtained from a calibration standard (external standard). Since it is not possible to spike solid minerals with any other substance, the two choices are:

- (i) to use an element contained in the mineral, which has been accurately analysed by another technique (electron microprobe),
- (ii) to use the known elemental stoichiometry when crystalline materials are analysed.

The concentrations  $C$  of each isotope ( $C(\text{analyte})_{\text{SAM}}$ ) in the sample are calculated from the count rates for each isotope using the equation (1)

$$C(\text{analyte})_{\text{SAM}} = I(\text{analyte})_{\text{SAM}} / S \quad (1)$$

$S$ : normalised sensitivity determined on the calibration standard (CAL) corrected for the volume (mass) of sample ablated.

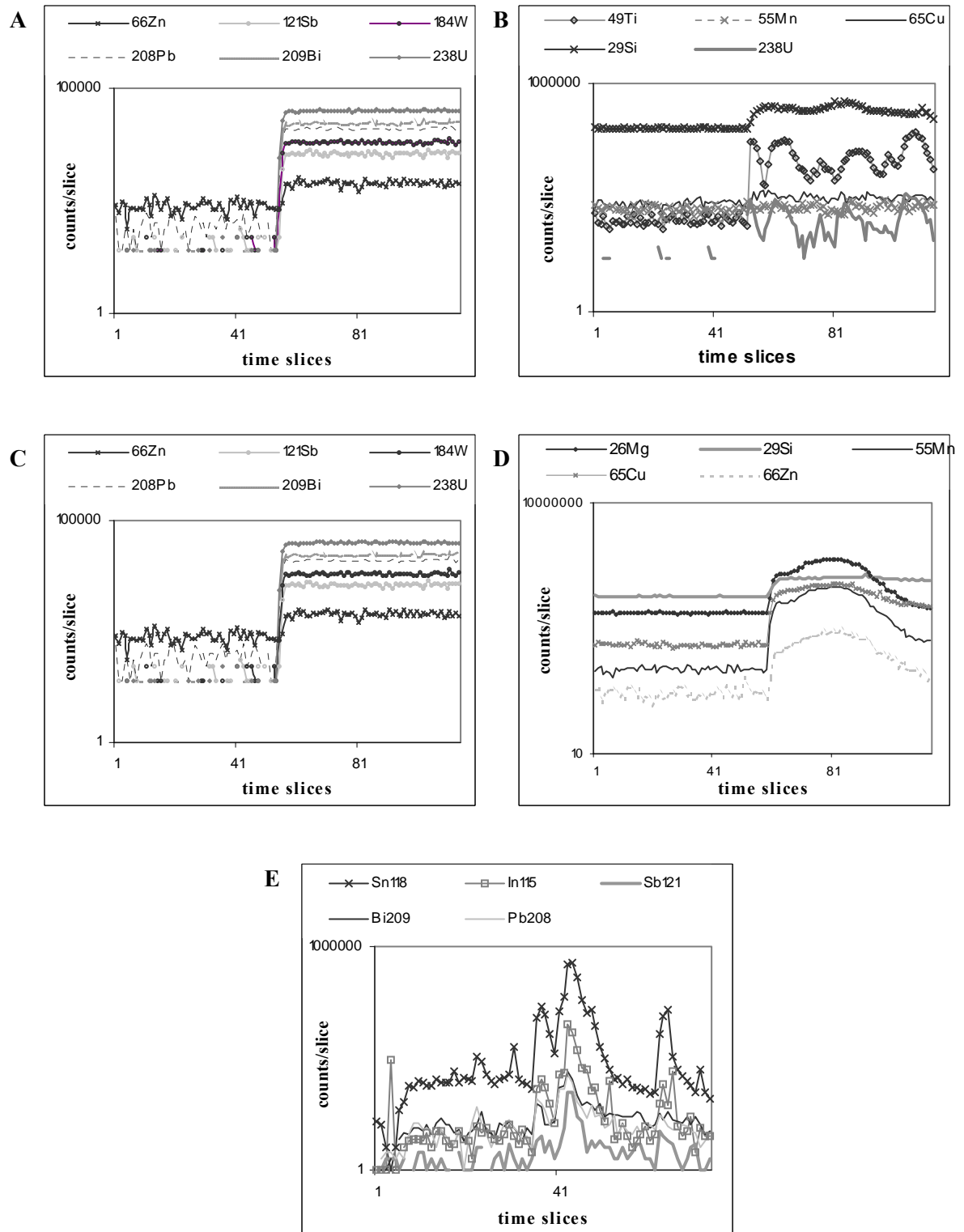


Figure 2. Time-resolved spectra of selected isotopes obtained on: A. NIST SRM 612 reference glass standard. B. Heterogeneous material. C. Iron oxides. D. Saprolite clays. E. LA-ICP-MS responses of Sn, In, Sb Bi and Pb produced by microchips of tin polishing plate encrusted in the sample.

$$S = I(\text{analyte})_{\text{CAL}} / C(\text{analyte})_{\text{CAL}} * (IIS_{\text{SAM}} / IIS_{\text{CAL}} * CIS_{\text{CAL}} / CIS_{\text{SAM}})$$

$I(\text{analyte})_{\text{CAL}}$ : intensity (count rate) of the analyte in the calibration standard

$C(\text{analyte})_{\text{CAL}}$ : concentration of the analyte in the calibration material

$IIS_{\text{SAM}}$ : intensity of the internal standard (Al, Si, Mn etc...) in the sample.

$IIS_{\text{CAL}}$ : intensity of the internal standard in the calibration material

$CIS_{\text{CAL}}$ : concentration of the internal standard in the calibration material

$CIS_{\text{SAM}}$ : concentration of the internal standard in the sample

For calibration material - or external standard - (CAL) the synthetic glasses NIST SRM 610, NIST SRM 612 and NIST SRM 616, and the Basalt Glass USGS BCR-2G have been used. A combination of 2 of these standards was chosen for better monitoring of the data. The trace element concentrations used for the NIST SRM 610 and SRM 612 are listed in Appendix 2.

The sensitivity (S) is subject to a mass dependent drift with time. The sensitivity ratios of the analyte and internal standard are corrected using a linear interpolation between the calibration samples analysed prior and after each batch of analyses (about 10 analyses). When the blanks are collected at the beginning and at the end of a batch of analyses, a drift correction on the background intensity is applied.

The limit of detection is different for each analysis as the amount of material ablated is usually different for each analysis. The conventional standard deviation of the blank ( $3\sigma$ ) approach is usually used.

## **2. 3. LA-ICP-MS analysis of regolith materials**

### **2. 3. 1. Introduction**

The regolith samples are structurally and compositionally heterogeneous. A method has been developed to accommodate the few problems introduced by this heterogeneity. Very few applications of LA-ICP-MS for analysing soils, clays and sediments have been reported. Most of these studies are assessing the methods and therefore report analyses of known materials such as standard reference soils and sediments (Durrant, 1999). For analyses, the samples were usually pressed into pellets without binder, or fused mixtures of soils and diluent (*e.g.* Baker *et al*, 1998; Motelica-Heino *et al*, 1998).

Pioneer studies conducted by Hale *et al.* (1984) tested the use of laser ablation as a means of introducing iron and manganese coatings on stream sediments into an ICP-MS. Radford and Burton (1999) performed *in situ* analyses of polished slabs of pisolithic laterite. However it seems that there is no previous report of *in situ* analysis of undisturbed regolith material (or soils or sediments) reporting quantitative measurements.

### **2. 3. 2. Homogeneous and heterogeneous regolith materials**

A regolith sample is an assemblage of crystals of various sizes usually randomly distributed. The size of the crystals is usually much smaller than the probe size (29 and 50  $\mu\text{m}$ ). A typical signal produced when analysing regolith samples is shown on Figure 2B. The total signal reflects the chemical signature of successive discs of material with a diameter of 29  $\mu\text{m}$  (or 50  $\mu\text{m}$ ) and a thickness of 0.5 to 1  $\mu\text{m}$ . For each time slice (usually 1s), the segment of signal represents the bulk composition of the material of the disc. The size of the crystals in the regolith is usually much smaller than the laser probe size (29 and 50  $\mu\text{m}$ ) except for a few residual fresh minerals. For example, the mineral grains of a kaolinitic plasma are typically less than 2  $\mu\text{m}$  in size. If the spatial resolution is quite poor laterally, it is however excellent in depth (0.5 to 1  $\mu\text{m}$ ).

Two main types of regolith material have been recognized (Figure 3):

1. The ablated volume consists of a homogeneous assemblage of small crystal (A). The assemblage can be mono-mineralic or poly-mineralic. A microcrystalline plasma composed of kaolinite and goethite is an example of such material.
2. The ablated volume is heterogeneous and presents mineralogical variations (B).

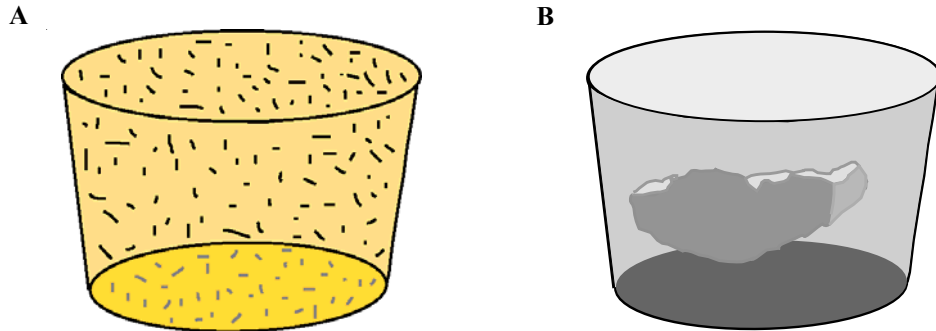


Figure 3. Types of regolith material

### **2. 3. 3. Nature of the ablated material**

The mineralogy and chemical compositions of the selected sites of the thin sections is carefully characterized and mapped with SEM-EDAX before ablation. The SEM observation of the pits after ablation is also useful in order to confirm the location of the analyses, and to assess the degree of homogeneity of ablated material. The inspection of the bottom and walls of the pit shown on Figure 4 indicates that the ablated sample which seemed mono-mineralic on surface is however composed of several phases in depth.

Visual inspection of the time resolved spectra, combined with a detailed knowledge of the mineralogy of the sample, provides a reasonably good idea of the nature of the ablated material. For this purpose, a few major element isotopes are systematically measured to serve as “navigators”. It is then usually possible to pick the time slice where a mineralogical change has occurred. For example, a drop in the silica signal will illustrate the transition from kaolinite to gibbsite. As mentioned above the high spatial resolution in depth allows the detection of minute grains less than 1  $\mu\text{m}$  in size on the spectra.

### **2. 3. 4. Data acquisition**

Samples can be scanned and ablated along a transect, or drilled in depth. Isotopes of major elements likely to be present in the ablated volume are systematically analysed for several purposes: 1) to serve as “navigators” *i.e.* to enable the identification of mineralogy of the ablated volume; 2) to enable the determination of the internal standard concentration.

### **2. 3. 5. Data processing**

#### *Qualitative results*

Observation of the isotopic responses allows a rapid assessment of some of the trace element associations and therefore the identification of the host-minerals. Trace element profiles often appear noisy due to fine scale mineralogical variations and analytical noises. The fine amplitude spikes have not been taken in account, as they cannot be safely discriminated from instrumental noises. Sharp spikes are also ignored whereas top rounded ones have been considered as real features of the spectra indicating the presence of a minute particle.

### *Quantitative results*

In order to achieve a quantitative analysis it is necessary to select an internal standard present in the sample and in the external standard (NIST glasses). The determination of the concentration standard is easily addressed when analysing a large individual crystal of a thin section (Microprobe analysis or stoichiometry). It is however more difficult to obtain a value for an internal standard concentration when the material is not a single crystal. In this case a stoichiometric value, normalised to 100% wt oxide or element, has been determined as follow:

- The concentrations of the isotopes are calculated according to Longerich's procedure using an arbitrary but possible  $CIS_{SAM}$  value based on the mineralogy;
- The concentrations of the most abundant isotopes in the phase are summed up;
- The value of  $CIS_{SAM}$  is adjusted to obtain a total of 100 wt. oxide or 100% element;
- The element concentrations and ratios such as Si/Al are checked to insure that they are in agreement with the stoichiometry of the assemblage. If it is not the case, overlooked phases or substitutions in some of the phases might account for the discrepancies.

The different methods, which have been used depending on the regolith type, are described below. Silica, Al or Mg were chosen as internal standards.

#### Type A: homogeneous regoliths

The signals produced by homogeneous samples are typically flat, similar to the ones obtained when ablating massive iron oxides (Figure 2C). The chemical composition of the assemblage is analysed by SEM-EDAX throughout the site to check for any possible spatial variation.

A mono-mineralic sample is treated like a single crystal. There is little or no chemical variation, therefore the normalised EDAX value (to 100 wt% or 100 % element) of a chosen element is used as the internal standard concentration.

For a poly-mineralic sample two methods are used: the  $CIS_{SAM}$  value is either the normalised value of a window SEM-EDAX analysis, or a stoichiometric normalised value when the proportions of the different phases vary in the ablated volume.

#### Type B: heterogeneous regoliths

The signals shown in Figure 2D are produced by the ablation of a volume of saprolite consisting of vermiculite and kaolinite. The variations in depth of the responses obtained for a combination of major diagnostic elements (e.g. K<sup>+</sup>, Si, Al, Fe) are used to decompose the signals into slices, each slice representing a single or group of minerals. Only phases large enough to be ablated during at least ten time slices are considered for quantitative results. An internal standard is chosen for each slice if necessary. The concentration of the internal standard is either an EDAX value or a stoichiometric value.

In the case of more complex mixture, the  $CIS_{SAM}$  is also a stoichiometric value. The value obtained for each isotope is the concentrations of this isotope in a volume of material containing x%Al<sub>2</sub>O<sub>3</sub>, y% SiO<sub>2</sub> and z%Fe<sub>2</sub>O<sub>3</sub> for example.

### **2. 3. 6. Interferences and contamination**

Problems are inherent to the technique or due to the nature of the sample. In the first category are polyatomic ion and oxide interferences.

The most relevant atomic interferences for this study are interferences with Ar atoms of the plasma such as  $^{40}\text{Ar} + ^{23}\text{Na} = ^{63}\text{Cu}$  and  $^{40}\text{Ar} + ^{28}\text{Si} = ^{68}\text{Zn}$ . Isotopes  $^{65}\text{Cu}$  and  $^{66}\text{Zn}$  are therefore analysed. Other examples are interferences with silver and gold such as  $^{91}\text{Zr}^{16}\text{O} = ^{107}\text{Ag}$ ,  $^{93}\text{Nb}^{16}\text{O} = ^{109}\text{Ag}$  and  $^{181}\text{Ta}^{16}\text{O} = ^{197}\text{Au}$ . It is necessary to analyse for the isotopes that can create interferences in order to discriminate between artefacts and true responses for the isotopes of interest.



Tin contamination and associated isotopes have been a major problem in the analyses of the samples. During the polishing of the thin sections, tin grains frequently set in or between crystals. Unfortunately the material of the plate certified “pure tin” also introduces anomalous concentrations of indium, bismuth, antimony and lead.

A careful inspection of the spectra is usually enough to discriminate between true trends and contamination. For this reason tin has been generally analysed but not quantified. Figure 2E shows Sn, Bi, In, Pb and Sb responses produced by such grains scattered in a mixture of clays and iron oxides.

Tin pollution is more likely to be present when scanning the sample surface. In this case, the track to be analysed is cleaned by a rapid and larger scan (65  $\mu\text{m}$ ) prior to ablation. Depth profiles are more useful because most of the spectrum under the top slices can still be used.

### 3. GEOLOGICAL SETTING OF THE SCUDDLES Zn-Cu DEPOSIT

#### 3. 1. Regional geology

The Scuddles Cu-Zn deposit is located in the Golden Grove district, about 400 km north-northeast of Perth, in the Murchison province of the Archaean Yilgarn Craton. The Scuddles and Gossan Hill prospects are the two major volcanogenic massive sulphide deposits of the Golden Grove area, in the Warriedar fold belt. The fold belt has been heterogeneously deformed (Baxter, 1982). Scuddles deposit occurs within the Scuddles Formation of the Gossan Hill Group, which consists of felsic to intermediate volcanoclastic sediments, lavas and associated autoclastic breccias. The sequence is more than 1 km thick and dips steeply west-southwest.

These rocks have been deeply modified by hydrothermal processes accompanying the formation of the Scuddles mineralisation, and subsequent greenschist grade regional metamorphism. Porphyritic dacitic and tholeiitic doleritic dikes postdating the hydrothermal events and predating regional metamorphism intrude the sequence (Ashley *et al.*, 1988; Mill *et al.*, 1990).

The mineralised horizon is up to 80 m thick in the central section of the deposit, and is dominated by sulphidic and cherty exhalative sediments and epiclastics. The footwall rocks mainly consist of felsic pyroclastics and epiclastics. The hanging-wall rocks consist of interbedded felsic to intermediate lavas, pyroclastics and epiclastics (Figure 5).

#### 3. 2. Mineralized horizon

Two lenses of massive sulphides are recognized, the “Main Lens” and the “Central Lens”. A zone of stockwork zinc mineralisation defines the “North Lens” further north. A 1 to 2 m thick layer of a magnetite-rich banded iron-formation, which is enriched in Mn and base metals, conformably caps the mineralized horizon. It is vertically zoned with an upper layer of massive Zn-Fe sulphides, 8 to 15 m thick, grading downwards to a pyritic zone. A zone of stockwork, stringer and disseminated Cu-Fe sulphides (pyrite and chalcopyrite) underlies the massive sulphide ore.

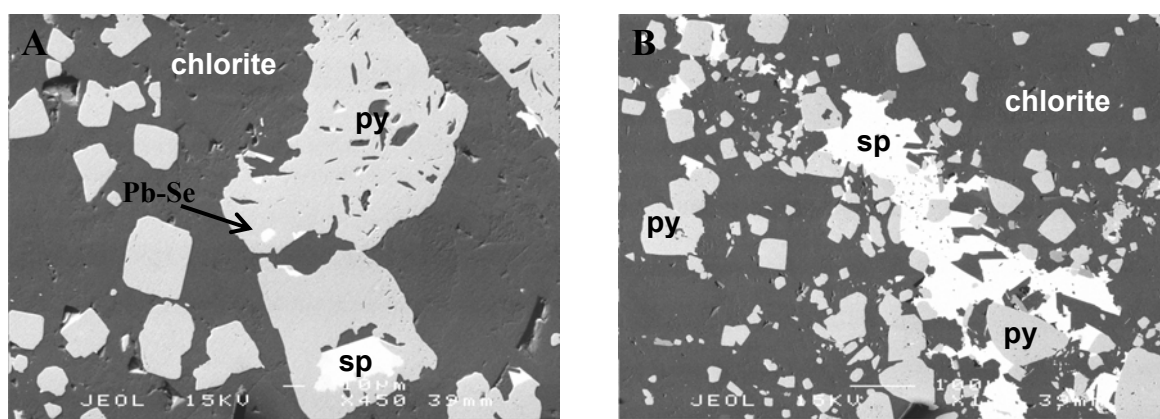


Figure 4. SEM micrographs (backscattered electron image) of the massive pyritic sulphide ore. A. Sphalerite (sp) exsolution and Pb-Se rich inclusions in pyrite (py). B. Pyrite (py) and sphalerite (sp).

Pyrite, sphalerite and chalcopyrite are the principal sulphide minerals (Figure 4). Accessory sulphides include galena and pyrrhotite, with rare arsenopyrite, tetrahedrite, mackinawite and gold. The SEM observations conducted during this project also show the presence of Pb-Se rich inclusions in pyrite (Figure 4). They are characterized by a Pb/Se ratio ranging from 7 to 11. A small amount of W was detected in one of these inclusions.

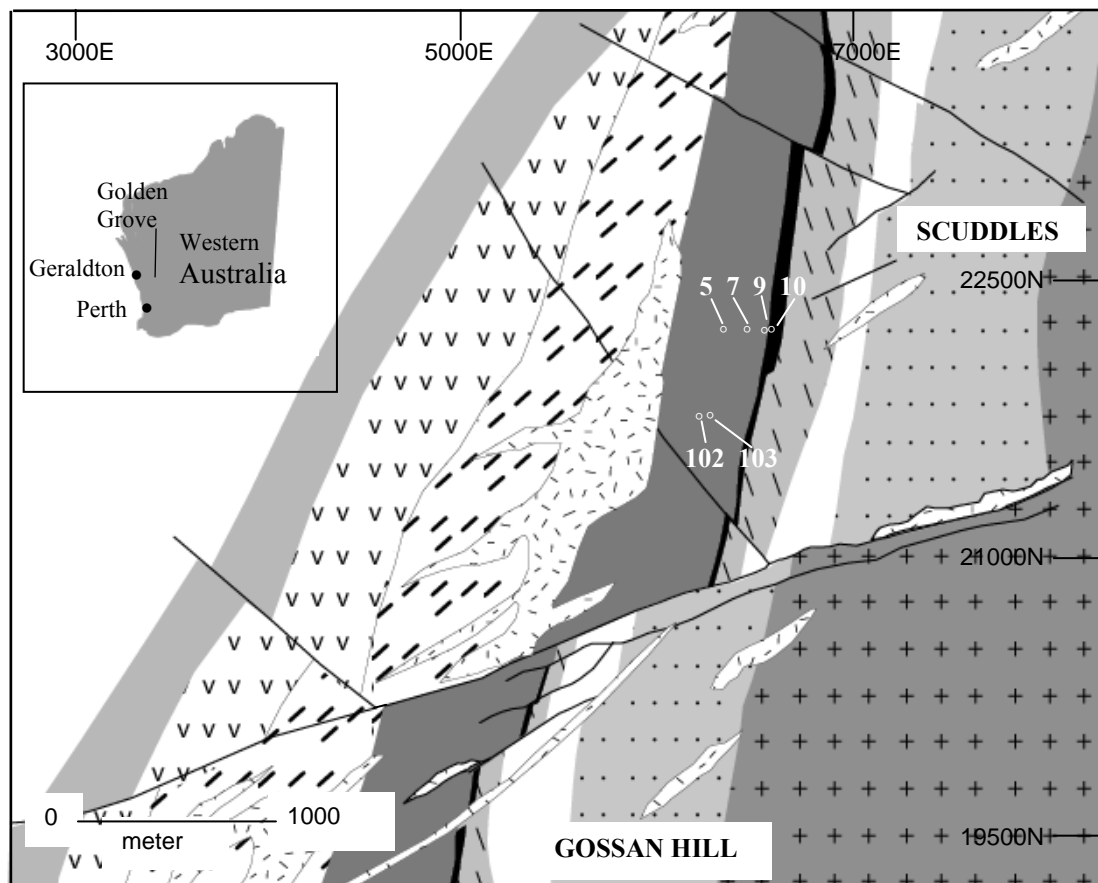
Gangue minerals include hydrothermal quartz, chlorite, and minor amounts of magnetite, sericite, carbonate, talc, amphibole, tourmaline, rutile and cassiterite traces (Ashley *et al*, 1988). The chlorite is a ripidolite according to the classification of Foster (1962) with a  $\text{Fe}^{2+}/\text{Fe}^{2+}+\text{Mg}^{2+}$  ratio of 0.6.

#### *Metal distribution in the mineralised horizon*

The main metals in Scuddles are Fe, Zn, Cu and Pb. Zinc, Pb, Ag, Sn and Fe are strongly concentrated in the massive Zn and pyritic sulphide zone whereas the Cu zone has high Cu and low Zn-Pb-Ag concentrations. Cobalt, As and Bi are also concentrated in the Zn-Fe and pyritic massive sulphides. Manganese is highest in the banded iron formation. Phosphorous is locally abundant in the Cu zone and Cr and Ni show patchy distributions in the mineralised horizon.

Hydrothermal alteration has affected all types of rocks and is responsible for mineralogical and chemical changes in the host rocks. Its effects are observed for up to 150 m into the hanging-wall, and several hundreds meters into the footwall. The primary mineralogical assemblage in the lower part of the hangingwall has been replaced by a quartz + sericite + chlorite assemblage, with characteristic epidote and minor titanite and sulphides. The only remaining primary minerals are quartz phenocrysts and partially altered chlorite and ilmenite. Footwall rocks have been replaced by chlorite + quartz + (sericite + minor carbonate, sulphides, talc) and characteristic rutile. The hydrothermal alteration resulted in a concentration of Fe, Mn, Mg, base metals, As,  $\text{H}_2\text{O}$ ,  $\text{CO}_2$  and S in the mineralised zone, most of the footwall and the lower part of the hangingwall. The breakdown of the primary feldspar resulted in Na, Ca and Sr depletion in these zones (Ashley *et al*, 1988).

The present dispersion of trace elements in the regolith is the expression of the combined effects of hydrothermal alteration and weathering. The geochemical patterns resulting from the hydrothermal episodes are partially controlling the supergene redistribution of the trace elements in the weathered mantle. Weathering processes have remodelled the primary geochemical distributions.



#### LEGEND





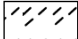
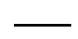





	Banded iron formation		Intrusive monzogranite
	Basalt		Intrusive dolerite and gabbro
	Upper volcanoclastic sediments		Fault
	Hanging wall succession		Drill hole
	Mineralised succession		
	Footwall succession		
	Basalt quartz arenites		

Figure 5. Local geology of the Scuddles area, Golden Grove (After Mill *et al.*, 1990).

Section 22240N: 5: drill hole SCRB05; 7: drill hole SCRB07; 9: drill hole SCRB09; 10: drill hole SCRB10.

Section 21760 N:

102: drill hole SCRB102; 103: drill hole SCRB103

## **4. THE REGOLITH**

### **4. 1. Introduction**

The climate in the Scuddles area is semi-arid, with an average annual rainfall of 260 mm. Vegetation consists of patches of grasses and shrubs and a low cover of mulga (*Acacia* sp). The area is a low relief peneplain with prominent ridges of resistant material (Smith and Perdrix, 1983).

### **4. 2. Description of the regolith units**

The lavas are deeply weathered in the hanging wall to a depth exceeding 100 m in places (Figure 6). The lower saprolite, 10 to > 60 m thick, roughly coincides with the modern water-table. Rock textures are well preserved. This horizon grades upwards to a white, cream or buff upper saprolite, 10 to 50 m thick. Saprolite merges into a mottled zone, 1 to 2 m thick. The pisolitic cover observed in the Golden Grove area is usually missing at Scuddles where the saprolite is locally capped by a 1 to 2 m thick silicified hardpan layer. The weathered rocks are covered by 0.5 m of locally transported colluvial material.

### **4. 3. Sampling, bulk mineralogical and chemical composition of the regolith units**

The samples selected by Normandy Mining Ltd for this study come from Rotary Air Blast (RAB) vertical drill holes that overlie ore grade massive sulphide mineralisation. Drill holes SCRB09 and SCRB10 are located directly above the mineralisation, and drill holes SCRB05, SCRB07, SCRB102 and SCRB103 intersect the weathered hanging-wall rocks (Figures 4 and 6). The results of the bulk X-ray diffraction analysis (SIROQUANT, Taylor and Clapp, 1992) are summarized in Table 1. Table 2 gives the location and bulk chemical composition of the samples.

The regolith is poorly differentiated and fresh mineralogical assemblages are still very well represented in the upper horizon. Chlorite remains mainly unweathered in saprolite overlying mineralisation, and ferromagnesian clays, such as corrensite, are abundant in the saprolite developed on the hanging wall rocks.

The chemical data show anomalous concentrations of Sb, In and Bi, as well as Cu, Pb and Zn in some samples, directly up dip from mineralisation, in drill holes SCRB09 and SCRB10, section 22240N. By contrast, samples in drill holes SCRB05, SCRB07, SCRB102 and SCRB103, located further west into the hanging wall lavas, are enriched in Cu, Pb and Zn, but not in Sb, Bi and In. Molybdenum is also associated with the ore although less strongly than Sb, Bi and In.

The oxidised zone is depleted in Mg, Zn and Cu, with almost complete Zn loss over mineralisation on 22240N (Finlay, 1998). The  $\text{Fe}^{2+}$  boundary shows a strong spatial correlation with the logging oxidation-front in the hanging wall sequence. There are also similarities between  $\text{Fe}^{2+}$  and Mg distributions.

Copper, Zn, Pb, Mn and Co contents decrease up the profile over mineralisation and in the hanging wall sequence. Bismuth, In and Sb are concentrated in the top horizons over mineralisation.

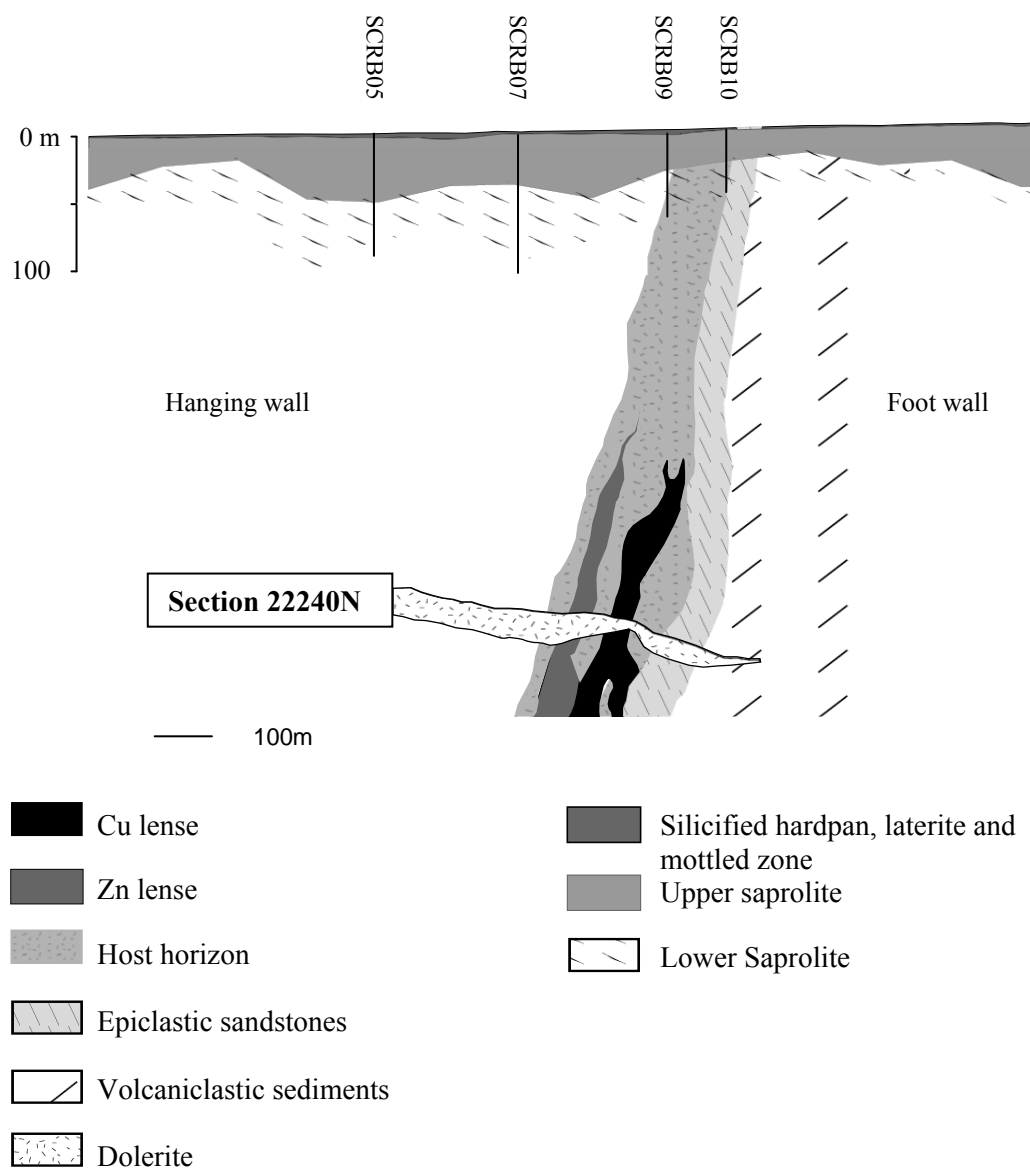


Figure 6. Cross-section along line 22240N showing the regolith stratigraphy and the mineralised horizon (After Finlay, 1998; Normandy Mining Ltd 2000)

Table 1. Quantitative mineralogy (SIROQUANT) of selected samples (%).  
(-: below detection limit)

Drill Holes	Regolith Unit	Depth (m)	Kaolinite	Muscovite	Quartz	Smectite	Chlorite	Corrensite
SCR005	Upper saprolite	14-15	35	13	52	-	-	-
SCR005	Upper saprolite	34-35	33	24	41	-	-	2
SCR007	Lower saprolite	54-55	19	26	48	-	-	7
SCR009	Silicified horizon	1-2	33	35	32	-	-	-
SCR009	Upper saprolite	14-15	23	40	37	-	-	-
SCR010	Upper saprolite	9-10	41	9	50	-	-	-
SCR010	Upper saprolite	14-15	47	45	8	-	-	-
SCR010	Lower saprolite	44-45	18	12	43	-	26	1
SCR0102	Lower saprolite	69-70	35	27	34	-	-	4
SCR0103	Upper saprolite	59-60	24	39	30	7	-	-

Table 2. Location and bulk chemical composition of the Scuddles samples.  
(a) SCRB05, SCRB07, SCRB09, SCRB10. (b) SCRB102; SCRB103.  
(-: below detection limit)

Drill Holes		SCRB005	SCRB005	SCRB007	SCRB009	SCRB009	SCRB010	SCRB010	SCRB010
Samples		579325	579329	579369	579397	579401	579414	579415	579421
Depth (m)		14 – 15	34 – 35	54 – 55	1 – 2	14 – 15	9 – 10	14 – 15	44 – 45
Regolith Unit		Upper saprolite	Upper saprolite	Lower saprolite	Silicified horizon	Upper saprolite	Upper saprolite	Upper saprolite	Lower saprolite
Local grid	Northing	22240.528	22240.528	22240.402	22239.927	22239.927	22239.314	22239.314	22239.314
	Easting	6424.593	6424.593	6520.508	6625.16	6625.16	6665.437	6665.437	6665.437
Bi ppm		0.1	0.1	0.1	0.6	0.4	47.3	2.7	0.4
In ppm		0.05	0.05	0.05	0.40	0.90	0.70	1.30	0.20
Mo ppm		1.1	3.3	4.4	2.1	1.8	0.5	16.2	2.3
Sb ppm		0.5	0.8	1.4	8.6	16.3	5.0	23.5	4.3
Cu ppm		306	1450	521	31	22	15	319	751
Pb ppm		276	816	2320	34	42	43	126	403
Zn ppm		126	1030	105	33	22	26	42	195
Mn ppm		48	871	222	10	9	13	55	578
Co ppm		6.0	21.0	10.0	2.5	2.5	2.5	2.5	9.0
Ni		9.0	29.0	15.0	2.5	2.5	2.5	2.5	14.0
Al %		8.15	7.67	6.08	6.51	6.11	6.60	6.48	5.02
Fe %		5.21	9.09	3.00	0.50	0.24	0.13	3.76	6.62
Ca %		0.03	0.06	0.04	0.01	0.00	0.01	0.00	0.03
K %		0.59	0.66	1.00	0.84	1.50	0.50	0.35	0.56
Mg %		0.19	0.40	0.30	0.07	0.03	0.02	0.02	0.78
Na %		0.06	0.03	0.12	0.10	0.12	0.03	0.02	0.06

Drill Holes		SCRB102	SCRB102	SCRB102	SCRB102	SCRB103	SCRB103	SCRB103	SCRB103
Samples		580856	580857	580861	580870	580874	580875	580879	580885
Depth (m)		4 – 5	9 – 10	29 – 30	69 – 70	4 – 5	9 – 10	29 – 30	59 – 60
Regolith Unit		Laterite	Upper saprolite	Upper saprolite	Lower saprolite	Laterite	Upper saprolite	Upper saprolite	Upper saprolite
Local grid	Northing	21759.268	21759.268	21759.268	21759.268	21759.726	21759.726	21759.726	21759.726
	Easting	6270.041	6270.041	6270.041	6270.041	6321.522	6321.522	6321.522	6321.522
Bi ppm		-	-	-	0.1	-	-	-	-
In ppm		-	-	-	0.05	-	-	-	-
Mo ppm		2.2	0.3	0.6	0.6	0.5	0.8	1.5	0.3
Sb ppm		0.4	0.3	0.4	0.3	0.3	0.2	0.2	0.3
Cu ppm		-	-	130	460	7	-	68	226
Pb ppm		15	11	51	508	13	12	108	547
Zn ppm		16	17	72	547	17	12	18	136
Mn ppm		16	26	38	157	37	17	40	242
Co ppm		-	-	-	15	-	-	-	10
Ni		-	-	-	-	-	-	-	-
Al %		12.66	10.89	9.94	8.16	9.48	8.94	6.05	9.79
Fe %		0.51	1.05	3.03	1.82	0.67	0.68	3.10	2.23
Ca %		0.01	-	0.01	0.01	0.01	0.01	-	0.04
K %		1.07	1.05	1.23	0.93	0.98	0.83	0.97	0.92
Mg %		0.19	0.38	0.27	0.44	0.28	0.25	0.21	0.46
Na %		0.03	0.05	0.02	0.03	0.06	0.05	0.04	0.05

## 5. MINERALOGY AND CHEMISTRY OF THE REGOLITH UNITS

### 5. 1. Lower saprolite

#### 5. 1. 1. Hanging wall

Two lower saprolite samples have been selected inside the hydrothermal alteration halo. Samples SCRB07 (54-55m) and SCRB102 (69-70m) are located about 100 m west and about 200 m south-west of the main Scuddles orebody respectively.

The material is yellow to pale yellow (2.5Y 8/6 to 2.5Y 8/2) and is composed of hydrothermal quartz, muscovite, kaolinite, corrensite and accessory ilmenite. The chemical composition of the lower saprolite minerals is given in Tables 3 and 4.

The clay fraction (<2 µm) contains kaolinite, mica and two types of corrensite: a low-charge corrensite and a high-charge corrensite (Figures 7A and 7B). Plumbogummite is also present in the clay fraction of sample SCRB07. Small quantities of gibbsite are present in the < 0.2 µm fraction.

#### *Mica*

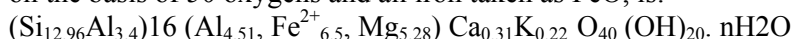
The mica, a muscovite with up to 4.9% FeO, occurs as large booklets often partially altered into kaolinite-mica intergrades.

#### *Corrensites*

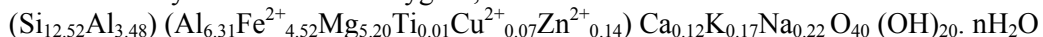
The low-charge corrensite is an expandable regular mixed-layered chlorite/smectite. The high-charge corrensite is a non-expandable regular interstratified chlorite/vermiculite. They are differentiated by their responses to ethylene-glycol solvation: the chlorite/vermiculite does not expand (002 reflection remains at 14 Å). The X-ray diffraction pattern of the heated material (Figure 7A) indicates the presence of two types of low-charge corrensite, one with a chlorite/smectite ratio close to 1, and another less abundant with a chlorite/smectite ratio >1. Two types of high-charge corrensites are also present, one with a high chlorite content and one with a chlorite/vermiculite close to 1 (Figure 7B).

Corrensite is a common alteration product of chlorite, either in supergene or low temperature hydrothermal systems. The low-charge corrensite contains a high iron level (FeO ~ 20%), suggesting that the primary chlorite is a brunsvigite-diabantite.

The average structural formula of a low-charge corrensite with a chlorite/smectite ratio of 1, calculated on the basis of 50 oxygens and all iron taken as FeO, is:



The average structural formula of the high-charge corrensite with an equal number of chlorite and vermiculite layers based on 50 oxygens, total Fe calculated as Fe<sup>2+</sup> is:



Copper and zinc are present in the high-charge corrensite (up to 2% ZnO, <1% CuO), probably in the vermiculite interlayers. Copper and Zn are not incorporated into kaolinite during corrensite weathering, but are released into the microenvironment.

#### *Kaolinite*

Kaolinite can constitute as much as 35% of the bulk sample. It results from the weathering of muscovite and corrensite. SEM observations show that large booklets of corrensite are partially replaced by packs of kaolinite layers (Figure 8A). Kaolinite contains very little iron (<1%) and does not inherit the corrensite Cu and Zn.



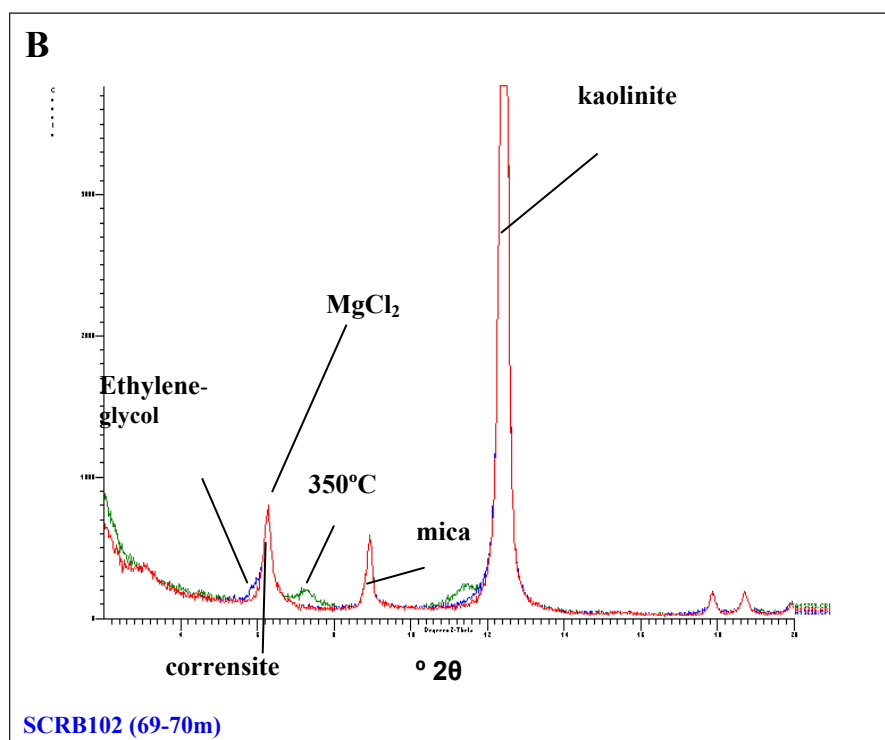
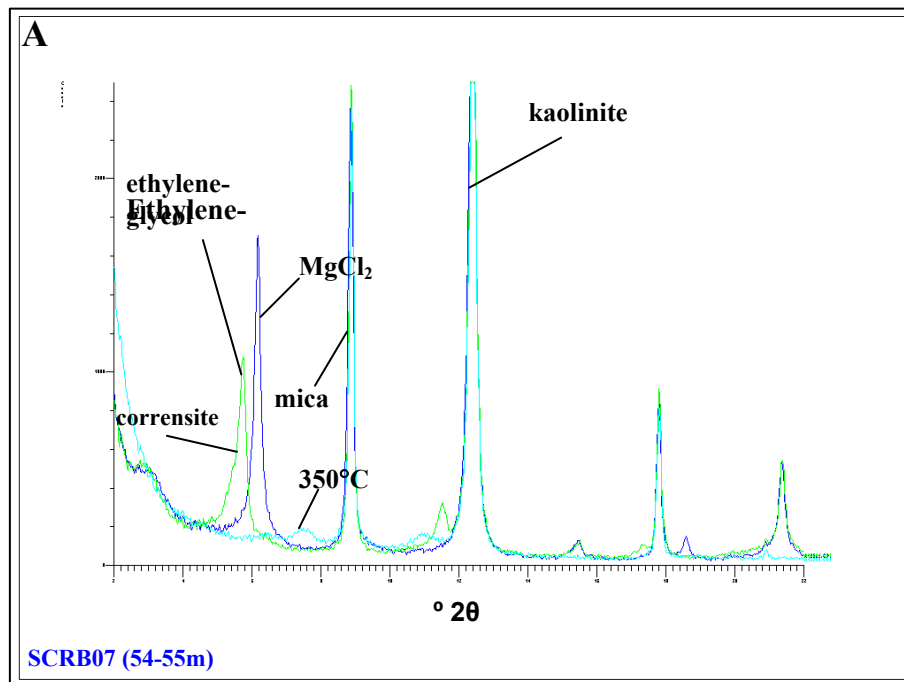


Figure 7. XRD diffraction patterns of the lower saprolite clay fractions.  
A. Low-charge corrensite. B. High-charge corrensite.

Table 3. Microprobe analyses (%) of the clays in the lower saprolite.

High-charge corrensite: chl/ver; low-charge corrensite: chl/smec; intergrades kaolinite-corrensite: kaol/corr; intergrades kaolinite-mica: kaol/mica. (-: below detection limit).

Analyses	Wt%	SiO <sub>2</sub>	Al <sub>2</sub> O <sub>3</sub>	FeO	MgO	CaO	K <sub>2</sub> O	Na <sub>2</sub> O	CuO	ZnO	Total
1 (SCRB102)	Chl/ver	36.6	26.3	11.2	7.74	0.34	0.31	0.39	-	-	82.88
2 (SCRB102)	Chl/ver	35.4	23.1	15.0	9.61	0.50	0.00	0.87	-	-	84.48
3 (SCRB102)	Chl/ver	33.0	19.8	18.1	12.49	0.50	0.62	0.53	-	-	85.04
4 (SCRB102)	Chl/ver	33.5	22.1	16.7	10.69	0.21	0.53	0.49	-	-	84.22
5 (SCRB102)	Chl/ver	35.8	24.5	11.1	6.85	0.39	0.16	0.00	0.61	1.09	80.50
6 (SCRB102)	Chl/ver	32.9	20.5	17.1	11.10	0.35	0.33	0.54	-	-	82.82
7 (SCRB102)	Chl/ver	33.4	21.1	15.5	10.2	0.35	0.12	-	0.93	2.13	83.73
8 (SCRB102)	Chl/ver	36.0	25.8	15.2	9.14	-	1.23	-	-	-	87.37
9 (SCRB102)	Chl/ver	32.6	21.9	13.5	8.30	0.22	-	-	0.68	1.46	78.66
10 (SCRB102)	Kaol/corr	31.3	22.5	5.3	2.81	-	-	0.84	-	-	62.75
11 (SCRB102)	Kaol/corr	43.1	34.5	2.5	1.05	-	-	0.75	-	-	81.90
12 (SCRB102)	Kaol/corr	43.5	34.8	1.3	0.93	-	-	0.74	-	-	81.27
13 (SCRB102)	Kaol/corr	29.4	22.0	1.4	1.06	-	-	-	-	-	53.86
14 (SCRB102)	Kaol/corr	33.2	24.5	8.4	4.55	0.14	-	-	-	0.77	71.56
15 (SCRB07)	Chl/smec	31.2	16.3	19.0	8.15	0.48	0.47	-	-	-	75.60
16 (SCRB07)	Chl/smec	33.0	17.1	20.6	9.23	0.49	0.79	-	-	-	81.21
17 (SCRB07)	Chl/smec	34.9	17.3	19.7	9.53	0.94	0.29	-	-	-	82.66
18 (SCRB07)	Chl/smec	33.1	17.8	20.1	9.25	1.06	0.24	-	-	-	81.55
19 (SCRB102)	Kaolinite	36.2	28.9	1.2	-	-	-	0.36	-	-	66.66
20 (SCRB102)	Kaolinite	42.3	34.5	0.7	-	-	-	0.57	-	-	78.07
21 (SCRB102)	Kaolinite	44.2	35.6	0.7	-	-	-	-	-	-	80.50
22 (SCRB102)	Kaolinite	35.8	28.8	0.4	-	-	-	-	-	-	65.00
23 (SCRB102)	Kaolinite	38.3	30.3	0.6	-	-	-	-	-	-	69.20
24 (SCRB102)	Kaolinite	42.2	34.0	0.3	-	-	-	-	-	-	76.50
25 (SCRB102)	Kaolinite	44.1	35.6	0.9	-	-	-	-	-	-	80.60
26 (SCRB102)	Kaolinite	44.0	36.0	0.5	-	-	-	-	-	-	80.50
27 (SCRB102)	Kaolinite	44.8	36.3	0.7	-	-	-	-	-	-	81.80
28 (SCRB102)	Kaolinite	45.0	36.8	0.4	-	-	-	-	-	-	82.20
29 (SCRB102)	Mica	48.8	26.3	4.9	2.71	-	9.97	-	-	-	92.68
30 (SCRB102)	Mica	48.4	29.0	4.1	2.46	-	10.64	0.87	-	-	95.47
31 (SCRB102)	Kaol/mica	46.0	37.7	0.7	-	-	2.22	-	-	-	86.62

Table 4. Microprobe analyses (%) of the Mn-oxides and associated minerals in the lower saprolite.  
Coronadite+Ti: coronadite + ilmenite; Coronadite+Pl: coronadite + plumbogummite;  
Pl+goethite: plumbogummite + goethite; Goethite + Si: goethite + Si-rich phase;  
coronadite+Al: coronadite + lithiophorite. (-: below detection limit).

Analyses	Mineralogy	SiO <sub>2</sub>	Al <sub>2</sub> O <sub>3</sub>	Fe <sub>2</sub> O <sub>3</sub>	TiO <sub>2</sub>	P <sub>2</sub> O <sub>5</sub>	Fe <sub>2</sub> O <sub>3</sub>	MnO <sub>2</sub>	CoO	K <sub>2</sub> O	CuO	PbO	CeO <sub>2</sub>	Total
SCRB102-1	Coronadite	4.1	0.4	5.1	1.34	-	5.06	44.04	-	-	1.55	32.68	-	94.27
SCRB102-2	Coronadite	4.0	0.5	5.7	1.81	-	5.65	43.78	-	-	1.45	35.50	-	98.39
SCRB102-3	Coronadite	4.7	0.5	5.4	1.80	-	5.69	46.34	-	-	1.35	34.17	-	99.95
SCRB102-4	Coronadite	3.8	0.3	7.0	1.27	-	7.03	40.92	-	-	1.59	34.57	-	96.48
SCRB102-5	Coronadite	4.2	0.4	6.5	1.53	-	6.45	40.9	-	-	1.31	34.53	-	95.82
SCRB102-6	Coronadite+Ti	3.9	0.4	9.5	1.90	-	9.52	39.5	-	-	1.91	33.36	-	99.99
SCRB102-7	Coronadite+Ti	2.4	0.4	9.1	4.8	-	9.12	38.68	-	-	2.61	32.97	-	100.08
SCRB102-8	Coronadite+Ti	2.2	0.2	9.7	1.80	-	9.68	39.43	-	-	2.73	34.18	-	99.92
SCRB102-9	Coronadite+Ti	2.3	0.0	8.9	3.97	-	8.92	39.66	-	-	2.57	33.68	-	100.00
SCRB102-10	Coronadite+clays	6.6	1.9	7.0	0.82	-	7.01	42.01	-	-	1.34	31.81	-	98.49
SCRB102-11	Coronadite+clays	8.4	3.9	6.2	0.54	-	6.24	40.14	-	-	1.15	30.65	-	97.22
SCRB102-12	Coronadite+clays	12.0	7.4	6.1	0.43	-	6.13	35.98	-	-	1.06	27.82	-	96.92
SCRB07-1	Coronadite	1.1	0.6	1.9	-	-	-	56.43	-	-	1.41	35.61	-	97.05
SCRB07-2	Coronadite	1.1	0.6	1.5	-	-	-	54.98	0.91	-	0.81	35.44	-	95.34
SCRB07-3	Coronadite	1.9	0.5	3.8	-	-	-	51.21	-	-	0.75	35.89	-	94.05
SCRB07-4	Coronadite	1.2	0.4	3.1	-	-	-	50.61	1.11	-	0.81	35.16	-	92.39
SCRB07-5	Coronadite	1.8	2.6	2.9	-	1.46	-	47.67	0.53	-	0.75	35.47	-	93.18
SCRB07-6	Coronadite	1.7	3.5	4.1	-	2.59	-	40.59	0.90	-	0.93	35.82	0.83	90.96
SCRB07-7	Coronadite+clays	3.2	3.5	4.8	-	1.57	-	41.81	1.03	-	0.97	35.17	-	92.05
SCRB07-8	Coronadite+clays	3.2	3.1	4.2	-	0.76	-	44.35	1.41	-	0.66	35.95	-	93.63
SCRB07-9	Coronadite+clays	1.8	1.0	5.7	-	-	-	46.89	0.99	-	0.99	36.44	0.52	94.33
SCRB07-10	Coronadite+clays	4.4	6.4	4.3	-	2.80	-	37.86	0.92	-	1.20	35.92	-	93.80
SCRB07-11	Coronadite+clays	5.0	5.0	3.8	-	-	-	40.85	0.74	-	0.88	34.34	-	90.61
SCRB07-12	Coronadite+clays	3.8	4.1	3.4	-	1.55	-	44.60	0.64	-	-	33.89	-	91.98
SCRB07-13	Coronadite+clays	6.0	4.1	4.0	-	2.03	-	40.46	1.25	-	0.70	34.87	-	93.41
SCRB07-14	Coronadite+clays	4.6	5.6	5.6	-	2.08	-	37.24	0.79	-	0.94	33.65	-	90.50
SCRB07-15	Coronadite+clays	4.4	5.3	4.9	-	2.02	-	37.65	0.88	-	0.99	34.27	-	90.41
SCRB07-16	Coronadite+clays	19.6	16.4	5.0	-	-	-	24.53	0.76	-	0.68	22.58	-	89.55
SCRB07-17	Coronadite+Pl	1.8	6.8	4.1	-	4.85	-	35.60	0.78	-	1.22	37.41	-	92.56
SCRB07-18	Coronadite+Pl	2.6	7.0	4.0	-	4.66	-	34.15	0.82	-	0.97	35.34	-	89.54
SCRB07-19	Coronadite+Pl	0.7	10.6	7.9	-	9.77	-	16.55	0.44	-	1.16	37.88	-	85.00
SCRB07-20	Coronadite+Pl	0.7	9.1	8.6	-	8.57	-	20.49	-	-	1.07	37.33	-	85.86
SCRB07-21	Coronadite+Pl	2.3	10.3	6.6	-	7.75	-	23.43	0.64	-	0.90	36.10	-	88.02
SCRB07-22	Pl+goethite	-	8.7	21.3	-	13.95	3.78	-	-	-	1.04	36.15	-	84.92
SCRB07-23	Pl+goethite	-	15.9	10.5	-	15.53	-	-	-	-	-	37.57	-	79.50
SCRB07-24	Pl+goethite	-	16.8	9.5	-	15.20	-	-	-	-	0.67	38.56	-	80.73
SCRB07-25	Pl+goethite	-	16.8	9.1	-	15.46	-	-	-	-	-	37.01	-	78.37
SCRB07-26	Pl+goethite	5.1	16.4	12.9	-	10.96	4.72	-	-	1.04	0.69	24.03	0.81	76.65
SCRB07-27	Goethite+ Si	27.8	1.9	55.5	-	0.99	-	-	-	-	1.46	1.01	-	88.66
SCRB07-28	Goethite+ Si	13.3	3.0	60.3	-	1.01	-	-	-	-	2.03	1.11	-	80.75
SCRB07-29	Goethite+ Si	10.3	3.0	62.2	-	1.08	-	-	-	-	2.11	1.11	-	79.80
SCRB07-30	Coronadite+Al	1.6	9.8	17.0	-	-	-	38.07	4.51	-	2.33	11.93	-	85.24

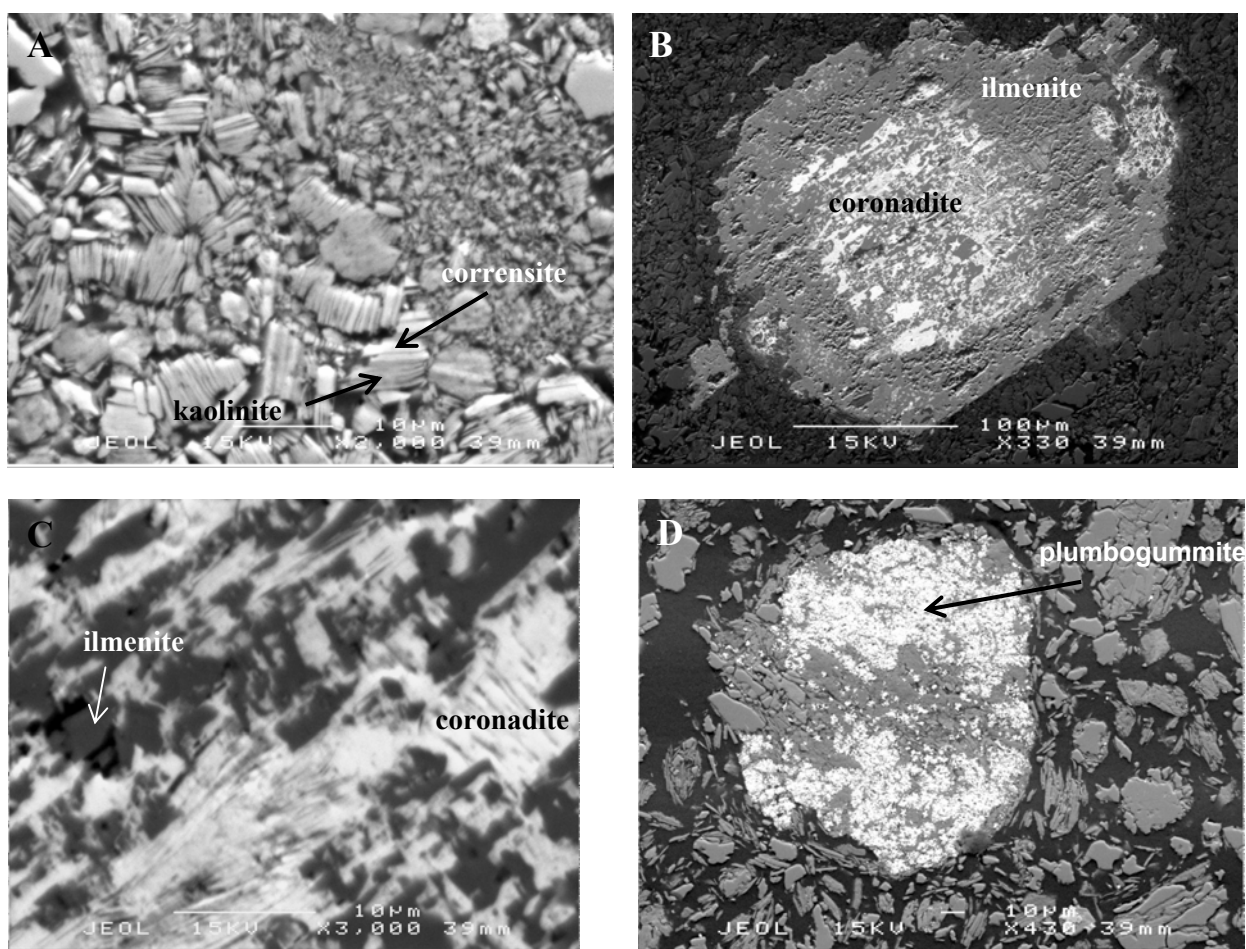


Figure 8. SEM micrographs (backscattered electron image). A. Weathering of corrensite to kaolinite. B. Coronadite nodule surrounded by a halo of tornebohmite. C. Coronadite replacing ilmenite. D. Plumbogummite accumulation.

#### *Quartz*

The quartz content of the samples varies with the degree of hydrothermal silification of the volcanic rocks. Sample SCRB07 consists of almost 50% quartz whereas SCRB102 contains 34% quartz. Some crystals present micrometric inclusions of Ti-rich mineral containing up to 9% PbO (Normalised wt% oxides= TiO<sub>2</sub>: 75%; PbO: 9.2%; Al<sub>2</sub>O<sub>3</sub>: 4.3%; SiO<sub>2</sub>: 7.5%; FeO: 4%).

#### *Ilmenite*

Primary ilmenite grains are commonly partially replaced by Mn oxides (Figures 8B and 8C). The non-altered ilmenite show various degrees of supergene alteration into anatase.

#### *Manganese oxides and plumbogummite*

The lower saprolite contains abundant millimetric brownish granules of Mn oxides (corodanite Pb<sub>2</sub>Mn<sub>8</sub>O<sub>16</sub>. nH<sub>2</sub>O) that partially replace clays, Ti-minerals and coat the quartz grains (Figures 8B and 8C). Coronadite is a Mn-oxide of the cryptomelane-hollandite-coronadite group characterised by a tunnel structure where MnO<sup>6</sup> octahedra form a framework with tunnels running through. Large cations and water molecules occupy the tunnels.

The general structural formula of these oxides is A<sub>0-2</sub> (B+Mn<sup>4+</sup>)<sub>8</sub>O<sub>16</sub>. xH<sub>2</sub>O. The A cations are K in cryptomelane, Ba in hollandite and Pb in coronadite. There is a wide range of chemical composition due to substitutions of Mn<sup>4+</sup> by di- and trivalent cations B to achieve charge balance, and to adsorption of ions on the surface of the oxides.

The chemical composition of coronadite varies with the distance from the mineralisation (Table 4). In sample SCRB102, the average chemical composition of the coronadite is 43% MnO<sub>2</sub>, 34% PbO and 6% Fe<sub>2</sub>O<sub>3</sub>. Most of the Mn oxides replace ilmenite crystals, thus explaining the high level of Ti (up to 2.2% TiO<sub>2</sub>). Copper (up to 2.7% CuO) has been detected in all areas probed.

In sample SCRB07, located closer to the Main Lens, “pure” coronadite is generally found in close association with plumbogummite, minor plumbojarosite and clays (Figure 8D). The average MnO<sub>2</sub> and PbO contents of the “purest” coronadite are 50.2% and 35.6% respectively. Copper is present with an average level of 0.9% CuO (up to 1.4% CuO). Cobalt is generally detected wherever coronadite is present (up to 1.4% CoO). Transmission electron microscopy observations have established that some Co occurs as lithiophorite domains included in coronadite (Figure 14C). Goethite is associated with plumbogummite or with a silica-rich phase (probably quartz microcrystals or amorphous silica). In both cases, Co is not detected indicating that neither plumbogummite nor goethite contains Co. The mixture goethite-silica bears as much as 2.1% CuO.

### **5. 1. 2. Over the mineralisation**

The lower saprolite over the mineralisation is very thin. The bulk sample (SCRB10, 44-45m) is light reddish brown (5YR 6/4, Munsell color charts), and consists of quartz (43%), Fe-rich chlorite (26%), kaolinite (18%), muscovite (12%) and corrensite (1%).

The X-ray diffraction analysis of the clay fraction indicates that the interstratified clay mineral is a regular interstratified chlorite/vermiculite mineral (high-charge corrensite), which results from the weathering of Fe-rich chlorite.

#### *Sulphide relicts*

The sample contains numerous relicts of mineralised material which have been pseudomorphosed by goethite and hematite. Quartz crystals contain inclusions of euhedral pyrite grains, about 20 µm across, pseudomorphed by Fe oxides. The sulphides have been dissolved, and the cavities filled or lined with colloform Fe oxides, resulting in a micro-boxwork texture characteristic of gossans (Figure 9A). Some Cu released by the sulphide weathering has been preferentially incorporated into goethite.

#### *Ferruginised saprolite*

Ferruginised chips of parent-rock are present as submillimetric to millimetric grains and display a skeletal morphology (Figure 9B). The SEM micrograph in Figure 9C shows a chlorite remnant surrounded by alternating bands of Fe oxides of slightly different goethite/hematite ratios. Copper is preferentially hosted in goethite with up to 4.4% CuO, whereas it does not exceed 1.3% in the more hematitic bands (Table 5). Lead displays a slight preference for hematite.

#### *Manganese oxides (Figure 9D)*

##### Hollandite-coronadite-cryptomelane series

Two populations have been identified: coronadite Pb<sub>2</sub>Mn<sub>8</sub>O<sub>16</sub>. nH<sub>2</sub>O and oxides of the coronadite-hollandite series with an intermediate composition (Pb, Ba)<sub>2</sub>Mn<sub>8</sub>O<sub>16</sub>. nH<sub>2</sub>O). Coronadite contains average MnO<sub>2</sub> and PbO concentrations of 58.3% and 28.4% respectively, up to 3.4% CuO, up to 1.6% CoO and 1% V<sub>2</sub>O<sub>5</sub> (Table 6). Lead and Ba equally share the sites in the tunnels of the structure of coronadite-hollandite, with average concentrations of 8% BaO and 9% PbO. Coronadite-hollandite hosts up to 2.3% CuO and 1% ZnO.

##### Lithiophorite

Lithiophorite occurs as large and homogeneous areas containing Co (up to 2.7% CoO), Cu (up to 3.5% CuO), Ni (up to 1.3% NiO) and Zn (up to 1.5% ZnO), and possibly as microdomains in coronadite (Table 6).

### *Hematite-Goethite*

Large areas of the chip imaged in Figure 9D are replaced by goethite associated with coronadite. Goethite contains up to 0.8% of CuO.

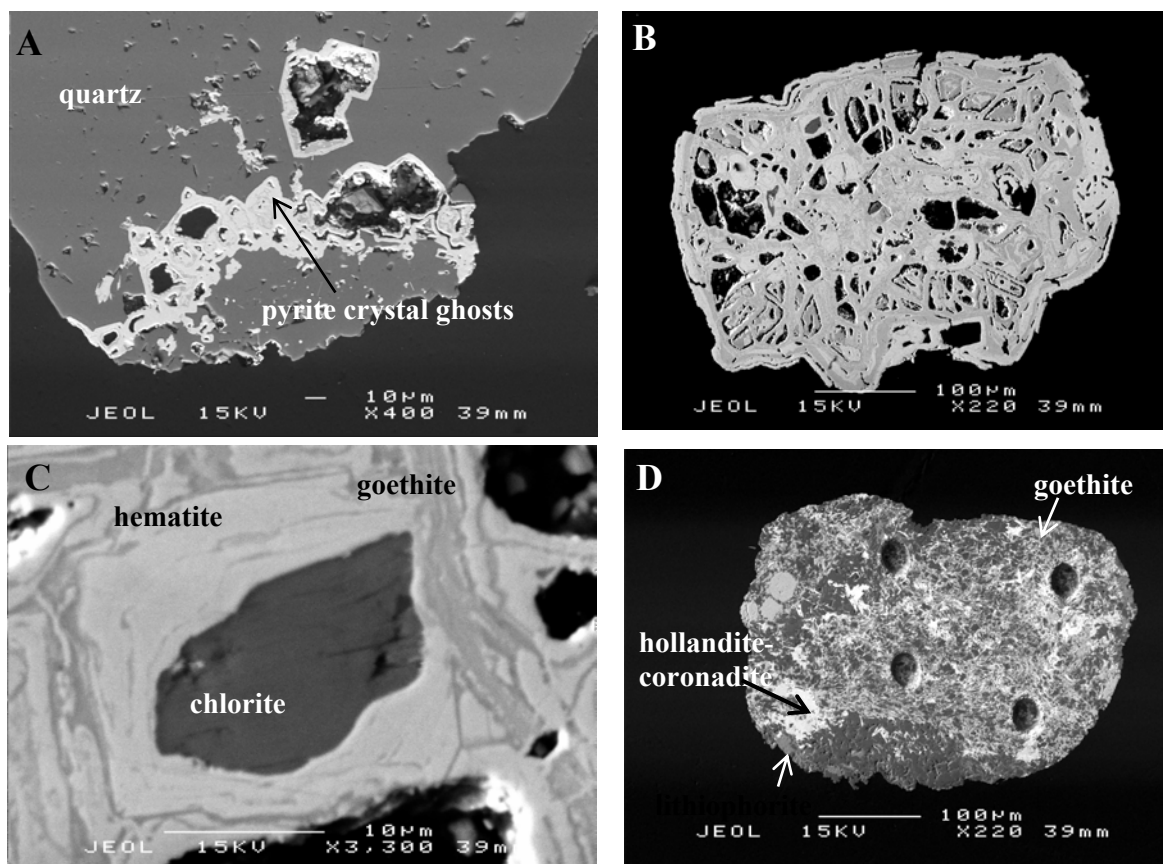


Figure 9. SEM micrographs (backscattered electron image). A. Pyrite crystals pseudomorphosed by Fe oxides in a quartz grain. B and C. Ferruginised saprolite with chlorite relict. D. Saprolite partially replaced by Mn and Fe oxides (the craters are laser ablation holes).

Table 5. Microprobe analyses (%) of the Fe oxides in the lower saprolite.  
(-: below detection limit)

Analyses	Mineralogy	SiO <sub>2</sub>	Al <sub>2</sub> O <sub>3</sub>	Fe <sub>2</sub> O <sub>3</sub>	CuO	PbO	Total
1	Goethite	2.5	2.0	78.3	2.20	0.67	85.67
2	Goethite	3.5	2.5	77.8	2.26	-	86.06
3	Goethite	5.0	4.5	69.6	4.45	-	83.55
4	Goethite	5.3	5.4	65.1	3.94	-	79.74
5	Goethite	4.8	4.8	65.4	3.98	-	78.98
6	Goethite	5.0	4.3	68.6	4.01	0.41	82.32
7	Goethite-hematite	2.4	1.5	85.9	1.17	0.59	91.56
8	Goethite-hematite	2.4	1.6	85.5	1.28	0.55	91.33
9	Goethite-hematite	2.3	1.7	87.8	0.91	0.64	93.35
10	Goethite-hematite	2.6	2.3	84.5	1.39	-	90.79
11	Goethite-hematite	2.0	1.5	87.9	0.70	0.60	92.70
12	Goethite-hematite	2.0	1.6	86.5	0.57	0.54	91.21

Table 6. Microprobe analyses (%) of the Mn-oxides and associated minerals in the lower saprolite.  
(-: below detection limit)

Analyses	Mineralogy	SiO <sub>2</sub>	Al <sub>2</sub> O <sub>3</sub>	Fe <sub>2</sub> O <sub>3</sub>	MnO <sub>2</sub>	CoO	CuO	NiO	BaO	PbO	ZnO	V <sub>2</sub> O <sub>5</sub>	Total
1	Ba-Pb Mn oxide	0.3	1.4	1.4	69.53	-	1.84	-	7.88	9.49	-	-	91.84
2	Ba-Pb Mn oxide	0.4	1.4	2.3	67.96	-	1.80	-	8.19	6.80	1.05	-	89.90
3	Ba-Pb Mn oxide	0.4	1.0	1.7	67.60	-	1.88	-	7.06	11.54	-	-	91.18
4	Ba-Pb Mn oxide	0.4	1.5	0.8	70.70	-	2.32	-	8.76	8.32	-	-	92.80
5	Ba-Pb Mn oxide + goethite	3.5	3.8	17.5	48.72	-	-	-	3.46	11.09	-	-	88.07
6	Coronadite	1.1	2.2	1.2	57.56	-	3.25	-	-	28.63	-	0.63	94.57
7	Coronadite	0.5	1.7	0.6	56.67	-	3.19	-	-	28.78	-	0.65	92.09
8	Coronadite	0.7	2.2	0.7	58.46	-	2.36	-	-	28.97	-	0.83	94.22
9	Coronadite	0.7	1.9	3.8	56.48	-	2.10	-	-	29.40	-	0.75	95.13
10	Coronadite	1.2	1.8	5.2	54.82	-	2.29	-	-	28.94	-	0.49	94.74
11	Coronadite	2.1	2.0	10.8	49.24	-	1.35	-	-	25.61	-	0.45	91.55
12	Coronadite	0.7	1.5	4.1	56.15	-	2.00	-	-	28.86	-	0.82	94.13
13	Coronadite	0.5	1.1	-	59.34	-	2.75	-	-	29.43	-	1.08	94.20
14	Coronadite	0.6	1.2	-	59.47	-	2.23	-	-	29.41	-	1.01	93.92
15	Coronadite	0.4	0.8	-	59.01	-	2.38	-	-	30.30	-	1.04	93.93
16	Coronadite	0.7	1.5	-	59.10	-	3.42	-	-	28.52	-	1.01	94.25
17	Coronadite	1.0	2.5	-	56.80	-	2.99	-	-	27.27	-	0.60	91.16
18	Coronadite	2.7	2.2	10.3	48.63	-	1.13	-	-	25.61	-	-	90.57
19	Coronadite + (lithiophorite ?)	0.6	1.9	1.2	61.17	1.25	2.01	-	1.04	22.89	-	-	92.06
20	Coronadite + (lithiophorite ?)	0.8	3.0	3.3	56.93	1.59	2.20	-	0.63	24.16	-	-	92.61
21	Coronadite + (lithiophorite ?)	2.8	4.2	4.8	53.00	1.11	1.60	-	-	25.66	-	-	93.17
22	Coronadite + (lithiophorite ?)	4.5	4.0	7.7	48.80	0.64	1.46	-	-	25.52	-	-	92.62
23	Coronadite + hollandite	3.5	5.7	7.4	53.38	-	0.91	-	3.13	12.34	-	-	86.36
24	Coronadite	1.8	3.0	8.2	55.07	-	1.57	-	0.89	23.22	-	-	93.75
25	Coronadite	3.3	5.0	4.0	56.85	-	1.49	-	0.87	21.85	-	-	93.36
26	Lithiophorite	6.7	18.9	-	45.91	2.72	3.24	1.27	-	-	1.49	-	80.23
27	Lithiophorite	8.7	19.1	-	48.32	1.13	3.46	0.86	-	-	1.20	-	82.77
28	Coronadite+goethite+ lithiophorite	3.0	3.8	18.1	42.04	2.33	1.57	-	-	18.66	-	-	89.50
29	Coronadite+goethite+ lithiophorite	3.5	4.6	10.7	45.86	2.42	1.86	-	-	21.57	-	-	90.51
30	Coronadite+goethite+ lithiophorite	3.8	2.9	17.8	43.96	0.49	1.06	-	-	21.96	-	-	91.97
31	Fe oxides + coronadite	2.5	2.1	84.7	1.66	-	0.68	-	-	0.50	-	-	92.14
32	Fe oxides + coronadite	6.4	3.9	78.8	1.81	-	-	-	-	-	-	-	90.91
33	Fe oxides + coronadite	2.9	1.9	82.2	2.84	-	0.65	-	-	0.36	-	-	90.85
34	Fe oxides + coronadite	2.2	1.3	83.5	1.34	-	0.69	-	-	0.68	-	-	89.71
35	Fe oxides + coronadite	2.2	1.6	83.0	1.52	-	0.72	-	-	0.53	-	-	89.57
36	Fe oxides + coronadite	2.1	3.7	80.8	3.38	-	0.87	-	-	1.18	-	-	92.03

## 5. 2. The upper Saprolite

### 5. 2. 1. *Hanging wall*

Two samples of upper saprolite were selected: SCRB05 (34-35 m) and SCRB103 (59-60m), located about 200 m West and South West of the main orebody. Sample SCRB103 is uniformly pale yellow (2.5Y 8/4, Munsell Soil Color Chart) and consists mainly of muscovite (39%), kaolinite (24%), quartz (30%) and smectites (7%). Sample SCRB05 is reddish yellow (7.5YR 6/6) and contains harder chips showing variegated bands (grey, yellow and red). The bulk sample is composed of quartz (41%), kaolinite (33%), muscovite (24%) and corrensite (2%).

#### *Clays*

The clay fraction extracted from sample SCRB103 comprises abundant kaolinite, smectites, mica, minor chlorite and possibly a smectite/kaolinite interstratified mineral. The chemical composition (EDAX) of the different clays is given in Table 7. The smectite is a nontronite (High Fe and low Mg contents) and is probably the weathering product of a low-charge corrensite.

The X-ray analysis of the clay fraction extracted from sample SCRB05 indicates a low-charge corrensite or regular interstratified chlorite/smectite mineral (Figure 10). The heat treatment indicates two types of corrensite, one with a chlorite/smectite ratio close to 1 and another containing more chlorite layers than smectites layers. The corrensite is Fe rich (>20% FeO) and contains copper (Table 8).

Fresh mica booklets are rare as they are partially altered to kaolinite (intergrades kaolinite/mica). The Pb and Mn in some analyses represent coronadite microcrystals. Analytical electron microscopy of kaolinite indicates substantial amounts of cerium as cerianite inclusions.

The major change occurring in this horizon is a local ferruginisation of the material. The backscattered electron image of Figures 11A and 11B show scattered concentrations of goethite and a large corrensite booklet partially replaced by kaolinite and goethite.

#### *Ilmenite*

Ilmenite has undergone two types of alteration by fluids rich in base metals (Figures 12A and 12B). Some ilmenite grains are partially replaced by coronadite (Pb-Mn oxide), and others by a Zn-rich oxide belonging to the ilmenite-ecandrewsite serie, with  $\text{Zn}^{2+}$  and  $\text{Mn}^{2+}$  substituting for  $\text{Fe}^{2+}$  (up to 7.7% ZnO). This type of alteration has only been observed in sample SCRB05.

#### *Manganese oxides and associated minerals*

The chemistry of the manganese oxides and associated minerals depends on the distance from the ore deposit.

#### Away from the mineralisation (SCRB103)

Small spheres similar to the one shown in Figure 12A are abundant in this sample. The nodules include an ilmenite crystal with surrounding minerals impregnated with coronadite. The nodule is encircled by a halo of scattered Ce-Al silicate grains which have been identified as tornebohmite-(Ce). Yttrium has also been detected in the tornebohmite-Ce. Coronadite coats quartz grains (Figures 12C and 12D) and replaces clays. Coronadite occurs as micrometric globules and ill-defined hexagons, and occasionally shows dissolution pits indicators of ongoing chemical reactions (Figure 12C). Transmission electron microscopy shows coronadite replacing clays along cleavages (Figure 12F), and that the reaction locally retains some of the clay micromorphology such as cleavages (Figure 12E). The Pb-Mn oxides have a grainy texture, and consist of randomly oriented particles 50 to 100 nm in size. Selected area electron diffraction patterns (SAED) show diffuse rings indicating the coronadite is poorly crystalline.

The Mn oxides contain an average of 43.3%  $\text{MnO}_2$ , 28.4% PbO and 12.0%  $\text{Fe}_2\text{O}_3$  (Table 9). The high Fe content indicates that  $\text{Fe}^{3+}$  is the dominant cation substituting for  $\text{Mn}^{4+}$  in the framework. The silica content is quite high and varies from 5.6 to 8.3%, and the alumina content from 0.6 to 1.1%. The



Analytical Electron Microscopy (AEM) data indicate the presence of Si and Al in various proportions even in areas without visible clay layers, suggesting that some Si and Al are located in coronadite. Aluminium can substitute for  $Mn^{4+}$  in the tunnel walls and Si might be absorbed at the surface of the oxides. Cerium has been detected in a few AEM spectra (Figure 13), and probably occurs as cerianite microdomains. The Cu grid is responsible for the Cu signal on this spectrum). Copper has not been detected in this sample located about 200m SW of the main Lens.

The replacement of mica or kaolinite by coronadite involves a complete dissolution of the clays and precipitation of the oxides with important element transfers: leaching of Al, Si and K and introduction of Mn, Pb and Fe into the alteration site. Some of the elements released by the dissolution of the clays remain at the reaction site and are incorporated in the Mn oxides.

#### Closer to the mineralisation (SCRB05)

The Mn oxides are very abundant in this sample (Figure 14A). The average coronadite contains 55.6%  $MnO_2$ , 27.0% PbO and 6.6%  $Fe_2O_3$  (Table 10). The Fe content varies from nil to 15.5%  $Fe_2O_3$  and correlates negatively with the  $MnO_2$  content, suggesting that most of Fe substitutes for  $Mn^{4+}$  in the structure of the oxides. Silica content does not exceed 1.5%, and Cu is abundant (up to 3.2% CuO). Up to 2.1% CoO is present in the oxides. Cerium (up to 2.2%  $CeO_2$ ) is detected in 7 analyses. The presence of Ba in some analyses (up to 2.4% BaO) is related to a lower Pb content suggesting an occasional shift of composition towards the hollandite pole.

Coronadite is locally associated with lithiophorite (Figure 14B) which contains up to 7.6% CoO and more copper than coronadite (up to 5.6% CuO). The TEM observations show that lithiophorite occurs as high contrasted domains about 150 nm across surrounded by grainy coronadite (Figure 14C). The AEM spectrum acquired on an area about 80 nm in diameter confirm that lithiophorite contains Co (Figure 15). The grid supporting the samples is partially responsible for the Cu signal.

#### *Al-goethite*

Aluminous goethite is also associated with coronadite (Figure 14D). The Fe oxide contains up to 1.3% ZnO, but no Cu or Co.

#### *Cerianite*

Cerium-rich microdomains similar to the ones observed in sample SCRB103 are scattered in coronadite (Table 10).

### **5. 2. 2. Over mineralisation**

The top of the upper saprolite is intensively silicified and weakly weathered. The bright white material contains up to 50% quartz, depending on the degree of hydrothermal silification. Some mica remains unaltered (up to 40%), and kaolinite is locally abundant (up to 40% in SCRB10).

The X-ray diffraction analysis of the clay fraction reveals the presence of a very small amount of an irregular chlorite-vermiculite interstratified mineral. The upper saprolite locally displays Fe-rich concretions, which are commonly banded. They mainly consist of aggregations or small balls (<2  $\mu m$ ) of microcrystalline kaolinite associated with goethite (Figure 17A).

The SEM observations show that the clay material consists of clusters of kaolinite and partially weathered mica booklets, 0.5 to 50  $\mu m$  thick. The large books display an intercalation of straight mica layers with slightly exfoliated kaolinite layers (Figure 16B). Kaolinite does not contain any iron (Table 11).

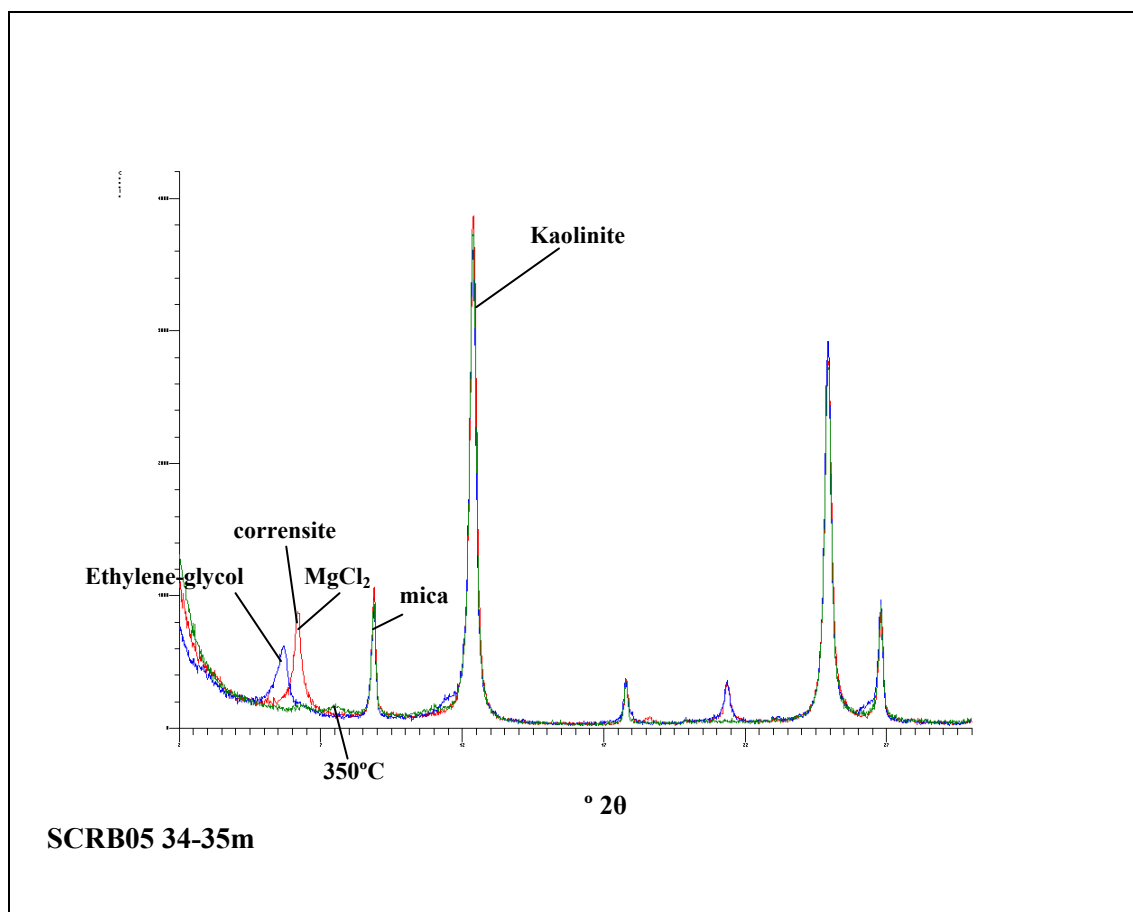


Figure 10. XRD diffraction pattern of the clay fraction in the upper saprolite (sample SCRB05).

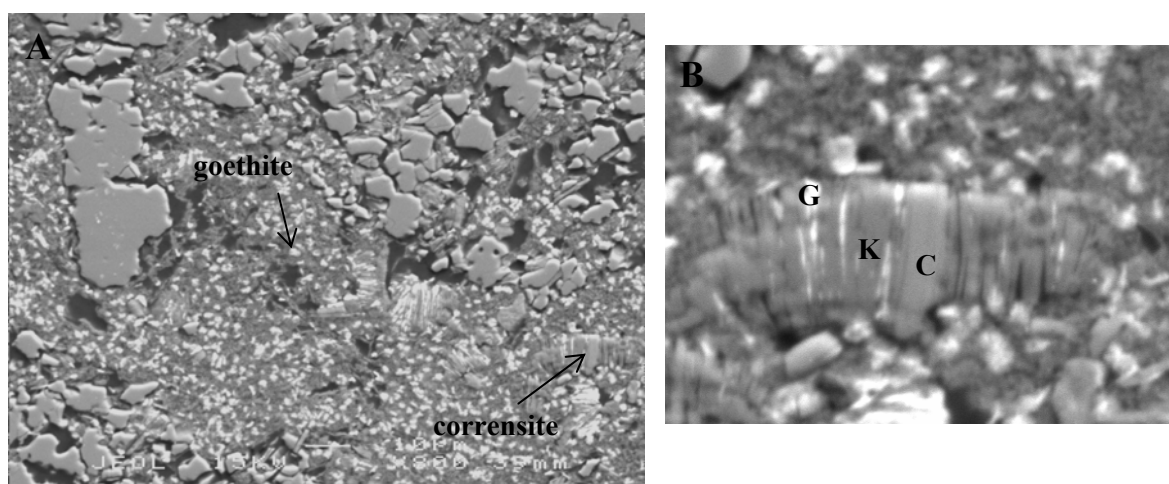


Figure 11. SEM micrographs (backscattered electron image) of the upper saprolite (SCRB05). A. Ferruginised saprolite showing iron oxides concentrations. B. Corrensite (C) booklet partially weathered into kaolinite (K) and goethite (G).

Table 7. Microprobe analyses (%) of the clays in the upper saprolite, sample SCRB103.  
(-: below detection limit).

Analyses	Mineralogy	SiO <sub>2</sub>	TiO <sub>2</sub>	Al <sub>2</sub> O <sub>3</sub>	FeO	MgO	CaO	K <sub>2</sub> O	Na <sub>2</sub> O	MnO	PbO	Total
1	Mica	48.6	-	28.8	3.5	2.45	-	9.98	-	-	-	93.33
2	Mica	45.1	0.46	29.8	4.4	1.56	-	9.71	0.38	-	-	91.41
3	Mica	40.6	-	27.0	4.3	1.04	-	8.26	-	4.73	3.38	89.31
4	Mica/kaolinite	46.9	-	31.6	3.1	-	-	6.11	-	-	-	87.71
5	Mica/kaolinite	45.0	-	31.5	2.9	-	-	6.89	-	-	-	86.29
6	Kaolinite/mica	45.5	-	35.7	1.0	-	-	1.49	-	-	-	83.69
7	Kaolinite/mica	41.3	-	31.6	2.0	0.4	-	1.93	-	-	-	77.23
8	Kaolinite	45.6	-	37.5	0.4	-	-	-	-	-	-	83.50
9	Kaolinite	45.5	-	37.0	0.7	-	-	-	-	-	-	83.20
10	Kaolinite	46.1	-	38.0	0.7	-	-	-	-	2.04	0.82	87.66
11	Smectite	30.4	-	10.5	18.8	2.41	0.42	0.32	-	-	-	62.85
12	Smectite	33.0	-	20.3	10.9	1.38	0.17	0.35	-	-	-	66.10
13	Smectite	31.6	-	12.3	11.5	1.52	0.14	0.63	-	-	-	57.69
14	Smectite	31.3	-	7.8	14.1	4.27	0.55	0.95	0.22	-	-	59.19
15	Smectite	31.6	-	11.3	12.4	3.2	0.52	0.79	0.16	-	-	59.97

Table 8. Microprobe analyses (%) of the upper saprolite minerals, sample SCRB05.  
(-: below detection limit)

Analyses	Mineralogy	SiO <sub>2</sub>	TiO <sub>2</sub>	Al <sub>2</sub> O <sub>3</sub>	FeO	MgO	CaO	K <sub>2</sub> O	V <sub>2</sub> O <sub>5</sub>	MnO	PbO	CuO	ZnO	Total
1	Mica	44.1	-	34.4	2.9	0.45	-	8.02	-	-	-	-	-	89.87
2	Mica/kaolinite	46	-	36.9	1.5	-	-	2.49	-	-	-	-	-	86.89
3	Corrensite	29.1	-	18.7	25.3	6.82	0.38	0.47	-	-	-	-	-	80.77
4	Corrensite	28.6	-	17.9	24.8	6.42	0.39	0.39	-	-	-	-	-	78.50
5	Corrensite	33.4	-	17.7	22.2	6.26	0.52	0.24	-	-	-	-	-	80.32
6	Corrensite	32	-	17.9	25.2	6.69	0.70	-	-	-	-	0.84	-	83.33
7	Corrensite	34.8	-	16.1	23.4	5.90	0.79	-	-	-	-	0.65	-	81.64
8	Ecandrewsite	-	51.5	-	36.0	-	-	-	-	3.10	-	-	7.10	97.70
9	Ecandrewsite	-	50.5	-	36.8	-	-	-	-	3.40	-	-	7.70	98.40
10	Ecandrewsite	-	50.5	-	40.8	-	-	-	-	3.20	-	-	5.40	99.90
12	Ecandrewsite+ ilmenite*	--	61.1	-	16.8	-	-	-	-	3.50	2.20	-	6.30	89.90
13	Weathered ilmenite	-	64.9	-	17.5	-	-	-	1.10	0.70	1.40	-	-	85.60

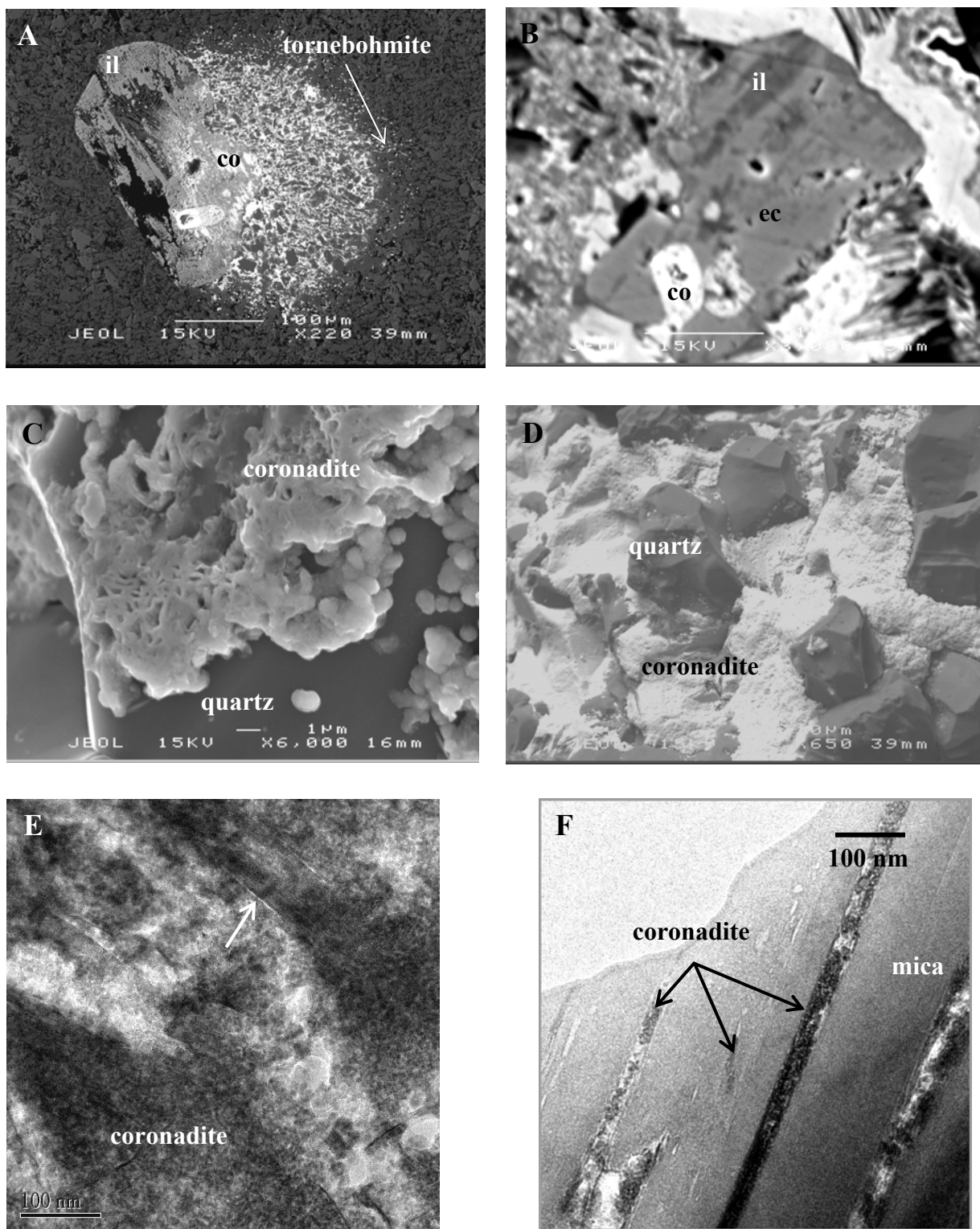


Figure 12. A. SEM micrograph (backscattered electron image) showing ilmenite (il) partially replaced by coronadite (co). B. SEM micrograph (backscattered electron image) of an ilmenite grain (il) partially replaced by eandrewsite (ec) and coronadite (co). C. SEM image micrograph (secondary electron image) of coronadite globules and dissolution pits. D. SEM image micrograph (secondary electron image) showing quartz crystals set into massive coronadite. E. TEM micrograph of kaolinite partially pseudomorphosed by coronadite with preservation of the clay fabric. F. TEM micrograph showing mica laths partially replaced by granular coronadite.

Table 9. Microprobe analyses (%) of the manganese oxides in sample SCRB103.

Analyses	Mineralogy	SiO <sub>2</sub>	Al <sub>2</sub> O <sub>3</sub>	Fe <sub>2</sub> O <sub>3</sub>	MnO <sub>2</sub>	PbO	Total
1	Coronadite	6.8	0.9	12.7	42.61	28.06	91.07
2	Coronadite	6.9	0.6	13.3	42.93	28.72	92.45
3	Coronadite	7.2	0.7	11.4	41.97	28.14	89.41
4	Coronadite	5.7	1.0	10.5	45.20	28.69	91.09
5	Coronadite	5.6	0.6	9.8	47.95	30.28	94.23
6	Coronadite	7.8	1.1	13.2	42.27	27.44	91.81
7	Coronadite	8.3	0.8	12.6	40.44	27.91	90.05
8	Coronadite	6.9	0.9	11.5	44.15	29.90	93.35
9	Coronadite+clays	8.9	3.7	13.3	42.89	26.08	94.87
10	Coronadite+clays	8.9	2.2	12.3	43.91	29.25	96.56

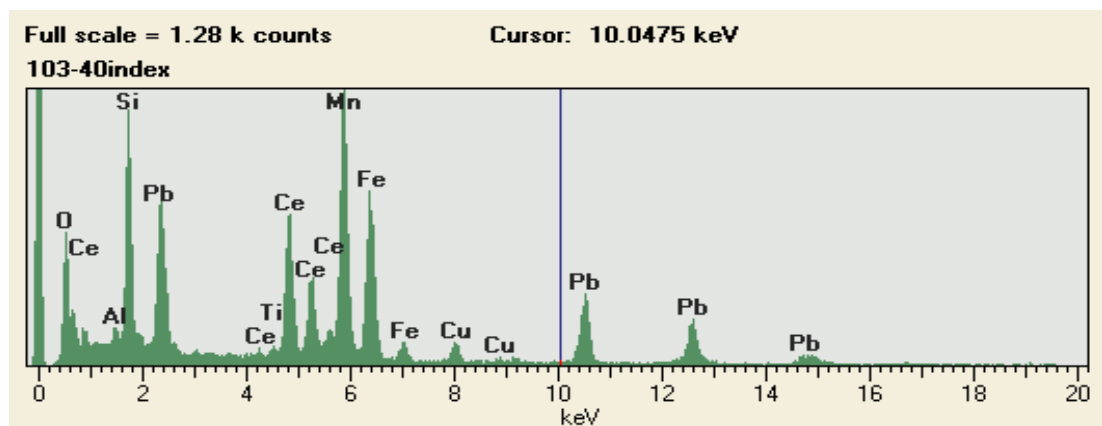


Figure 13. Analytical Electron Microscopy (AEM) spectrum of Ce-rich coronadite in sample SCRB103.

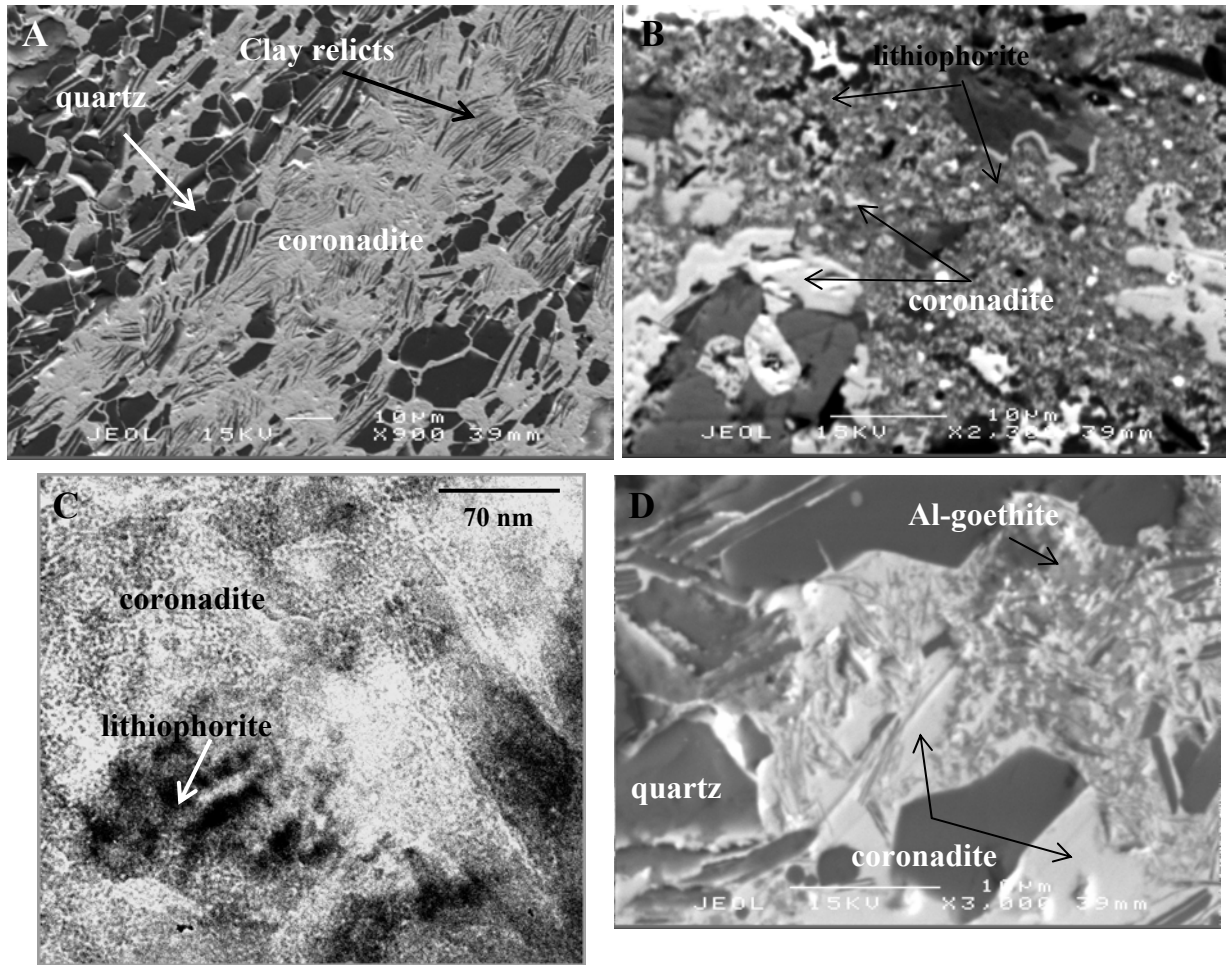


Figure 14. A. SEM micrograph (backscattered electron image) showing the impregnation of clays by coronadite. B. SEM micrograph (backscattered electron image) showing the lithiophorite-coronadite association. C. TEM micrograph of a lithiophorite domain in coronadite. D. SEM micrograph (backscattered electron image) showing Al-goethite mixed with coronadite.

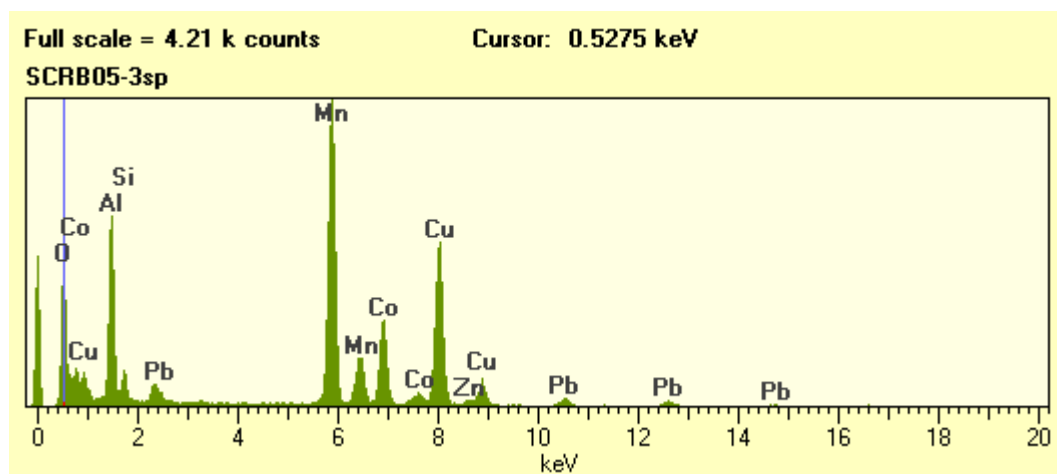


Figure 15. Analytical Electron Microscopy (AEM) spectrum of lithiophorite associated with coronadite in sample SCRB05.



Table 10. Microprobe analyses (%) of the Mn oxides and associated minerals in sample SCRB05.  
(-: below detection limit).

	Mineralogy	SiO <sub>2</sub>	Al <sub>2</sub> O <sub>3</sub>	Fe <sub>2</sub> O <sub>3</sub>	MnO <sub>2</sub>	CoO	BaO	CuO	PbO	CeO <sub>2</sub>	Total
1	Coronadite	0.5	1.4	6.3	57.00	-	-	2.42	29.67	-	97.29
2	Coronadite	0.5	1.3	4.5	57.88	-	-	2.63	29.29	-	96.10
3	Coronadite	0.7	1.7	4.4	58.95	-	-	2.15	28.31	-	96.21
4	Coronadite	0.8	1.0	13.1	47.71	-	-	1.55	29.29	-	93.45
5	Coronadite	0.5	1.2	3.7	57.99	-	-	2.11	29.77	-	95.27
6	Coronadite	0.8	1.1	10.8	49.10	-	-	1.73	28.82	-	92.35
7	Coronadite	1.2	1.1	12.2	46.62	-	-	1.73	29.58	-	92.43
8	Coronadite	1.3	1.3	4.3	54.25	1.21	-	1.63	28.66	0.93	93.58
9	Coronadite	1.5	1.5	1.6	52.87	2.13	-	1.85	31.31	1.19	93.95
10	Coronadite	1.5	0.3	0.7	55.42	0.84	-	1.71	33.83	0.68	94.98
11	Coronadite	0.9	1.8	5.7	56.75	-	1.40	2.22	23.47	0.69	92.93
12	Coronadite	0.5	1.8	3.1	59.32	-	2.33	2.72	22.33	-	92.10
13	Coronadite	1.0	1.5	13.2	48.81	-	-	1.76	27.08	-	93.35
14	Coronadite	1.0	1.7	9.2	52.60	-	-	2.15	26.48	-	93.13
15	Coronadite	0.7	3.2	5.1	56.75	-	-	2.10	26.70	-	94.55
16	Coronadite	0.8	1.8	5.5	57.06	0.79	2.38	1.67	22.62	-	92.62
17	Coronadite+cerianite	1.5	2.0	0.7	61.69	-	-	1.32	27.42	2.19	96.82
18	Coronadite	0.9	3.0	6.1	58.38	-	-	1.82	25.92	-	96.12
19	Coronadite	0.9	1.5	15.5	46.32	-	-	1.54	28.45	-	94.21
20	Coronadite	1.1	2.0	0.8	62.72	-	-	1.51	29.00	-	97.13
21	Coronadite	0.8	2.8	12.7	48.95	-	-	1.42	26.68	-	93.35
22	Coronadite	1.3	2.3	13.5	47.22	-	0.70	1.61	25.13	-	91.76
23	Coronadite	1.0	2.3	0.0	63.31	-	-	1.94	28.37	-	96.92
24	Coronadite	0.9	3.0	2.5	60.82	-	0.59	1.70	25.98	-	95.49
25	Coronadite	1.6	2.2	10.4	55.60	-	1.73	1.62	22.11	-	95.26
26	Coronadite	0.8	2.1	7.9	59.55	-	1.45	1.10	23.17	-	96.07
27	Coronadite	0.6	2.0	2.6	64.25	-	1.11	1.74	23.85	-	96.15
28	Coronadite	1.3	2.1	12.6	51.47	-	0.86	1.66	24.32	-	94.31
29	Coronadite	1.0	1.8	9.9	55.70	-	1.15	1.78	24.63	-	95.96
30	Coronadite	0.8	1.7	9.0	56.31	-	1.26	1.45	24.58	-	95.10
31	Coronadite	0.6	3.6	3.9	55.85	-	-	3.14	26.66	0.80	94.55
32	Coronadite	1.8	0.6	3.4	55.64	-	-	1.33	30.21	1.15	94.13
33	Coronadite	0.3	1.8	2.5	61.28	-	-	3.22	25.94	-	95.04
34	Coronadite+clay	2.2	4.7	12.6	47.66	-	1.33	2.26	18.40	-	89.15
35	Coronadite+clay	1.7	2.1	4.5	53.85	-	-	2.92	28.82	-	93.89
36	Coronadite+clay	3.1	1.7	5.9	50.36	-	-	1.00	30.56	-	92.62
37	Coronadite+clay	2.0	2.4	10.3	46.30	1.67	-	1.60	27.29	-	91.56
38	Coronadite+clay	3.6	4.3	16.1	43.86	0.58	0.54	1.15	20.39	-	90.52
39	Coronadite+clay	4.7	4.5	5.1	49.43	-	-	2.41	27.63	-	93.77
40	Coronadite+clay	4.4	4.3	1.9	54.41	-	-	3.30	25.66	-	93.97
41	Lithiophorite-coronadite	0.3	17.9	1.3	42.20	7.59	-	5.59	1.69	-	76.57
42	Lithiophorite-coronadite	2.6	16.9	9.5	36.87	6.62	-	3.23	4.21	-	79.93
43	Lithiophorite-coronadite	1.6	9.8	17.5	38.08	4.51	-	2.33	11.93	-	85.75
44	Lithiophorite-coronadite	1.0	9.4	7.0	45.63	5.17	-	2.96	14.16	-	85.32
45	Lithiophorite-coronadite	9.2	16.7	2.3	40.99	5.89	0.74	2.40	9.75	-	87.97
46	Lithiophorite-coronadite	8.7	15.2	2.2	40.75	6.07	0.68	2.60	10.44	-	86.64
47	Lithiophorite-coronadite	3.7	14.2	1.3	42.20	7.47	0.51	3.59	9.16	-	82.13
48	Lithiophorite-coronadite	8.2	15.0	1.6	39.95	5.93	-	2.67	10.61	-	83.96
49	Lithiophorite-coronadite	5.0	10.3	2.2	49.19	4.41	1.11	2.67	13.43	-	88.31
50	Lithiophorite-coronadite	2.4	7.2	3.8	51.60	2.94	0.98	2.87	15.66	-	87.45
51	Al-goethite	2.8	8.3	65.9	1.18	-	-	-	0.55	-	78.73
52	Al-goethite	4.1	9.9	64.4	1.68	-	-	-	0.44	-	80.52
53	Al-goethite	3.5	7.7	61.5	5.50	-	-	-	3.33	-	81.53
54	Goethite + Mn oxides	2.2	3.1	20.9	43.95	-	0.52	-	20.69	-	91.36
55	Ce-domain	4.1	1.0	4.3	6.51	-	-	-	8.21	64.65	88.77
56	Ce-domain	6.8	5.2	4.4	16.39	-	-	-	11.02	43.40	87.21
57	Ce-domain	2.3	1.1	8.1	28.91	-	-	-	13.93	32.17	86.51

TEM examination of a <13 µm fraction (suspension onto holey carbon grid) shows pseudo-hexagonal plates about 200 nm across of kaolinite. A few minute size spherical grains of Sn oxide (cassiterite) <0.5 µm in diameter (Figure 16A), and of spinel about 1 µm in diameter (Fe, Cr, Ni and Sb) are scattered in the material. The latter are probably related to the Fe-Cr spinel rimmed by magnetite in Cr-bearing chlorite described by Ashley *et al* (1988).

#### *Quartz*

Hydrothermal quartz occurs as large crystals (up to 100 µm) containing various solid inclusions. Sphalerite inclusions, 4 µm to 20 µm wide, are abundant (Figure 16C), and contain up to 5% FeO. Xenotime YPO<sub>4</sub> or churchite YPO<sub>4</sub>·2H<sub>2</sub>O, baryte, chlorite and rutile inclusions have also been identified. These inclusions have been protected from dissolution and remain throughout the profile. When located in non-disturbed material, these inclusions are reliable mineralogical indicators of the underlying mineralisation. No inclusions were observed in the interlocked large crystals of quartz (up to 1 mm long) filling the wider veins (about 2 mm wide) cutting through the material.

#### *Plumbogummite*

Plumbogummite PbAl<sub>3</sub>(PO<sub>4</sub>)<sub>2</sub>(OH)<sub>5</sub> (H<sub>2</sub>O) is a significant accessory mineral, occurring as small diffuse grains (<5 µm) between crystals of hydrothermal quartz. The chemical composition indicates some isomorphic substitutions of Pb by Ce, La and Ca (about 3% Ce<sub>2</sub>O<sub>3</sub>, 3% La<sub>2</sub>O<sub>3</sub> and 3% CaO).

#### *Rutile*

Rutile also occurs as large laths partially replaced by silica (Figure 16E) and as inclusions in hydrothermal quartz grains (Figures 16D and 16F). It contains low levels of V and Fe (Table 11). According to Ashley *et al* (1988), rutile is a characteristic accessory phase in the mineralised horizon and footwall rather than titanite which is restricted to the hangingwall.

### **5. 3. Silicified horizon and laterite**

#### **5. 3. 1. Hanging wall**

A lateritic horizon overlies the saprolite developed over the hanging wall lavas. It contains hard ferruginous fragments set in a clay-rich matrix. It locally grades upwards into a more nodular and pisolitic unit. The pisoliths present anomalous Bi-Sn-Mo-Sb-As associations (Smith and Perdrix, 1983). According to these authors, gossan fragments and cassiterite grains have been mechanically dispersed and incorporated into the concretionary rims of pisoliths and therefore would be responsible for the secondary dispersion haloes observed in the pisolitic lateritic residuum.

The variety of Mn-oxides nodules observed in all the saprolite samples is not present in the top horizon. The coarse fraction contains chips of Fe impregnated material, hematitic grains, chromite-rich grains and residual weathered ilmenite. Quartz grains are coated with Mn and Fe oxides and clays. The Mn oxides contain little or no Pb, and Ba is the main cation in the Mn oxide tunnels (Table 12). Barium can be present in a large variety of Mn oxides such as hollandite, todorokite, psilomelane. Copper is not detected in the Mn-coating and hematite.

#### **5. 3. 2. Over mineralisation**

The surface horizon (or hardpan) over mineralisation is very similar to the top of the upper saprolite. Muscovite-kaolinite intergrades and quartz are the principal constituents. Accessory minerals are rutile laths and large Ti-weathered ilmenite grains (Figure 17B) and plumbogummite.



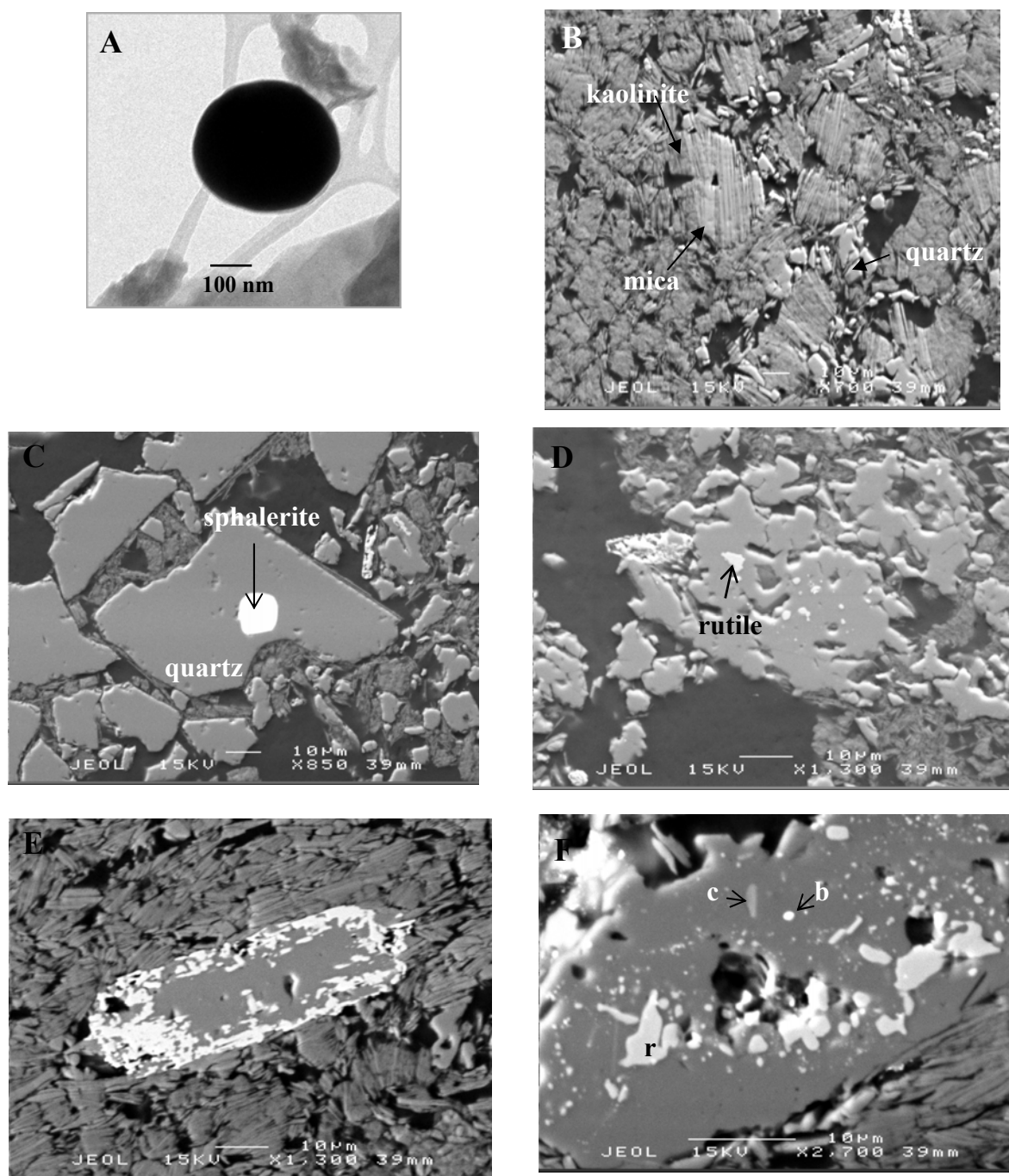


Figure 16. A. TEM micrograph of a cassiterite grain in the <13  $\mu\text{m}$  fraction. B. SEM micrograph (backscattered electron image) of mica booklets partially altered into kaolinite. C. SEM micrograph (backscattered electron image) showing a sphalerite inclusion in hydrothermal quartz crystal. D. SEM micrograph (backscattered electron image) of hydrothermal quartz with rutile inclusion. E. SEM micrograph (backscattered electron image) of a rutile crystal partially replaced by silica. F. SEM micrograph (backscattered electron image) of a quartz grain containing various types of inclusions: rutile (r), baryte (b), and chlorite (c).

Table 11. Microprobe analyses (%) of the clays in the silicified surface horizon over mineralisation.  
(-: below detection limit).

Analyses	Mineralogy	SiO <sub>2</sub>	Al <sub>2</sub> O <sub>3</sub>	K <sub>2</sub> O	TiO <sub>2</sub>	V <sub>2</sub> O <sub>5</sub>	Fe <sub>2</sub> O <sub>3</sub>	Total oxides
1	Mica	45.6	36.5	10.1	-	-	-	92.20
2	Mica-kaolinite	39.9	32.7	6.5	-	-	-	79.10
3	Mica-kaolinite	43.4	33.4	7.9	-	-	-	84.70
4	Kaolinite	39.9	33.1	-	-	-	-	73.00
5	Kaolinite	45.5	38.0	-	-	-	-	83.50
6	Rutile	3.9	-	-	94.10	1.05	0.83	99.88
7	Rutile	-	-	-	96.57	0.97	0.82	98.36
8	Rutile	-	-	-	97.73	0.87	0.70	99.30

Table 12. Microprobe analyses of the Mn-oxides and associated minerals.  
(-: below detection limit). \*: Iron as FeO.

Mn+Fe+Qt: Mn oxides + Fe oxides + quartz; Mn + clays: Mn oxides + clays;  
Fe+Mn: Fe oxides + Mn oxides.

Mineralogy	SiO <sub>2</sub>	Al <sub>2</sub> O <sub>3</sub>	Fe <sub>2</sub> O <sub>3</sub>	MnO <sub>2</sub>	K <sub>2</sub> O	CaO	BaO	Cr <sub>2</sub> O <sub>3</sub>	PbO	CeO <sub>2</sub>	TiO <sub>2</sub>	Total
Mn+Fe+Qt	13.1	3.3	21.0	42.97	0.42	0.46	5.48	-	1.05	1.12	-	88.90
Mn+Fe+Qt	11.3	2.4	19.5	48.33	0.44	0.30	6.92	-	1.24	1.20	-	91.63
Mn+Fe+Qt	17.3	1.5	34.1	27.73	0.40	0.38	4.00	-	1.00	2.55	-	88.96
Mn + clays	30.9	24.4	6.9	25.56	0.65	0.21	2.22	-	-	0.92	-	91.76
Mn+Fe+Qt	18.5	4.5	34.0	24.56	0.38	0.24	3.12	-	1.12	0.72	-	87.14
Fe+Mn	37.5	27.6	22.9	1.65	0.60	-	0.48	-	-	-	-	90.73
Cr-rich grain	4.5	0.8	30.4*	3.42	-	-	-	32.34	-	-	-	41.06
Ilmenite	-	-	46.2	3.65	-	-	-	-	-	-	50.12	99.97

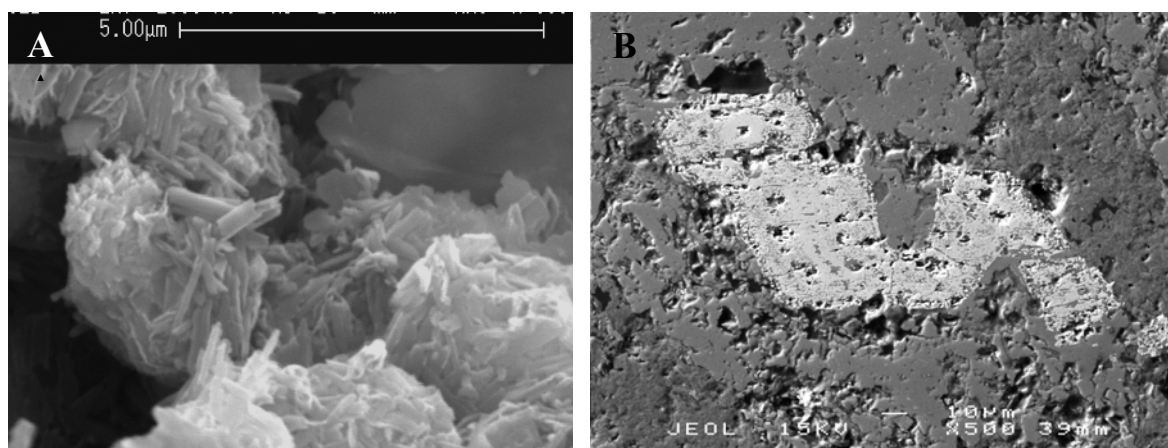


Figure 17. A. SEM micrograph (secondary electron image) showing balls of kaolinite associated with goethite in the mottled upper saprolite. B. SEM micrograph (backscattered electron image) of a weathered ilmenite grain in the surface horizon.

## 6. DETERMINATION OF TRACE ELEMENTS IN REGOLITH MATERIAL BY LASER ABLATION-INDUCTIVELY COUPLED PLASMA-MASS SPECTROMETRY (LA-ICP-MS)

### 6. 1. Introduction

The residence of some abundant trace elements such as Cu, Co and Zn in the Scuddles regolith minerals has been identified using analytical electron microscopy. However, the surface expression of the mineralisation consists of anomalous Sb, In and Bi levels, which are beyond the detection limit of EDAX. The chemical composition of the minerals in the regolith developed over the mineralisation and on the hanging wall lavas has been further characterised by *in situ* LA-ICP-MS analyses.

The general description of the technique and the data reduction method are described in Section 2 and Appendix 3. The detailed mineralogy documented in section 5 provides the necessary background for the interpretation of the LA-ICP-MS analyses.

### 6. 2. Lower saprolite

Eighty analyses were carried out on selected mineral phases of the lower saprolite samples over the mineralisation and further west. The calculated concentrations are given in Tables 13, 14, 15, 16 and 21.

#### 6. 2. 1. Hanging-wall

Two lower saprolite samples have been analysed, one located directly west to the Main Lens (SCRB07, 54-55 m) and the other further south-west SCRB102 (69-70m).

##### *Mica*

Fresh muscovite from sample SCRB07 (54-55 m) has a homogeneous trace element composition (Figure 18A). It contains about 200 ppm V, up to 175 ppm Cr and 600 ppm Ti. Barium (650 ppm) and Pb (up to 158 ppm) substitute for K in the interlayer. These levels are very similar to those obtained in hydrothermal muscovite in the Boddington Gold deposit, (Le Gleuher, 2002). The mica booklets, partially altered to kaolinite, are comparatively depleted in V, Ba, Ti and Pb indicating these elements are not incorporated into kaolinite.

##### *Goethite*

Figure 18B shows the isotopic responses of a volume consisting of mica-kaolinite intergrades and goethite in sample SCRB07. The goethite-rich slices — *i.e.* Fe-rich or K-poor — at the top of the pit are significantly enriched in Cu (0.63%), Zn (870 ppm), As (200 ppm) and P (0.28%). Goethite contains Sb (up to 21 ppm), and small amounts of Mo, Ni and Co (<10 ppm).

##### *Interstratified clays*

Both high- and low-charge corrensites have been identified in the lower saprolite. The high-charge corrensite (chlorite/vermiculite) analysed in sample SCRB102 contains high levels of Cu and Zn (about 0.30%), Ni (up to 340 ppm) and Co (up to 80 ppm). Zinc content exceeds Cu in a few booklets. Arsenic, Sb and Mo are not present. The distribution of selected traces in corrensite, mica and kaolinite is shown in Figure 18C. The base metals have been trapped into the vermiculite during the chlorite alteration into corrensite. This reaction either involved hydrothermal or low temperature fluids carrying the base metals. The low-charge corrensite (chlorite/smectite) in sample SCRB07 shows similar trends with lower levels (Figure 18D). This is particularly evident for the Zn content which is roughly 1/3 that of Cu.

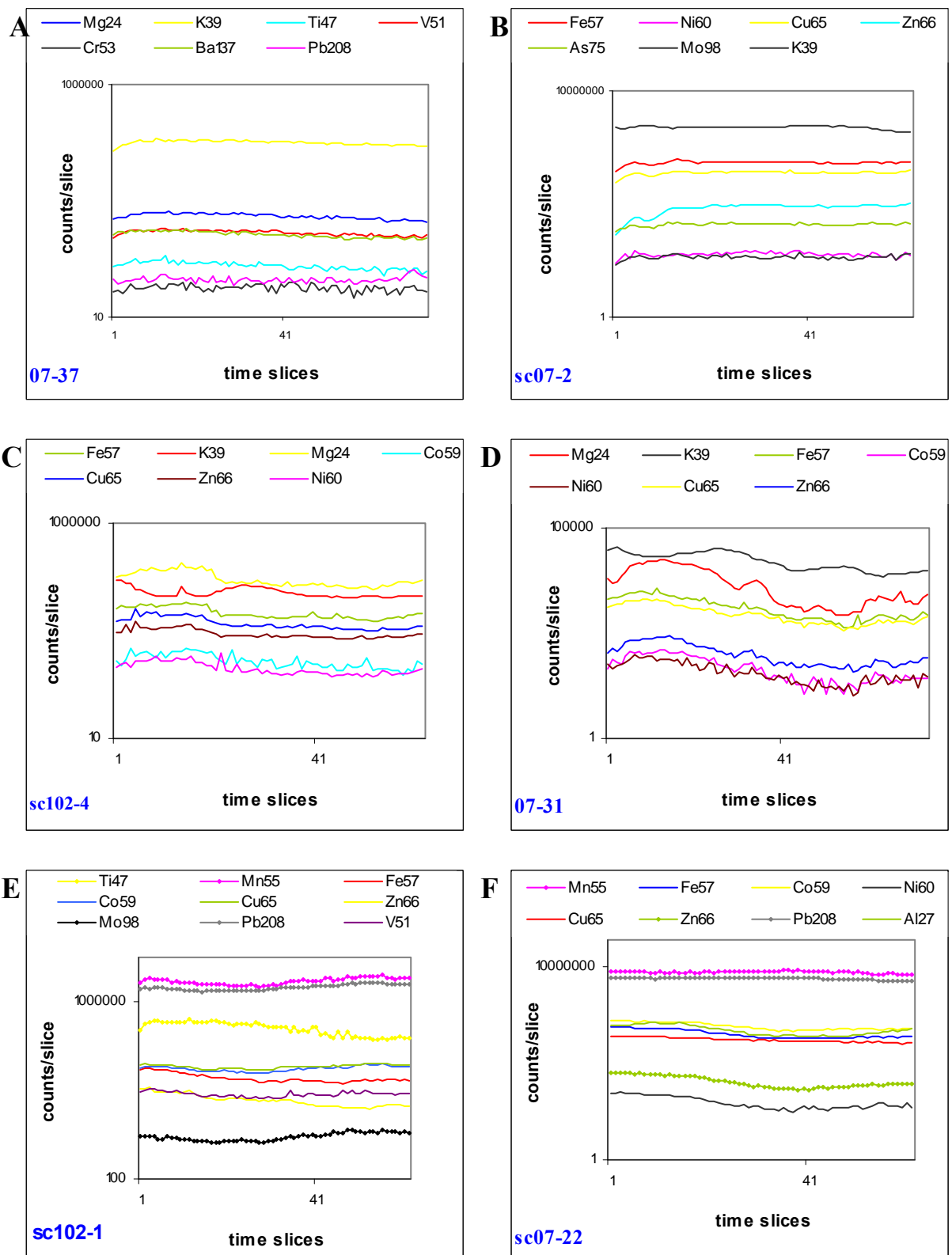


Figure 18. LA-ICP-MS time resolved spectra of selected isotopes in Scuddles lower saprolite minerals. Muscovite. B. Kaolinite-muscovite intergrade and goethite. C. High-charge corrensite, muscovite and kaolinite. D. Low-charge corrensite, muscovite and quartz. E. Coronadite and ilmenite (SCR102). F. Coronadite, goethite and lithiophorite(SCR07).

### *Manganese oxides and associated minerals*

The manganese oxides and associated minerals host a large variety of trace elements with concentrations related to the distance to the orebody.

Figure 18E shows spectra acquired on a Mn-rich nodule consisting of an ilmenite grain partially replaced by coronadite in a sample away from the mineralisation (SCRB102). Copper, Co and Mo are associated with coronadite, whereas Ti, Fe and Zn present similar distributions. Coronadite contains up to 1% Cu, and 0.2% Co hosted in lithiophorite microdomains scattered in the coronadite. The Mn oxides also contain abundant Mo (up to 150 ppm), V (up to 500 ppm) and Ce (up to 0.15%), the latter probably occurring as cerianite-rich granules. The high Zn level (up to 0.37%) is contained in ilmenite areas partially altered into ecandrewsite.

Closer to the main orebody (SCRB07), coronadite contains lower levels of Cu (to 0.7%). Cobalt (up to 0.7%), Ni and Zn (up to 550 ppm) are correlated with Al and Fe, suggesting that they are hosted either by aluminous goethite or by a mixture of lithiophorite and goethite (Figure 18F). Vanadium (to 0.2%) and Ce (up to 0.4%) are more abundant than in SCRB102 but Mo is comparatively depleted ( $\leq 12$  ppm).

### *Plumbogummite*

Plumbogummite is abundant in sample SCRB07 and generally occurs in close association with coronadite. The phosphates contain Ce (Figure 19A), and lanthanides La and Pr possibly forming complexes of the type  $\text{Ln}(\text{P}_2\text{O}_7)^{2+}$ .

### *Ilmenite*

Spectra obtained on ilmenite partially replaced by coronadite (Figures 19B and 19C) indicate that fresh ilmenite contains W (up to 9 ppm), Sb (up to 11 ppm), Ta (up to 36 ppm) and abundant Nb (up to 540 ppm).

### *Gold and silver*

Silver contents vary from 280 ppm to 0.65% in altered ilmenite. A similar level (390 ppm) has also been detected in a pit containing quartz and mica. There is no obvious relationship between Ag, Si, Mn and Fe levels indicating that Ag is not associated with quartz, coronadite or Fe oxides (Figure 19D). Unfortunately as Zn was not analysed, it not possible to check if Ag is hosted by or associated with ecandrewsite. The homogeneous Ag distribution does not argue for a distinct minute argentiferous phase. The few ppb of Au detected in some analyses seem to be due to interferences with Ta.

## **6. 2. 2. Over mineralisation**

Sample SCRB10 (44-45 m) situated directly up dip from mineralisation was analysed.

### *Iron oxides*

The location of the probed sites in a ferruginised chip is shown in Figure 20. The spatial resolution of the quantitative analyses (29  $\mu\text{m}$  probe) does not allow the distinction between goethite and hematite layers. However, goethite and hematite can be distinguished by the Fe intensity variations on the depth profiles (Figures 19E and 19F)

The Fe oxides contain up to 2% Cu, 0.4% Zn, 0.4% Pb and 0.15% As. Up to 950 ppm Mg, 570 ppm P, 220 ppm V, 740 ppm Mn, 70 ppm Co, 130 ppm Ni and 90 ppm Mo are present. High levels of Se (up to 45 ppm) and Sb (up to 39 ppm) are detected. The Fe distribution suggests that the top of the pit is enriched in hematite (Fe intensity slightly higher), whereas the bottom contains more goethite (Figures 19E and 19F). Preferential trace-elements-mineral associations are evidenced: Cu, Zn, Mn, Co, Mg, and in a lesser way P, are associated with goethite, whereas Al, Pb and possibly As are preferentially hosted in hematite.

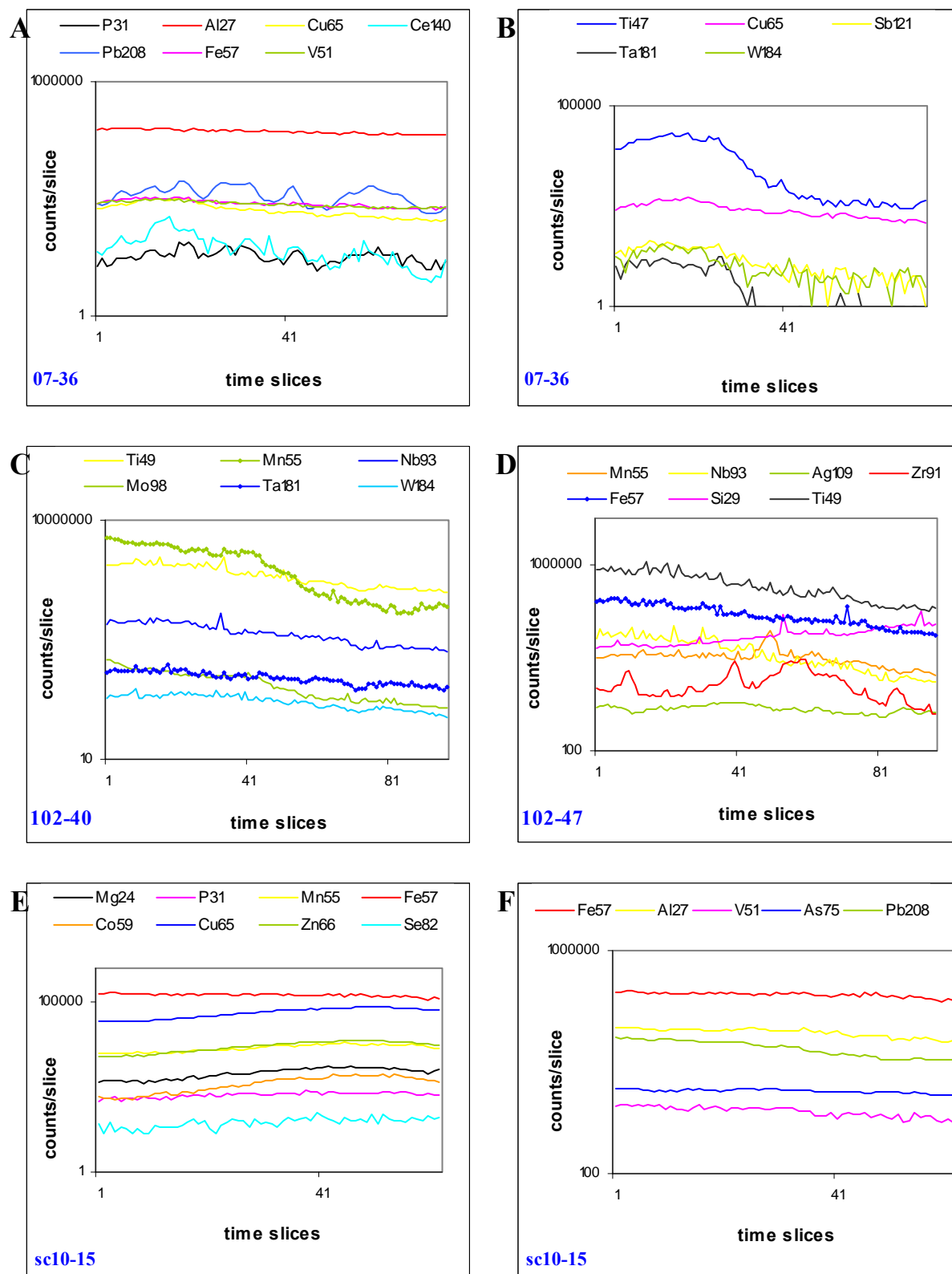


Figure 19. LA-ICP-MS time resolved spectra of selected isotopes in Scuddles lower saprolite minerals. A. Plumbogummite and mica. B and C. Weathered ilmenite. D. Silver distribution. E and F. Goethite and hematite in a gossan chip.

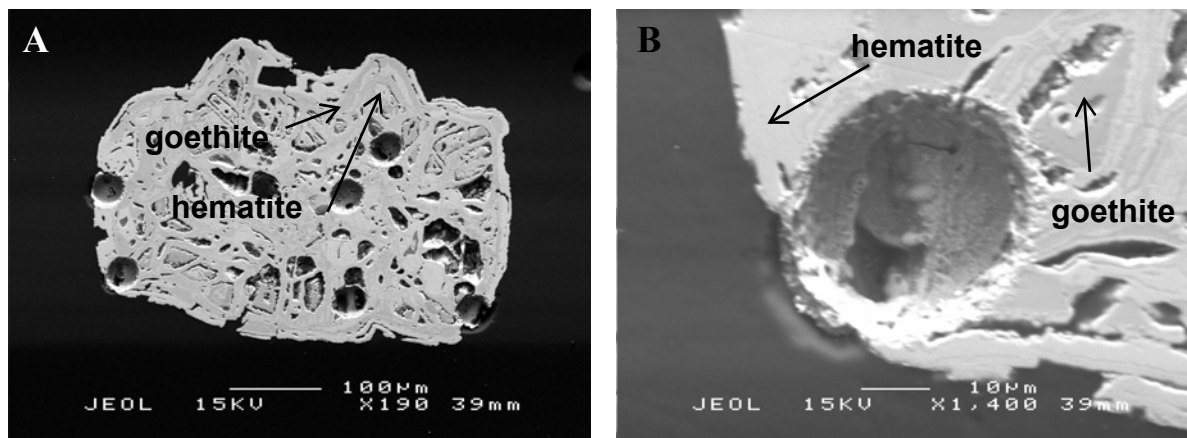


Figure 20. SEM micrographs (backscattered electron image). A. Location of the LA-ICP-MS ablation pits in a ferruginised saprolite chip. B. Close up showing the probe size compared with the goethite-hematite banding.

#### *Manganese oxides and associated minerals*

The Mn oxides are characterised by a homogeneous isotopic signature (Figure 21A). They consist of coronadite-hollandite containing high levels of Cu (up to 2%), Co (up to 0.8%), Zn (up to 700 ppm), V (up to 0.6%) and Ce (up to 0.1%). Nickel and Co are abundant (up to 0.8%) and their distribution suggests that they are hosted by lithiophorite (Figure 21B).

### **6. 3. Upper saprolite**

#### **6. 3. 1. Hanging-wall**

Two samples of upper saprolite developed on hanging wall lavas have been analysed: SCRB103 (59-60 m) and SCRB05 (34-35 m). The calculated concentrations are given in Tables 17, 18, 19, 20 and 22.

#### *Clays*

Figure 21C shows the responses of selected isotopes obtained when probing an assemblage consisting of smectites at the top of the pit and mica-kaolinite intergrades below. The smectitic slice is enriched in Cu (>0.25%), Zn (0.12%), Pb (0.7%), Ni (>150 ppm) and Co (>50 ppm). Smectites and parent low-charge corrensite show similar trends suggesting that smectites inherit the corrensite smectitic layers during weathering.

The analyses of mica-kaolinite booklets show that kaolinite does not incorporate the cations released during muscovite alteration such as V, Ba and Ti. Moreover, kaolinite has not incorporated any of the abundant base metals present in the environment.

#### *Manganese oxides*

LA-ICP-MS analyses of coronadite from sample SCRB103 indicate that Cu (>0.17%) which had remained undetected with the electron microprobe is also present (Figure 21D). Cerium and V are abundant (respectively to 0.23% and 0.16%) and up to 21 ppm Mo is present in assemblages composed of mica and coronadite. Cobalt (>470 ppm) is hosted in associated lithiophorite.

Closer to the mineralisation (SCRB05), coronadite is associated with areas of lithiophorite large enough to be detected on the spectra. Figure 21E illustrates the responses obtained on a volume of coronadite and mica with abundant lithiophorite towards the bottom of the pit. Lithiophorite contains abundant Co (>2.8%) and Ni (>0.13%). Cerium (up to 0.56%) occurs in the coronadite and microdomains detected

during the TEM analyses. The distributions of Zn and Ti (Figures 21E and 22A) indicate that Zn is both located in ilmenite-eandrewsite and in coronadite (up to 0.3% Zn). Molybdenum occurrence is erratic, with a maximum value of 160 ppm detected in a relatively Fe-poor material.

#### *Iron oxides*

Iron and Mn-rich assemblages are relatively enriched in P (> 0.10%) and As (> 140 ppm), suggesting these elements are located in goethite which has been commonly observed associated with coronadite in sample SCRB05.

#### *Cerium phases*

Figures 22A and 22B show isotopic responses obtained on material containing micrometric Ce-rich domains. The silica response indicates that Ce is not only present in tornebohmite crystals around the Mn-rich nodules observed in sample SCRB103, but probably as cerianite. It contains high levels of V (>100 ppm) and P (>223 ppm).

#### *Weathered ilmenite*

High levels of W (up to 100 ppm) and Sb (up to 79 ppm) have been detected in weathered ilmenite in sample SCRB103. The distributions of these elements clearly show that the surrounding mica does not contain these two elements (Figure 22C). Zinc is present in ilmenite-eandrewsite.

### **6. 3. 2. Over mineralisation**

Analyses have been performed on two saprolite samples, SCRB10 (14-15 m) and SCRB10 (9-10 m). Iron oxides found in close association with kaolinite were targeted in the former, whereas the “clean” white clays were probed in the latter. Large sulphide inclusions in quartz grains were also analysed.

#### *Clays*

Clusters of mostly fresh muscovite are abundant in the upper saprolite over mineralisation. The freshest mica contains about 600 ppm Ba, 270 ppm V, little Sc (68 ppm) and Cr (35 ppm). Figure 22D shows that kaolinite only partially inherits cations from the mica.

Twenty assemblages composed of various proportions of mica, kaolinite and quartz all contain high Bi contents ranging from 4 to 170 ppm. To ensure that these data were valid, contamination introduced by the Sn polishing plate has been considered and rejected as Sn and Bi are not related (Figure 23B). Bismuth appears to be hosted by several phases associated with the clays, the most common being rutile and a Pb-rich phase. These phases occur as large grains a few micrometers in size or as numerous submicrometric granules scattered among the clays as suggested by some Bi responses (Figures 22F, 23A, 23B and 23C).

#### *Iron-oxides*

Sample SCRB10 presents local iron-stained mottles consisting of kaolinite and iron oxides. The iron-rich material is enriched in a large variety of traces. Compared to the iron oxides present in the lower saprolite, the mottles are depleted in Cu (0.4%), Zn (250 ppm), As (370 ppm) and Pb (730 ppm). One analysis shows a high level of Sb (441 ppm), Mo (222 ppm) and Ti (0.14%). Low levels of Bi are detected in all analyses. The iron oxides also contain V (to 0.18%), P (to 420 ppm) and Cr (to 0.1%). Cobalt, Ni and Ce levels are low (<20 ppm). The homogeneous distribution of Ti in the microsample suggests that it occurs as scattered nanograins or has been scavenged by iron oxides (Figure 22E). Antimony, Fe, Ti and Cr distributions show that some Sb is associated with the iron oxides.

#### *Rutile*

Figures 22F, 23A and 23B show that rutile hosts W, Nb, Ta, Bi, Mo and Sb. Bismuth is abundant with a concentration of 310 ppm in a slice of material containing a rutile grain. Tungsten and Nb concentrations are 36 and 73 ppm respectively in the same slice.



#### *Pb-Bi bearing minerals*

Micron-sized grains containing Bi, Pb, Ba, Cu and often Ce and La are scattered in the material (Figure 23C). The mineralogy of these phases has not been established, but S and P responses indicate that they are not a Pb-Bi sulphide or a phosphate. The nature of the traces suggests a carbonate, (beyerite?).

#### *Sulphides*

Two inclusions of sphalerite in quartz crystals have been probed in sample SCRB10 (9-10m). As no sulphide standard was available, the concentrations were not calculated (See Appendix 4). However, the time-resolved spectra provide useful information about the nature of the trace elements present in sphalerite (Figures 23E and 23F). Apart from Fe, sphalerite inclusion contains Cu, Mn, Co, Pb and In. Antimony and As are not present in the sulphide. The inclusion is homogeneous regarding In, Co and Fe. There are significant variations in Cu concentrations and in a lesser way in Mn and Pb concentrations between different areas of the sample. Similar high Cu levels in sphalerite have been attributed to chalcopyrite inclusions by Axelsson and Rodushkin (2001).

#### *Silver*

Silver is abundant in sample SCRB10 (9-10 m) and has been detected in all samples analysed. Its level varies from 210 ppm to 0.14%. The spectra indicate that silver does not occur as mineral inclusions in quartz, but is associated with the clay fraction of the probed microsample (Figure 23B).

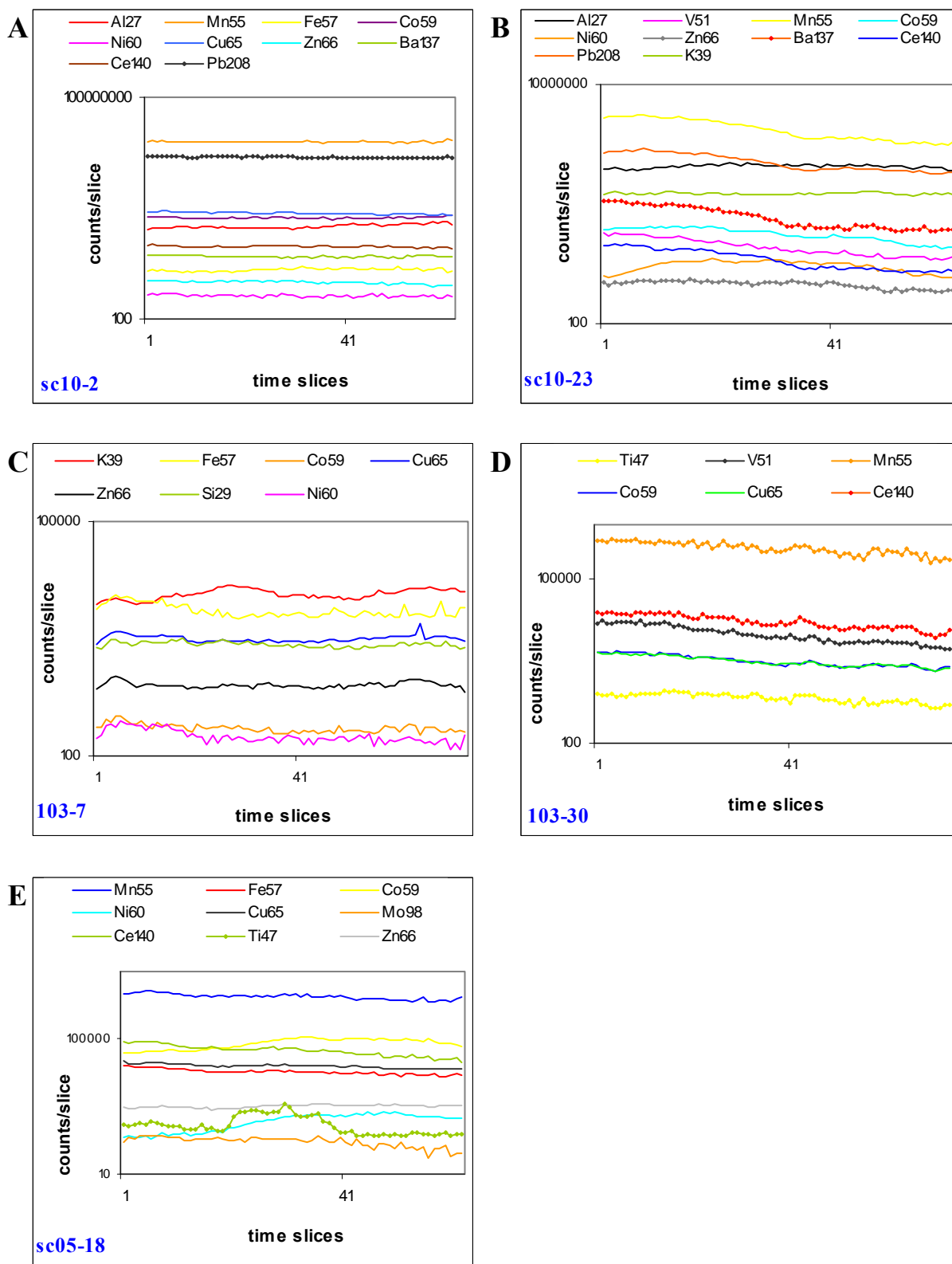


Figure 21. LA-ICP-MS time resolved spectra of selected isotopes in Scuddles lower and upper saprolite minerals. A. Coronadite-hollandite. B. Coronadite, lithiophorite and muscovite. C. Smectite and mica-kaolinite assemblage. D. Coronadite and mica. E. Coronadite, lithiophorite and ilmenite.

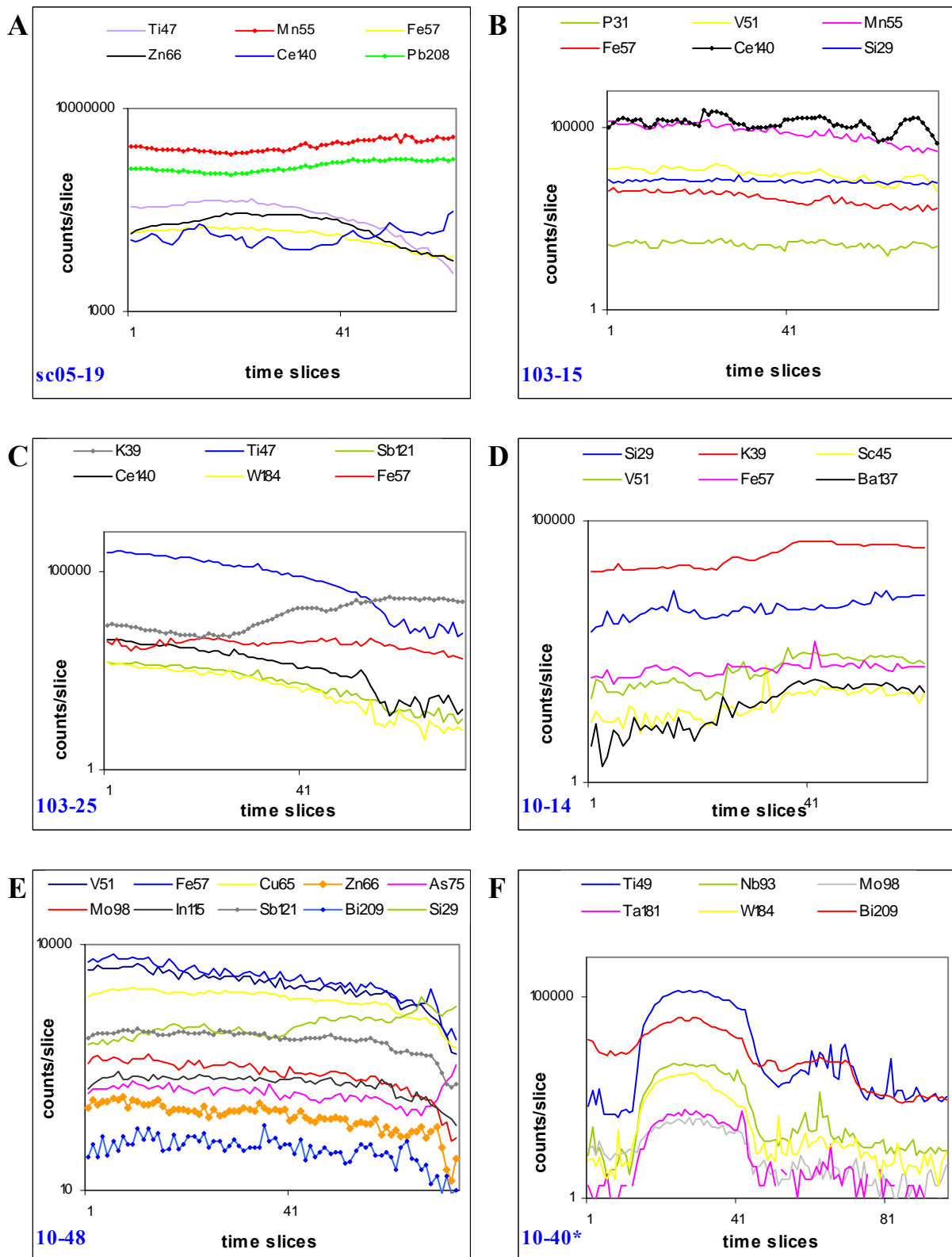


Figure 22. LA-ICP-MS time resolved spectra of selected isotopes in Scuddles upper saprolite. Coronadite and altered ilmenite-eandrewsite. B. Cerium-rich phases and mica. C. Ilmenite. D. Mica-kaolinite booklets. E. Kaolinite, Fe-oxides and quartz. F. Rutile.

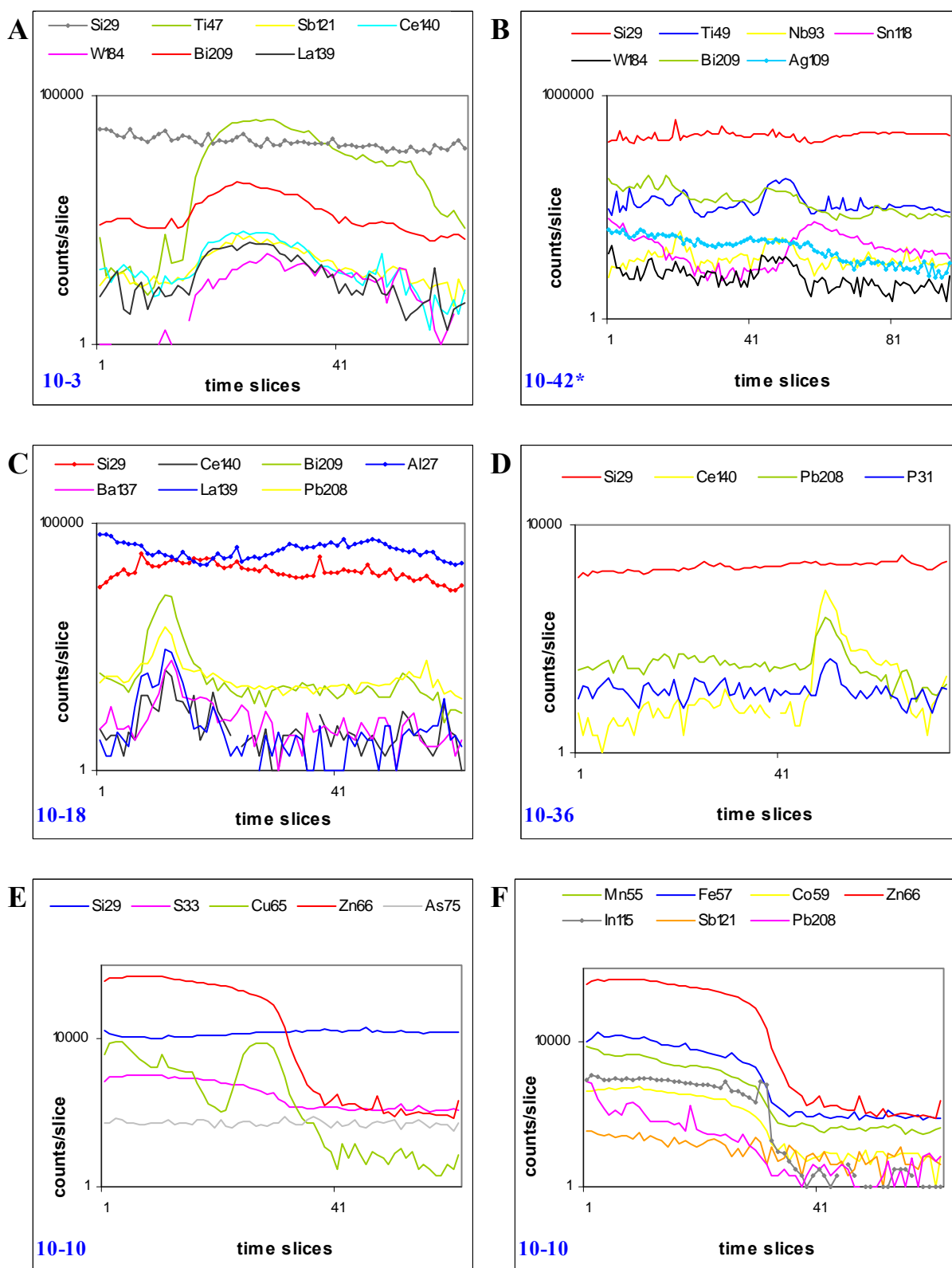


Figure 23. LA-ICP-MS time resolved spectra of selected isotopes in Scuddles minerals. A. Rutile. B. Rutile and Bi-rich phase. C. Pb-Bi rich phase. D. Plumbogummite grain. E and F. Sphalerite inclusions in quartz crystals.

Table 13A. LA-ICP-MS analyses of the lower saprolite minerals (Sample SCRB102, 69-70m). All data in ppm, except for Al and Si in wt% oxides, Ti, Mn and Fe in % element. Internal standard: Al stoichiometric values normalised to 100% wt oxides. (-: below detection limit).

Analyses	Mineralogy	<sup>24</sup> Mg	<sup>27</sup> Al	<sup>29</sup> Si	<sup>31</sup> P	<sup>39</sup> K	<sup>45</sup> Sc	<sup>47</sup> Ti	<sup>51</sup> V	<sup>53</sup> Cr	<sup>55</sup> Mn	<sup>57</sup> Fe	<sup>59</sup> Co
102-14	Ilmenite + coronadite	179	0.3	1.4	228	-	31	42.13	385	248	5.69	5.4	710
sc102-2	Ilmenite + coronadite	645	0.7	3.0	127	-	20	31.81	414	170	10.84	5.7	1250
sc102-9	Ilmenite + coronadite	169	0.3	1.5	316	-	20	27.55	348	106	13.55	3.9	1783
sc102-1	Ilmenite + coronadite	265	0.7	3.9	140	-	21	22.79	498	153	15.84	5.4	1798
sc102-3	Ilmenite + coronadite	211	0.6	4.1	151	-	13	16.48	510	126	19.11	5.5	2011
102-19	Mica/kaolinite	6719	33.5	50.2	239	8.99	31	0.12	471	28	-	3.0	5
sc102-8	Kaolinite/mica	1291	38.0	58.2	38	1.64	8	0.02	117	43	-	0.8	1
sc102-10	Kaolinite/mica	3798	40.0	55.9	-	0.58	6	0.02	88	37	0.01	1.3	10
102-11	Corrensite + mica	30159	25.0	59.2	-	0.05	7	0.03	61	38	0.06	7.3	68
sc102-4	Corrensite+kaolinite+qtz	25225	25.0	59.7	58	0.26	7	0.55	66	132	0.25	5.4	89
sc102-7	Corrensite+quartz	22588	14.4	73.7	54	0.06	5	0.04	35	54	0.04	5.4	47
102-18	Corrensite + clays	17061	33.5	54.9	0	0.23	7	0.03	92	71	0.04	5.4	43
102-17	Quartz + corrensite	7076	5.9	88.5	111	0.27	7	0.31	39	29	0.01	2.1	18
sc102-5	Kaolinite+qtz	4904	34.0	61.3	66	0.04	6	0.23	77	143	0.11	2.0	28
sc102-6	Quartz+clays	2193	39.0	59.5	46	-	4	0.14	72	38	0.02	1.0	9
102-12	Quartz mainly	2827	1.7	96.1	-	0.10	3	0.02	8	5	0.01	0.8	6
102-13	Quartz mainly	5941	4.3	92.0	-	0.19	5	0.03	18	24	0.01	1.5	12
102-15	Quartz + mica	2526	15.3	80.4	128	1.83	12	0.08	112	19	0.01	1.0	4
102-16	Quartz + mica	1132	5.4	91.8	64	1.03	5	0.04	18	10	-	0.8	1

Table 13B. LA-ICP-MS analyses of the lower saprolite minerals (Sample SCRB102, 69-70m). All data in ppm except for Pb in % element. Internal standard: Al stoichiometric values normalised to 100% wt oxides.(-: below detection limit).

Analyses	<sup>60</sup> Ni	<sup>65</sup> Cu	<sup>66</sup> Zn	<sup>75</sup> As	<sup>98</sup> Mo	<sup>121</sup> Sb	<sup>137</sup> Ba	<sup>139</sup> La	<sup>140</sup> Ce	<sup>141</sup> Pr	<sup>184</sup> W	<sup>208</sup> Pb	<sup>209</sup> Bi
102-14	14	5271	3726	66	59	11	63	69	479	25	4	10.38	1
sc102-2	31	6324	3002	52	88	5	27	69	728	33	2	16.75	1
sc102-9	10	10280	2193	88	129	11	17	169	1315	49	7	22.07	2
sc102-1	22	8076	2313	55	129	8	24	104	1315	49	4	22.78	1
sc102-3	23	8887	1866	60	153	6	20	112	1535	53	5	26.05	1
102-19	13	808	92	13	3	-	2197	80	121	22	1	0.17	-
sc102-8	12	431	115	-	-	-	290	10	9	2	-	0.03	-
sc102-10	51	742	571	-	-	-	127	10	3	2	-	0.03	-
102-11	345	3568	3299	-	-	-	13	71	8	15	-	0.08	-
sc102-4	267	2630	2381	-	3	-	49	109	113	23	-	0.39	-
sc102-7	253	2557	2901	-	-	-	13	91	55	18	-	0.09	-
102-18	223	2419	2341	-	-	-	44	61	13	12	-	0.08	-
102-17	76	838	1306	-	1	-	67	178	255	32	-	0.13	-
sc102-5	73	1112	760	-	1	-	11	50	75	13	-	0.20	-
sc102-6	34	719	553	-	1	-	3	7	6	2	-	0.08	-
102-12	24	261	416	-	-	-	33	18	14	2	-	0.02	-
102-13	70	794	1177	-	-	-	79	18	15	4	-	0.05	-
102-15	16	332	231	-	-	-	509	198	291	32	1	0.06	-
102-16	6	147	110	-	-	-	326	65	81	10	-	0.04	-

Table 14A. LA-ICP-MS analyses of the lower saprolite minerals (Sample SCRB07, 54-55 m). All data in ppm, except for Al and Si in wt% oxides, and Mn and Fe in % element. Internal standard: Al stoichiometric values normalised to 100% wt oxides.

Analyses	Mineralogy	<sup>24</sup> Mg	<sup>27</sup> Al	<sup>29</sup> Si	<sup>31</sup> P	<sup>39</sup> K	<sup>45</sup> Sc	<sup>47</sup> Ti	<sup>51</sup> V	<sup>53</sup> Cr	<sup>55</sup> Mn	<sup>57</sup> Fe	<sup>59</sup> Co
sc07-1	Mica+kaolinite+goethite	0.18	26.0	42.6	1873	8.35	40	470	298	164	0.01	13.5	7
sc07-2	Mica+kaolinite+goethite	0.13	22.0	46.1	2799	6.13	39	1257	251	144	0.02	15.6	10
sc07-22	Coronadite+Fe	-	1.0	3.9	1486	0.03	7	62	2206	37	28.58	7.3	2990
sc07-24	Coronadite+Fe+qtz	-	1.3	11.8	1971	0.09	7	215	1808	43	25.50	6.1	3264
sc07-20	Clays+coronadite+Fe	0.01	5.4	7.9	1837	0.29	7	1400	937	43	23.17	6.9	9559
sc07-25	Coronadite+Fe+qtz	0.01	6.2	8.5	1942	0.19	7	104	1045	43	23.09	6.1	8998
sc07-10	Kaolinite+coronadite	0.02	7.1	7.5	8635	0.52	13	114	1023	74	22.70	3.7	8479
sc07-5	Coronadite+plumbogummite	0.01	7.8	6.5	14638	0.25	15	357	1047	76	22.10	2.7	6353
sc07-7	Clays+coronadite	0.04	7.6	11.6	3218	1.29	14	189	912	62	21.36	6.4	7659
sc07-9	Coronadite+quartz	0.01	1.8	35.0	1736	0.26	5	187	1490	44	21.08	0.9	3230
sc07-4	Coronadite+quartz	0.02	3.7	20.1	2211	0.68	9	498	1110	47	20.99	5.1	5081
sc07-6	Clay+qtz+coronadite	0.03	5.8	20.1	2058	1.32	13	406	911	60	19.39	6.2	5876
sc07-18	Quartz+coronadite+clays	0.02	9.0	26.6	3946	0.89	10	244	983	46	19.25	1.8	4677
sc07-11	Coronadite+quartz+clays	0.02	5.1	24.3	4873	0.95	10	377	887	53	19.19	3.0	6592
sc07-13	Clays+coronadite+ quartz	0.01	14.8	20.8	4045	0.44	11	187	685	50	18.35	2.8	5574
sc07-12	Clays+coronadite+plumbo	0.01	15.0	14.8	10803	0.43	16	160	709	62	18.30	3.2	5267
sc07-8	Coronadite+quartz+clays	0.02	4.9	28.8	4168	0.89	11	3875	906	52	18.22	2.8	5271
sc07-14	Clays+coronadite+(Plumbo?)	0.07	16.3	20.8	3706	3.03	27	218	957	72	17.32	2.4	5258
sc07-15	Clays+coronadite+(Plumbo?)	0.02	17.7	23.6	5961	1.13	12	113	749	50	15.71	2.4	5582
sc07-17	Quartz+coronadite	0.01	1.3	51.4	449	0.26	4	6086	1074	24	15.48	1.1	2311

Table 14B. LA-ICP-MS analyses of the lower saprolite minerals (Sample SCRB07, 54-55 m). All data in ppm, except for Pb in % element. Internal standard: Al stoichiometric values normalised to 100% wt oxides.

Analyses	<sup>60</sup> Ni	<sup>65</sup> Cu	<sup>66</sup> Zn	<sup>75</sup> As	<sup>98</sup> Mo	<sup>115</sup> In	<sup>121</sup> Sb	<sup>137</sup> Ba	<sup>139</sup> La	<sup>140</sup> Ce	<sup>141</sup> Pr	<sup>184</sup> W	<sup>208</sup> Pb	<sup>209</sup> Bi
sc07-1	19	5457	743	172	10	-	16	491	19	25	3	1	0.77	-
sc07-2	21	6303	870	205	11	-	21	404	35	38	5	2	1.35	-
sc07-22	21	3990	174	35	4	-	2	17	19	2776	6	1	35.07	-
sc07-24	18	3969	211	42	6	-	3	25	35	2939	8	1	32.37	-
sc07-20	45	5365	474	33	9	-	3	38	33	2168	10	2	34.14	-
sc07-25	31	5914	421	34	10	-	2	31	33	3795	10	1	33.82	-
sc07-10	19	6850	394	80	12	-	4	88	158	2396	34	2	35.14	-
sc07-5	17	6945	270	106	8	-	4	113	300	2541	64	3	37.41	-
sc07-7	21	7172	557	83	11	-	6	113	57	1917	10	2	29.85	-
sc07-9	7	3796	97	25	6	-	2	31	33	1673	7	1	24.19	-
sc07-4	16	5471	413	73	8	-	6	68	38	1944	8	2	29.38	-
sc07-6	17	6336	548	85	10	-	7	102	30	1954	6	3	27.27	-
sc07-18	14	4995	202	47	7	-	3	85	59	2761	12	1	25.17	-
sc07-11	15	5596	312	56	10	-	4	91	219	2152	44	2	28.58	-
sc07-13	19	5777	306	44	8	-	2	55	64	2647	14	1	25.96	-
sc07-12	18	6502	310	74	7	-	3	88	173	2357	38	2	29.36	-
sc07-8	13	4978	251	49	8	-	5	84	71	1638	15	2	26.57	-
sc07-14	15	4709	250	46	8	-	3	223	59	2309	12	2	23.76	-
sc07-15	16	4826	303	68	8	-	3	107	92	2038	17	1	23.61	-
sc07-17	6	2869	64	14	4	-	3	32	4	1827	1	8	16.91	-

Table 15A. LA-ICP-MS analyses of the lower saprolite minerals (Sample SCRB07, 54-55 m). All data in ppm, except for Al and Si in wt% oxides, and Fe in % element. Internal standard: Al stoichiometric values normalised to 100% wt oxides.

Analyses	Mineralogy	<sup>24</sup> Mg	<sup>27</sup> Al	<sup>29</sup> Si	<sup>31</sup> P	<sup>39</sup> K	<sup>47</sup> Ti	<sup>51</sup> V	<sup>53</sup> Cr	<sup>55</sup> Mn	<sup>57</sup> Fe	<sup>59</sup> Co
07-37	Mica	0.20	35.0	50.5	42	9.87	631	216	105	5	1.6	1
07-35	Mica	0.24	34.5	50.5	42	9.51	568	217	159	7	1.7	1
07-33	Mica	0.20	34.5	50.8	34	9.37	598	212	115	6	1.9	1
07-32	Mica	0.20	35.0	51.4	34	9.37	578	214	175	5	1.7	1
07-36	Mica + (plumbogummite?)	0.20	32.5	48.5	204	9.11	23103	217	175	10	2.7	2
07-34	Mica + Ti-ml +(plumbogummite)	0.23	31.0	47.6	113	8.77	48312	220	146	11	2.3	2
07-39	Quartz+mica+corrensite+ilmenite	0.54	10.0	82.1	70	2.17	742	46	58	46	2.5	8
07-31	Quartz + mica + corrensite	0.35	10.6	81.6	238	1.60	870	49	32	37	2.9	8
07-30	Mica + corrensite+quartz	3.27	15.8	55.4	186	1.62	587	92	121	321	14.4	62
07-40	Mica + corrensite+quartz	2.26	19.5	57.6	105	2.89	323	106	169	212	10.6	44

Table 15B. LA-ICP-MS analyses of the lower saprolite minerals (Sample SCRB07, 54-55 m). All data in ppm. Internal standard: Al stoichiometric values normalised to 100% wt oxides. (-: below detection limit).

Analyses	<sup>60</sup> Ni	<sup>65</sup> Cu	<sup>66</sup> Zn	<sup>75</sup> As	<sup>98</sup> Mo	<sup>121</sup> Sb	<sup>137</sup> Ba	<sup>140</sup> Ce	<sup>181</sup> Ta	<sup>184</sup> W	<sup>208</sup> Pb	<sup>209</sup> Bi
07-37	2	19	11	-	-	1	650	-	-	1	61	-
07-35	3	40	17	-	-	1	543	1	-	1	139	-
07-33	5	85	15	2	-	1	574	1	-	1	158	-
07-32	4	44	17	-	-	-	578	-	-	1	109	-
07-36	10	233	23	6	-	5	570	8	1	4	1209	-
07-34	9	229	32	6	-	13	542	12	2	8	569	-
07-39	18	350	113	4	-	1	161	19	-	1	981	-
07-31	21	564	116	3	-	1	117	16	-	-	1878	-
07-30	136	2847	929	20	-	1	191	106	-	1	6483	-
07-40	87	1767	658	7	-	-	255	91	-	-	4858	-

Table 16A. LA-ICP-MS analyses of the lower saprolite minerals (Sample SCRB10, 44-45 m). All data in ppm, except for Al and Si in wt% oxides, and Mn and Fe in % element. Internal standard: Al stoichiometric values normalised to 100% wt oxides.

Analyses	Mineralogy	<sup>24</sup> Mg	<sup>27</sup> Al	<sup>29</sup> Si	<sup>31</sup> P	<sup>39</sup> K	<sup>45</sup> Sc	<sup>47</sup> Ti	<sup>51</sup> V	<sup>53</sup> Cr	<sup>55</sup> Mn	<sup>57</sup> Fe	<sup>59</sup> Co	<sup>60</sup> Ni
sc10-15	Fe oxides	293	1.7	3.3	328	2	52	51	120	27	0.04	65.9	41	23
sc10-18	Fe oxides	250	1.9	3.6	358	54	47	84	149	36	0.04	65.3	64	31
sc10-17	Fe oxides	363	2.0	3.8	406	-	57	77	130	34	0.04	64.3	42	34
sc10-14	Fe oxides	957	2.4	4.2	465	12	51	15	160	40	0.04	63.7	30	74
sc10-19	Fe oxides	100	1.6	8.2	304		24	24	129	36	0.03	62.9	14	10
sc10-13	Fe oxides	244	3.2	4.2	577	15	74	24	221	54	0.03	62.8	68	92
sc10-12	Fe oxides+chlorite	15129	6.9	8.3	311	89	52	64	169	66	0.07	56.8	73	134
sc10-20	Fe oxides+quartz	198	5.1	39.7	219	2	233	2248	147	52	0.01	37.8	6	8
sc10-21	Fe oxides+quartz+clays	200	13.5	39.3	144	239	29	990	130	60	0.01	32.9	6	20
sc10-2	Coronadite	116	1.2	0.8	34	307	12	15	4952	-	38.45	0.6	3678	129
sc10-3	Coronadite	96	1.0	0.7	37	160	12	3	6078	2	38.17	0.1	3185	144
sc10-4	Coronadite	107	1.1	0.8	34	530	13	4	6002	0	37.97	0.1	3218	146
sc10-5	Coronadite+mica	1553	5.0	6.7	56	8033	24	132	3328	3	32.41	3.7	4710	193
sc10-6	Coronadite+mica+Ti	891	6.8	10.9	31	13069	25	8249	1130	13	31.30	1.9	6065	198
sc10-8	Coronadite + mica	969	7.8	11.2	56	11311	22	108	3766	18	29.35	3.4	2619	135
sc10-10	Coronadite+mica	475	9.8	17.7	55	12009	22	2105	2911	24	26.09	2.1	3507	74
sc10-22	K/m+coronadite+Fe	306	18.0	20.3	114	9965	25	120	1066	48	22.05	5.9	994	88
sc10-23	K/m+coronadite+Fe	637	18.5	21.6	106	11166	36	5591	784	65	20.49	10.4	1335	1270
sc10-9	Coronadite+Ti+qtz+mica	701	4.2	24.1	100	6137	72	142291	1716	62	14.38	5.7	2123	72
sc10-24	K/m+coronadite+Fe	643	18.5	25.4	86	24937	50	31635	1236	83	14.06	10.9	485	73
sc10-7	K/m+ coronadite+ Al-Co	857	21.0	39.3	42	16652	26	319	934	27	13.78	1.7	8449	476
sc10-11	Quartz+coronadite+mica	1259	4.7	54.4	71	7161	13	194	880	14	13.68	2.2	4631	202
sc10-25	K/m+coronadite+Fe	377	14.8	19.2	170	7972	31	366	855	126	12.67	26.8	558	248

Table 16B. LA-ICP-MS analyses of the upper saprolite minerals (Sample SCRB10, 44-45 m). All data in ppm except for Pb in % element. Internal standard: Al stoichiometric values normalised to 100% wt oxides. (-: below detection limit).

Analyses	<sup>65</sup> Cu	<sup>66</sup> Zn	<sup>75</sup> As	<sup>82</sup> Se	<sup>98</sup> Mo	<sup>121</sup> Sb	<sup>137</sup> Ba	<sup>139</sup> La	<sup>140</sup> Ce	<sup>141</sup> Pr	<sup>184</sup> W	<sup>208</sup> Pb	<sup>209</sup> Bi
sc10-15	18439	2962	1519	45	24	19	2	6	21	4	-	0.30	-
sc10-18	16907	2866	1139	39	37	18	4	6	17	4	-	0.33	-
sc10-17	20500	3385	1299	46	32	17	3	7	20	5	-	0.31	-
sc10-14	16347	3008	1074	43	52	18	4	6	16	5	-	0.35	-
sc10-19	8465	861	1301	22	21	39	2	4	10	3	-	0.47	2
sc10-13	23727	3902	1208	45	92	15	3	5	10	4	-	0.32	-
sc10-12	13219	2623	779	21	43	13	11	5	14	3	-	0.31	-
sc10-20	4223	490	692	19	13	23	6	34	67	17	4	0.35	3
sc10-21	3808	391	390	9	12	10	9	7	13	3	1	0.26	1
sc10-2	19366	408	26	1	47	1	1812	179	401	91	-	30.96	-
sc10-3	21382	403	24	2	53	1	1618	197	258	101	-	31.16	-
sc10-4	21409	414	25	1	53	1	1620	198	260	102	-	30.69	-
sc10-5	15270	449	33	2	46	-	2177	230	380	91	1	25.03	-
sc10-6	14486	312	17	-	11	1	4342	104	244	52	3	21.75	-
sc10-8	13299	279	32	-	40	1	1759	158	249	72	1	24.22	-
sc10-10	11231	230	25	1	35	1	1092	107	1060	52	1	22.31	-
sc10-22	5187	250	37	1	11	3	6485	185	370	57	0	14.10	-
sc10-23	5947	705	62	3	18	8	17687	286	277	90	1	8.65	-
sc10-9	7408	280	57	3	14	19	1061	97	292	42	19	14.70	-
sc10-24	4184	354	65	1	9	13	4870	140	231	45	7	9.17	-
sc10-7	7391	392	12		12	-	1843	69	201	32	-	9.91	-
sc10-11	6772	311	18		12	1	1193	66	167	31	-	11.53	-
sc10-25	4955	484	192	7	14	22	11822	244	200	77	1	5.80	1



Table 17A. LA-ICP-MS analyses of the upper saprolite minerals (Sample SCRB103, 59-60 m). All data in ppm, except for Al and Si in wt% oxides, and Ti, Mn and Fe in % element. Internal standard: Al stoichiometric values normalised to 100% wt oxides.

Analyses	Mineralogy	<sup>24</sup> Mg	<sup>27</sup> Al	<sup>29</sup> Si	<sup>31</sup> P	<sup>39</sup> K	<sup>47</sup> Ti	<sup>51</sup> V	<sup>53</sup> Cr	<sup>55</sup> Mn	<sup>57</sup> Fe	<sup>59</sup> Co
103-31	Mica/kaolinite	0.71	30.5	54.3	39	7.15	0.12	204	11	0.00	3.8	5
103-27	Mica/kaolinite	0.54	32.5	55.9	42	5.39	0.18	142	20	0.00	2.8	4
103-18	Kaolinite/mica	0.45	34.5	56.2	50	4.87	0.06	156	8	0.13	1.8	8
103-28	Kaolinite/mica	0.61	32.0	55.9	45	4.85	0.07	150	20	0.00	4.0	7
103-22	Kaolinite/mica	0.33	36.0	56.1	65	4.02	0.06	103	14	0.00	1.7	3
103-32	Kaolinite/mica	0.50	33.5	55.9	53	3.94	0.06	131	15	0.00	3.6	5
103-17	Kaolinite/mica	0.33	35.5	57.2	52	3.51	0.04	121	7	0.07	1.6	6
103-23	Kaolinite/mica	0.25	36.0	57.8	47	2.80	0.03	84	10	0.00	1.6	2
103-16	Kaolinite/mica	0.17	38.0	58.5	69	1.28	0.02	95	14	0.19	1.3	13
103-29	Kaolinite/mica	0.21	37.5	59.3	52	1.13	0.02	54	14	0.00	1.4	3
103-6	kaolinite+quartz	0.09	32.0	64.4	41	0.41	0.02	38	14	0.00	1.5	3
103-33	Mica/kaolinite +Ti	0.51	28.0	57.5	67	3.60	1.94	120	32	0.00	4.2	8
103-14	Mica+coronadite	0.64	29.0	49.7	179	6.02	0.11	850	25	2.74	3.0	103
103-30	Mica+coronadite	0.28	11.5	24.8	267	3.14	0.17	1612	391	16.61	6.1	477
103-12	Mica+coronadite	0.33	19.0	34.3	183	3.63	0.15	857	136	12.04	5.5	451
103-13	Mica+coronadite	0.26	19.5	34.3	187	2.60	0.15	1003	149	11.73	4.8	426
103-15	Mica+tornebohmite	0.29	30.5	50.0	223	2.86	0.08	1003	33	3.75	2.7	159
103-7	Smectites+quartz+m/k	3.22	16.0	45.8	43	1.28	0.03	110	34	0.02	20.4	48
103-8	Smectites + quartz + m/k	4.09	19.0	48.6	47	2.05	0.03	86	24	0.02	15.9	53
103-19	Ti + mica	0.23	2.4	6.5	238	0.59	51.01	324	63	0.02	5.5	9
103-20	Ti + mica+ coronadite	0.05	1.7	6.6	222	0.12	25.58	1192	388	14.18	6.2	552
103-24	Ti + mica	0.07	6.4	12.3	77	0.41	46.94	263	46	0.01	3.3	4
103-25	Ti	0.07	1.0	2.8	59	0.23	56.55	318	50	0.01	3.2	3

Table 17B. LA-ICP-MS analyses of the upper saprolite minerals (Sample SCRB103, 59-60 m). All data in ppm, except for Pb in element %. Internal standard: Al stoichiometric values normalised to 100% wt oxides. (-: below detection limit).

Analyses	<sup>60</sup> Ni	<sup>65</sup> Cu	<sup>66</sup> Zn	<sup>75</sup> As	<sup>98</sup> Mo	<sup>115</sup> In	<sup>118</sup> Sn	<sup>121</sup> Sb	<sup>137</sup> Ba	<sup>140</sup> Ce	<sup>184</sup> W	<sup>208</sup> Pb	<sup>209</sup> Bi
103-31	22	251	67	-	-	-	2	-	1290	1	-	0.05	-
103-27	20	192	56	-	-	-	3	-	810	3	-	0.04	-
103-18	17	98	37	1	-	-	2	-	743	329	-	0.15	-
103-28	39	437	113	-	-	-	4	-	794	3	-	0.07	-
103-22	24	121	53	1	-	-	1	-	610	2	-	0.03	-
103-32	31	341	107	1	-	-	2	-	633	1	-	0.08	-
103-17	20	129	48	-	-	-	1	-	576	130	-	0.13	-
103-23	22	110	43	-	-	-	1	-	455	1	-	0.02	-
103-16	26	163	56	1	-	-	1	-	196	348	-	0.22	-
103-29	28	192	76	-	-	-	-	-	169	-	-	0.03	-
103-6	26	174	67	5	-	-	-	-	71	1	-	0.04	-
103-33	45	554	180	4	1	-	5	12	561	8	7	0.15	-
103-14	13	413	63	5	2	-	2	-	1009	9919	-	2.68	-
103-30	8	1697	82	10	22	-	1	2	502	1259	-	20.45	-
103-12	16	1327	115	7	10	-	1	1	616	1340	-	13.99	-
103-13	11	1364	95	7	10	-	1	1	456	2328	-	14.95	-
103-15	16	512	66	6	4	-	1	-	512	12503	-	4.10	-
103-7	157	2573	1250	5	-	-	-	-	12	3	-	0.73	-
103-8	130	2240	1131	4	-	-	1	-	6	4	-	0.52	-
103-19	55	604	154	18	2	-	20	64	162	1408	101	0.27	-
103-20	25	1650	188	18	18	-	10	36	32	1851	36	16.61	-
103-24	31	293	110	18	7	-	15	55	92	84	64	0.21	1
103-25	16	205	112	29	6	-	18	80	74	101	84	0.16	1

Table 18A. LA-ICP-MS analyses of the upper saprolite minerals (Sample SCRB05, 34-35 m). All data in ppm, except for Al and Si in wt% oxides, and Mn and Fe in % element. Internal standard: Al stoichiometric values normalised to 100% wt oxides. Kaol = Kaolinite; qtz = Quartz

Analyses	Mineralogy	<sup>24</sup> Mg	<sup>27</sup> Al	<sup>29</sup> Si	<sup>31</sup> P	<sup>39</sup> K	<sup>45</sup> Sc	<sup>47</sup> Ti	<sup>51</sup> V	<sup>53</sup> Cr	<sup>55</sup> Mn	<sup>57</sup> Fe	<sup>59</sup> Co
sc05-1	Mica+kaol?+qtz+PbMn	1006	19.0	25.8	450	2.70	34	491	806	37	18.40	2.1	4822
sc05-2	Kaol-mica-PbMn-	841	17.5	15.1	449	1.54	24	469	473	24	24.21	3.3	28109
sc05-3	Mica+Kaol-PbMn	549	15.1	15.7	285	1.39	20	286	448	14	26.98	1.5	13659
sc05-4	Kaol+PbMn	205	8.8	9.2	363	0.39	8	282	643	7	32.74	1.9	3062
sc05-5	Kaol+PbMn	711	23.0	24.4	308	1.33	20	349	319	18	18.46	2.2	19744
sc05-6	Mica+kaol+PbMn	668	16.3	26.2	333	1.15	18	320	426	15	21.41	2.0	19413
sc05-7	Kaol+bit of mica+qtz+PbMn	339	21.6	26.9	633	0.54	14	328	498	19	15.63	4.5	1657
sc05-8	Kaol+bit of mica+qtz+PbMn	421	15.5	18.5	873	0.82	16	552	584	20	19.72	5.9	3811
sc05-9	MnPb+lithiophorite+kaol+qtz	237	4.9	1.9	1681	0.07	12	4448	891	19	28.82	10.2	12076
sc05-10	Kaol-mica-PbMn+qtz	349	27.5	34.0	196	0.70	16	126	114	21	14.02	0.6	963
sc05-11	Kaol+bit mica+PbMn+qtz	363	14.0	15.9	718	1.28	21	326	427	33	24.48	3.3	2710
sc05-12	Kaol+PbMn	229	10.7	12.6	1077	0.45	12	600	513	22	24.24	7.5	2327
sc05-13	Mica-kaol+PbMn	437	13.5	26.6	718	1.30	21	528	457	35	18.81	6.0	2391
sc05-14	Kaol-mica-PbMn	277	16.0	19.1	746	0.45	13	435	471	14	20.49	7.4	2725
sc05-15	Kaol-mica-PbMn	380	9.7	11.7	609	0.50	13	1012	1112	29	26.92	4.8	14124
sc05-16	Kaol-PbMn	344	7.3	7.8	619	0.33	11	328	1078	28	30.01	5.1	11589
sc05-17	Coronadite	157	3.6	3.7	935	0.03	8	391	1737	20	30.72	6.3	12714
sc05-18	Kaol+Pb-Mn	356	16.5	19.8	716	0.43	12	589	1043	31	19.81	5.6	8914
sc05-19	Ti ml+kaol+goethite+PbMn+Fe	259	4.2	7.3	719	0.38	25	142015	515	49	15.14	15.1	2840
sc05-20	Kaol+PbMn+mica	505	20.5	24.0	524	0.93	16	315	466	19	17.88	2.5	3258
sc05-21	qtz+PbMn	198	4.1	42.8	734	0.20	11	732	563	17	16.60	4.1	4363
sc05-22	Kaol+mica+qtz+PbMn	413	8.2	23.1	731	0.71	14	540	620	27	22.46	6.5	3438
sc05-24	Kaol+PbMn	293	8.1	11.5	632	0.47	12	475	666	17	28	6.5	5723

Table 18B. LA-ICP-MS analyses of the upper saprolite minerals (Sample SCRB05, 34-35 m). All data in ppm, except for Pb in % element. Internal standard: Al stoichiometric values normalised to 100% wt oxides.

Analyses	<sup>60</sup> Ni	<sup>65</sup> Cu	<sup>66</sup> Zn	<sup>75</sup> As	<sup>98</sup> Mo	<sup>115</sup> In	<sup>121</sup> Sb	<sup>137</sup> Ba	<sup>139</sup> La	<sup>140</sup> Ce	<sup>141</sup> Pr	<sup>184</sup> W	<sup>208</sup> Pb	<sup>209</sup> Bi
sc05-1	149	7082	485	35	22	-	-	3065	111	3808	28	2	15.66	1
sc05-2	1336	19024	3254	41	104	-	-	3678	116	3257	21	11	14.11	1
sc05-3	530	13134	1400	19	57	-	-	5110	94	872	13	5	16.57	-
sc05-4	60	14739	597	22	19	-	-	6910	135	734	15	4	21.73	1
sc05-5	876	12494	2082	24	68	-	-	2408	83	1346	18	8	11.94	1
sc05-6	904	14781	2116	21	77	-	-	4270	106	2511	17	8	12.85	-
sc05-7	32	9082	1121	71	41	-	-	433	123	2604	23	6	15.61	4
sc05-8	39	10090	1324	111	78	-	1	719	141	1569	25	22	20.24	6
sc05-9	692	18849	3594	146	103	-	1	837	246	7496	42	10	23.82	5
sc05-10	14	4675	144	8	2	-	-	378	24	3993	6	1	12.08	-
sc05-11	21	9758	499	65	30	-	-	2057	78	2786	12	8	19.93	1
sc05-12	19	9873	939	149	126	-	2	764	134	688	20	26	22.71	3
sc05-13	54	7094	808	86	39	-	-	2757	175	828	24	8	16.27	1
sc05-14	73	7685	1008	88	31	-	-	3026	213	917	29	6	17.59	1
sc05-15	413	10756	849	58	31	-	-	5678	204	3583	43	3	21.87	3
sc05-16	288	12905	933	57	29	-	-	7424	245	3537	43	3	23.35	3
sc05-17	282	11649	813	90	52	-	-	2891	200	5633	54	3	28.14	3
sc05-18	204	7516	735	70	28	-	-	991	127	3780	40	2	19.50	2
sc05-19	110	9011	35060	116	25	-	3	1850	118	1787	20	11	12.42	2
sc05-20	25	10774	822	56	160	-	1	553	50	1556	11	25	17.35	3
sc05-21	149	11090	1185	72	68	-	-	1139	102	7758	20	9	15.49	4
sc05-22	98	11271	1302	75	29	-	-	2502	156	1365	26	4	19.27	2
sc05-24	150	12105	1157	56	28	-	-	4767	211	1466	30	4	21.48	2

Table 19A. LA-ICP-MS analyses of the upper saprolite minerals (Sample SCRB10, 14-15 m). All data in ppm, except for Al and Si in wt% oxides, and Fe in % element. Internal standard: Al stoichiometric values normalised to 100% wt oxides

Analyses	Mineralogy	<sup>24</sup> Mg	<sup>27</sup> Al	<sup>29</sup> Si	<sup>31</sup> P	<sup>39</sup> K	<sup>47</sup> Ti	<sup>51</sup> V	<sup>53</sup> Cr	<sup>55</sup> Mn	<sup>57</sup> Fe	<sup>59</sup> Co	<sup>60</sup> Ni
10-35	Quartz+mica	387	14.0	80.3	59	18479	738	112	556	31	2.4	1	9
10-36	Quartz+mica	343	15.0	79.3	69	17989	13549	90	292	11	0.4	2	9
10-34	Quartz+mica	323	6.2	91.1	51	13077	1217	45	348	16	0.3	2	4
10-38	Quartz mainly	296	0.8	99.0	43	265	141	2	10	21	0.2	-	3
10-37	Quartz mainly	478	0.8	98.1	56	167	514	7	11	181	0.5	4	4
10-40	Quartz mainly	139	0.4	96.8	63	259	1152	3	14	13	0.2	2	2
10-43	Quartz mainly	226	1.7	95.6	47	2766	191	12	85	26	0.3	1	3
10-44	Kaolinite+ Fe oxides+quartz	485	21.0	37.0	152	359	743	470	854	556	28.4	3	18
10-48	Kaolinite+ Fe oxides+quartz	207	15.3	45.6	426	1352	1393	1805	1069	268	27.2	12	39
10-50	Kaolinite+ Fe oxides+quartz	236	19.5	48.8	142	114	336	463	617	80	22.0	3	13
10-32	Kaolinite+ Fe oxides+quartz	498	27.5	44.9	113	537	394	311	485	429	18.6	3	22
10-30	Quartz+Fe oxides+kaolinite	768	9.7	66.7	100	222	360	275	374	562	16.2	2	7
10-33	Kaolinite+quartz+Fe oxides	829	21.5	58.0	159	854	357	264	427	362	14.5	3	21
10-46	Kaolinite+quartz+Fe oxides	489	25.0	53.4	91	558	295	244	377	282	13.9	2	28
10-39	Kaolinite+quartz+Fe oxides	459	22.0	59.0	91	173	429	239	357	258	13.0	3	25
10-42	Kaolinite+quartz+Fe oxides	446	27.5	52.9	99	445	451	247	331	185	12.6	3	29
10-31	Quartz+kaolinite+Fe oxides	435	15.5	65.8	99	240	1585	221	338	238	12.6	3	16
10-47	Quartz+kaolinite+Fe oxides	461	32.0	50.2	94	448	242	198	365	318	11.7	2	25
10-45	Quartz +kaolinite+ Fe oxides	306	9.6	74.3	77	277	498	158	267	176	10.2	2	11
10-49	Quartz+kaolinite+Fe oxides	242	32.0	53.3	97	55	167	202	476	37	9.6	3	24
10-41	Quartz+kaolinite	208	12.6	83.6	43	71	448	47	78	26	1.3	2	15

Table 19B. LA-ICP-MS analyses of the upper saprolite minerals (Sample SCRB10, 14-15 m). All data in ppm. Internal standard: Al stoichiometric values normalised to 100% wt oxides.

Analyses	<sup>65</sup> Cu	<sup>66</sup> Zn	<sup>75</sup> As	<sup>98</sup> Mo	<sup>115</sup> In	<sup>121</sup> Sb	<sup>137</sup> Ba	<sup>140</sup> Ce	<sup>184</sup> W	<sup>208</sup> Pb	<sup>209</sup> Bi
10-35	153	51	13	3	1	2	184	2	1	80	-
10-36	100	22	5	-	-	4	183	11	6	44	-
10-34	14	49	4	-	-	2	161	11	-	18	-
10-38	4	8	-	-	-	1	9	-	-	4	-
10-37	26	10	7	3	-	3	7	6	-	18	-
10-40	11	7	3	1	-	2	32	31	-	25	-
10-43	11	19	3	-	-	1	48	10	-	16	-
10-44	745	79	108	29	3	29	2	6	1	908	7
10-48	3599	252	372	222	-	441	6	13	1	730	9
10-50	804	63	125	26	6	45	5	5	-	663	3
10-32	701	92	82	15	-	17	3	5	1	552	9
10-30	541	54	72	14	1	12	2	3	-	438	3
10-33	850	81	69	18	2	13	4	4	-	433	2
10-46	560	64	63	12	2	9	2	5	-	525	2
10-39	608	60	61	14	2	8	3	9	1	478	2
10-42	588	70	49	14	1	12	2	4	1	405	3
10-31	659	66	63	13	1	10	3	8	1	310	2
10-47	626	63	51	10	2	7	2	3	-	367	2
10-45	347	39	42	9	1	8	5	4	-	273	2
10-49	603	54	56	11	4	18	4	3	-	306	2
10-41	250	42	12	4	-	2	4	3	-	70	-

Table 20A. LA-ICP-MS analyses of the upper saprolite minerals (Sample SCRB10, 9-10 m). All data in ppm, except for Al and Si in wt% oxides, and Fe in % element. Internal standard: Al stoichiometric values normalised to 100% wt oxides.

Analyses	Mineralogy	<sup>24</sup> Mg	<sup>27</sup> Al	<sup>29</sup> Si	<sup>31</sup> P	<sup>39</sup> K	Sc45	<sup>47</sup> Ti	<sup>51</sup> V	<sup>53</sup> Cr	<sup>55</sup> Mn	<sup>57</sup> Fe	<sup>59</sup> Co
10-12	Mica-kaolinite	1515	35.0	53.7	15	8.37	68	3594	271	35	9	-	1
10-13	Mica-kaolinite	1332	38.0	51.1	22	7.64	61	359	244	34	11	-	1
10-25	Kaolinite+mica+quartz	517	34.0	62.2	4	2.31	19	586	127	68	13	-	3
10-14	Kaolinite+mica+quartz	500	38.5	58.4	85	2.06	31	290	162	64	7	-	4
10-16	Kaolinite+mica+quartz	385	30.5	66.8	49	1.26	17	239	145	67	7	-	3
10-29	Quartz+mica+kaolinite	306	13.0	78.0	-	1.25	10	314	62	34	9	-	2
10-24	Quartz+mica+kaolinite	332	27.0	69.4	137	1.15	15	283	93	57	7	-	3
10-26	Quartz+mica+kaolinite	309	39.0	59.8	-	0.87	8	334	120	497	4	-	5
10-23	Quartz+mica+kaolinite	189	11.7	86.8	15	0.70	10	1627	51	26	4	-	2
10-17	Quartz+mica+kaolinite	136	8.5	90.3	45	0.18	3	319	26	17	6	-	2
10-15	Quartz+mica+kaolinite	345	28.5	70.3	49	0.76	10	297	83	41	9	0.1	3
10-27	Quartz+kaolinite	148	3.3	96.2	-	0.26	4	1223	17	21	5	-	1
10-28	Quartz+kaolinite	115	3.9	94.5	-	0.24	4	315	20	29	4	-	1
10-2	Quartz+kaolinite	119	38.5	60.9	38	-	12	165	85	63	2	-	4
10-3	Quartz+kaolinite	91	29.0	64.8	39	-	26	32450	165	63	5	-	3
10-4	Quartz+kaolinite	172	35.0	64.6	32	-	12	265	90	68	3	-	3
10-5	Quartz+kaolinite	134	39.0	60.4	79	0.02	16	358	94	69	3	-	4
10-6	Quartz+kaolinite	185	30.0	70.5	38	0.01	7	585	67	60	9	-	3
10-7	Quartz+kaolinite	104	38.0	61.7	51	0.01	10	524	106	80	3	-	4
10-8	Quartz+kaolinite	95	31.0	67.5	49	0.01	14	7674	102	60	3	-	4
10-18	Quartz+kaolinite	125	5.3	93.9	33	0.04	3	195	11	9	6	-	1
10-19	Quartz	154	1.5	97.9	36	0.05	2	169	4	6	6	-	2
10-20	Quartz	108	1.5	97.7	42	0.04	2	1048	4	1	5	-	1
10-21	Quartz	244	0.1	96.9	172	0.00	25	8070	6	2	13	-	1
10-22	Quartz	137	0.4	99.8	37	0.01	5	2096	3	-	7	-	1

Table 20B. LA-ICP-MS analyses of the upper saprolite minerals (Sample SCRB10, 9-10 m). All data in ppm. Internal standard: Al stoichiometric values normalised to 100% wt oxides.

Analyses	<sup>60</sup> Ni	<sup>65</sup> Cu	<sup>66</sup> Zn	<sup>75</sup> As	<sup>98</sup> Mo	<sup>115</sup> In	<sup>121</sup> Sb	<sup>137</sup> Ba	<sup>139</sup> La	<sup>140</sup> Ce	<sup>141</sup> Pr	<sup>184</sup> W	<sup>208</sup> Pb	<sup>209</sup> Bi
10-12	2	123	-	2	1	1	4	674	9	4	-	2	47	32
10-13	5	17	-	-	-	1	1	639	5	3	-	-	22	4
10-25	28	48	60	-	2	3	5	193	5	6	-	-	61	59
10-14	30	50	32	-	1	3	4	211	1	1	-	1	31	27
10-16	27	53	31	6	-	3	6	172	5	3	-	-	42	48
10-29	12	53	34	-	1	1	7	123	4	8	-	-	170	78
10-24	27	45	84	-	1	-	6	140	19	24	2	-	155	3032
10-26	45	72	98	-	2	4	5	85	1	1	-	-	30	39
10-23	14	21	37	-	-	1	10	69	1	2	-	2	60	25
10-17	10	15	20	1	-	1	5	24	1	2	-	-	36	14
10-15	31	59	12	9	-	3	1	78	1	1	-	1	28	36
10-27	3	9	14	-	1	-	5	31	-	1	-	-	27	23
10-28	3	9	16	-	-	1	5	30	1	1	-	-	38	17
10-2	45	60	78	5	1	2	4	5	2	2	-	-	24	44
10-3	43	45	96	6	1	2	19	10	4	8	1	12	27	140
10-4	51	51	169	4	-	2	4	3	1	2	-	-	20	45
10-5	59	65	208	6	1	2	4	7	12	14	2	-	100	52
10-6	30	54	45	6	1	2	9	11	2	2	-	-	32	37
10-7	55	61	131	7	1	2	4	5	2	2	-	-	27	46
10-8	39	52	94	7	1	2	7	5	2	3	-	4	53	59
10-18	6	11	15	-	-	1	4	12	1	1	-	-	33	14
10-19	2	4	6	-	-	-	3	13	-	1	-	-	27	13
10-20	1	5	5	-	-	-	4	10	1	1	-	-	29	13
10-21	1	6	2	10	1	-	6	73	3	7	-	1	62	176
10-22	1	3	3	1	1	-	3	5	3	2	-	-	31	16

Table 21. LA-ICP-MS analyses of the lower saprolite minerals (Sample SCRB102, 69-70 m). All data in ppm, except for Al and Si in wt% oxides, and Fe, Ti and Mn in % element. Internal standard: Al stoichiometric values normalised to 100% wt oxides. (-: below detection limit).

Analyses	Mineralogy	<sup>27</sup> Al	<sup>29</sup> Si	<sup>49</sup> Ti	<sup>55</sup> Mn	<sup>57</sup> Fe	<sup>77</sup> Se	<sup>82</sup> Se	<sup>91</sup> Zr	<sup>93</sup> Nb	<sup>95</sup> Mo	<sup>98</sup> Mo	<sup>107</sup> Ag	<sup>109</sup> Ag	<sup>115</sup> In	<sup>118</sup> Sn	<sup>181</sup> Ta	<sup>184</sup> W	<sup>197</sup> Au	<sup>209</sup> Bi
102-40	Ilmenite + coronadite + mica	2.6	6.8	39.83	3.75	12.2	2	1	164	439	33	29	174	282	-	17	29	8	10	1
102-41	Ilmenite + coronadite + mica	2.7	7.9	39.76	2.07	13.8	3	-	136	516	24	22	153	313	-	9	36	9	13	1
102-43	Ilmenite + coronadite + mica	6.3	13.3	29.92	6.93	13.4	5	5	277	367	51	45	306	374	-	36	31	8	10	2
102-45	Ilmenite + coronadite + mica + quartz	0.4	4.5	35.92	8.75	6.3	3	3	163	451	102	93	344	442	-	10	32	8	9	3
102-46	Ilmenite + coronadite + quartz	0.3	2.0	43.79	4.59	10.3	5	3	521	518	60	56	266	327	-	8	27	5	8	2
102-47	Ilmenite + coronadite + mica + quartz	3.7	16.7	34.62	0.03	16.1	2	1	540	428	13	13	6561	6585	-	8	34	10	13	-
102-48	Ilmenite + coronadite + mica + quartz	2.1	7.7	40.61	5.22	11.9	1	1	168	359	48	44	294	370	-	9	24	9	9	1
102-44	Quartz + mica	11.8	78.4	1.50	0.21	4.8	-	-	36	21	2	2	394	393	-	36	2	1	-	-

Table 22. LA-ICP-MS analyses of the upper saprolite minerals (Sample SCRB10, 9-10 m). All data in ppm, except for Al and Si in wt% oxides, and Fe, Ti and Mn in % element. Internal standard: Al stoichiometric values normalised to 100 % wt oxides.

Analyses	Mineralogy	<sup>27</sup> Al	<sup>29</sup> Si	<sup>49</sup> Ti	<sup>55</sup> Mn	<sup>57</sup> Fe	<sup>91</sup> Zr	<sup>93</sup> Nb	<sup>98</sup> Mo	<sup>109</sup> Ag	<sup>115</sup> In	<sup>181</sup> Ta	<sup>184</sup> W	<sup>197</sup> Au	<sup>209</sup> Bi
10-40	Quartz+kaolinite	5.3	91.8	1.6	-	0.1	119	9	-	216	2	-	4	-	45
10-41	Kaolinite +quartz	35.0	64.6	0.0	-	0.2	315	1	1	1102	2	-	-	-	56
10-42	Kaolinite + quartz	18.5	79.1	0.2	-	0.2	81	2	1	1470	2	-	1	-	30
10-44	Kaolinite+qtz	11.5	85.7	-	0.05	0.5	71	1	-	936	1	-	-	-	19
10-46	Quartz+kaolinite	14.0	83.3	0.2	-	0.2	74	2	1	1127	2	-	-	-	30
10-40(2)	Rutile slice	14.0	60.5	14.7	-	0.1	165	73	3	553	5	4	36	-	318

## 7. MINERALOGY AND CHEMISTRY OF SIZE FRACTIONS

### 7. 1. Introduction

Selected samples were separated into size fractions by settling velocity and sieving, and the fractions analysed by standard ICP-MS in order to compare with *in situ* analyses. The following samples have been analysed: SCRB102 (69-70 m), SCRB103 (59-60 m), SCRB07 (54-55m), SCRB09 (14–15 m) and SCRB10 (9-10 m).

Several size fractions were retrieved from the bulk samples, and in some cases sufficient material was obtained for X-ray diffraction analyses. The detailed protocol is described in Appendix 3. The following size fractions have been extracted:

1. A coarse residue obtained by washing away the finer material;
2. A decanted <5.5  $\mu\text{m}$  fraction;
3. A decanted clay fraction with particle size <2  $\mu\text{m}$ ;
4. A <0.2  $\mu\text{m}$  fraction obtained by centrifugation of the clay fraction <2  $\mu\text{m}$ ;
5. A decanted <20  $\mu\text{m}$ ;
6. A sieved fraction >13  $\mu\text{m}$ ;
7. A sieved fraction with particle sizes comprised between 5.5 and 13  $\mu\text{m}$  and
8. A “heavier” and “lighter” 5.5-13  $\mu\text{m}$  fractions obtained by decantation.

Samples consist of a mixture of quartz, booklets of mica and kaolinite of various crystal sizes and therefore are present in all the fractions. Smectites and corrensites tend to be concentrated in the finer fractions. Manganese oxides are present in the coarse residue as nodules and in the fine fractions. Iron oxides occur in the fine fractions. Quartz and accessory minerals are concentrated in the coarse residue and >13  $\mu\text{m}$  fraction. The mineral fractionation has been most effective in concentrating Mn oxides in the coarse fraction and smectites in the <2  $\mu\text{m}$  fraction.

### 7. 2. Distribution of the trace elements in the size fractions

Five size fractions have been selected for each sample and analysed with ICP-MS. Tables 23A and 23B give the particle size of the fractions and their trace elements concentrations. Figure 24 illustrates Cu, Zn, Pb and Mn distributions in the 25 fractions.

#### 7. 2. 1. Hanging wall: samples SCRB103, SCRB102 and SCRB07

Manganese is significantly concentrated in the coarse residue in the three samples where they are hosted in coronadite nodules. Lead is also enriched in the coarse residue as a major component of the Mn-oxides. It is also abundant in the other fractions, especially in SCRB07, where it is present as plumbogummite. Copper is enriched in the clay fraction (<2  $\mu\text{m}$ ) and preferentially in the fine clays (<0.2  $\mu\text{m}$ ) in sample SCRB103, in the smectites. The relatively low abundance of Cu in the coarse residue reflects the low Cu content of coronadite in this sample. Copper is abundant in all fractions in samples SCRB102 and SCRB07, with a slight preference for the clay fraction and the coarse residue. It is hosted by coronadite in the coarse residue, and in corrensite booklets which are present in all the size fractions. Zinc is abundant in the fine fractions (5.5- 13  $\mu\text{m}$  “lighter”, 0-2  $\mu\text{m}$  and <0.2  $\mu\text{m}$ ) of the three samples where it is hosted in smectites and corrensite. It is also concentrated in SCRB102 coarse residue in ilmenite-ecandrewsite. Cobalt is enriched in the coarse residue in samples SCRB102 and SCRB07 where it is present in lithiophorite and coronadite. It is relatively more abundant in SCRB103 clay fraction (<0.2  $\mu\text{m}$ ), in the smectites. Cerium is enriched in the coarse fraction of sample SCRB103, and in a lesser way in SCRB102 and SCRB07. It occurs as tornebohmite and cerianite observed in close association with the coronadite nodules. Phosphorus, abundant in all fractions of sample SCRB07, is located in plumbogummite. Tungsten is concentrated in the coarse residue of the three samples, in altered ilmenite. Antimony is greatly concentrated in SCRB07 clay fraction (<2  $\mu\text{m}$ ), possibly in

goethite. It has not been detected in the other hanging wall samples. Molybdenum occurs in SCRB102 coarse residue and in the fine clay fraction ( $<0.2\ \mu\text{m}$ ) extracted from SCRB103. However, LA-ICP-MS data show that Mo is present in coronadite in both samples. The presence of Mo in SCRB103 clay fraction suggests that it is hosted by Mn oxides replacing kaolinite and mica booklets. Surprisingly Mo has not been detected in SCRB07 size fractions although it is present in the bulk sample. Arsenic levels are low in all the fractions, the highest anomalies being in goethite in SCRB07.

#### **7. 2. 2. Over mineralisation: samples SCRB09 (14-15 m) and SCRB10 (9-10)**

Low Mn contents are present in isolated Mn oxide grains in all size fractions. Lead is evenly distributed in all the fractions in SCRB09, and is slightly enriched in SCRB10 clay fraction ( $<2\ \mu\text{m}$ ) and  $<20\ \mu\text{m}$  fraction. It is hosted in coronadite and plumbogummite. The occurrence of plumbogummite in all fractions is confirmed by the distribution of P. Copper and Zn contents are low, and are relatively enriched in the finer fractions, specially in the  $<2\ \mu\text{m}$  fraction where they are hosted in the Fe oxides. Molybdenum, Sb and As, enriched in the clay fraction ( $<2\ \mu\text{m}$ ), are contained in the Fe oxides. Bismuth, which remained undetected in SCRB09, is concentrated in all the fractions in SCRB10 with a slight preference for the finest. These data are in agreement with the LA-ICP-MS results which show that Bi occurs in minute phases scattered among the clays booklets of various sizes, and in rutile grains. Tellurium has only been detected in sample SCRB10 where it occurs preferentially in the clay fraction ( $<2\ \mu\text{m}$ ).

#### **7. 3. Effectiveness of the method**

The separation of the bulk samples into size fractions by settling velocity and sieving is a simple method which has achieved the desired goal of concentrating some elements of interest such as Cu, Zn, Mo, As, Sb, W. The coarse and clay fractions are the most effective for improving anomalies. Iron oxides, smectites and corrensite, the main constituents of the  $<2\ \mu\text{m}$  fraction, concentrate elements.

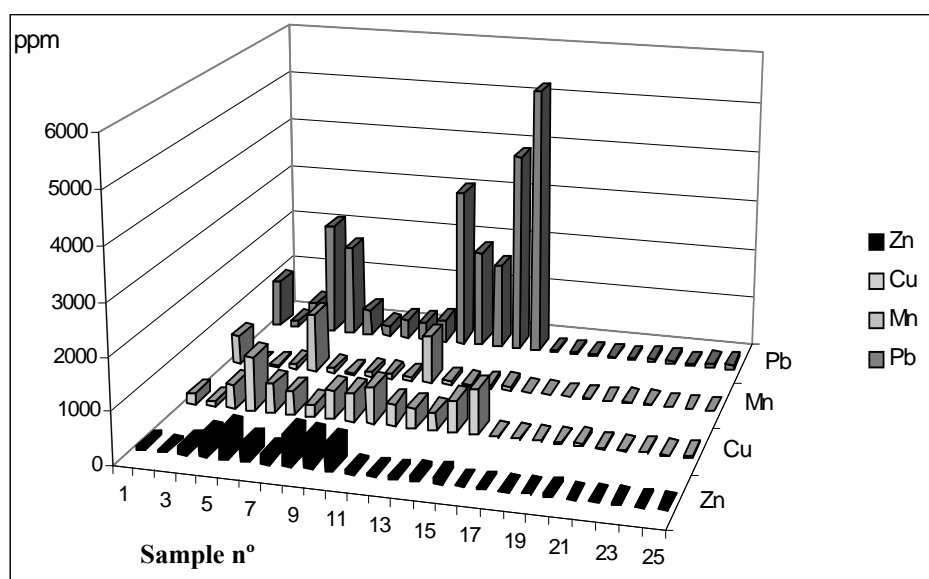


Figure 24. Copper, Zn, Mn and Pb distributions in the 25 size fractions. 1 to 5: SCRB103; 6 to 10: SCRB102; 11 to 15: SCRB07; 16 to 20: SCRB09; 21 to 25: SCRB10. The details of the size fractions are given in Table 23A and 23B.

Table 23A. Trace element concentrations in the size fractions.  
(-: no data available); Bulk: Normandy Mining Ltd data.

	Size fraction	Sample n°	Mn	Co	Ni	Cu	Zn	Pb	Ge	Rb	Sr	Cd	Ce
			ppm	ppm	ppm	ppm	ppm	ppm	ppm	ppm	ppm	ppm	ppm
SCRB103	Coarse residue	1	561.4	8.4	14.6	225.6	81.4	942.0	0.7	12.5	3.8	0.0	199.7
	5.5-13 µm heavier	2	10.6	2.1	7.6	104.3	34.0	126.3	0.0	28.2	2.4	0.0	14.2
	<2 µm	3	31.0	8.4	29.1	476.4	170.8	551.1	0.0	6.1	2.0	0.0	6.9
	<0.2 µm	4	95.5	19.5	80.8	1060.5	374.3	2212.8	1.3	5.3	2.8	0.0	14.2
	Bulk		242.0	10.0	<5	226.0	136.0	547.0	-	-	-	-	-
SCRB102	Coarse residue	5	1149.7	35.1	38.2	565.3	528.0	1788.5	0.0	38.3	5.5	0.0	90.5
	>13 µm	6	96.8	7.3	28.5	453.1	339.4	513.6	0.0	19.6	2.7	0.0	52.6
	5.5-13 µm heavier	7	36.5	4.0	16.5	240.7	185.6	219.6	0.0	18.3	2.1	0.0	15.2
	5.5-13 µm lighter	8	95.7	10.5	45.7	563.0	583.9	375.4	0.9	51.0	5.9	0.0	63.6
	<5.5 µm	9	94.1	10.1	45.0	557.6	567.7	348.2	0.8	31.4	5.2	0.0	50.6
	<2 µm	10	74.7	8.8	45.6	714.2	500.0	442.7	0.0	6.5	1.7	0.0	22.4
SCRB07	Bulk		157.0	15.0	29.0	460.0	547.0	508.0	-	-	-	-	-
	Coarse residue	11	922.2	19.7	14.3	432.2	60.5	3133.1	0.0	31.9	15.4	0.0	33.1
	>13 µm	12	71.7	5.3	13.3	390.2	52.1	1929.8	0.0	35.1	17.3	0.0	39.9
	5.5-13 µm heavier	13	44.6	4.2	12.2	344.9	47.9	1687.0	0.0	18.3	3.1	0.0	18.5
	5.5-13 µm lighter	14	68.1	7.4	23.1	610.0	86.2	3968.1	0.8	51.4	25.3	0.0	19.2
	<2 µm	15	86.4	9.6	30.7	869.3	106.8	5310.8	0.8	50.6	22.1	0.0	24.1
SCRB09	Bulk		222.0	10.0	15.0	521.0	105.0	2320.0	-	-	-	-	-
	Coarse residue	16	2.7	0.0	0.0	11.5	0.0	38.9	0.7	29.5	8.7	0.0	5.9
	>13 µm	17	4.2	0.0	0.4	15.8	17.5	33.4	0.7	24.1	0.3	0.0	9.0
	5.5-13 µm	18	2.5	0.0	2.3	17.1	4.9	31.5	1.1	47.4	10.4	0.0	12.1
	<5.5 µm	19	3.3	0.0	5.7	25.5	20.3	21.0	1.7	66.2	20.9	0.0	21.7
	<2 µm	20	4.5	0.8	9.6	60.5	44.8	30.8	2.5	55.5	6.8	0.0	8.6
SCRB10	Bulk		9.0	<5	<5	22.0	22.0	42.0	-	-	-	-	-
	Coarse residue	21	9.3	0.8	2.9	9.1	0.0	53.2	0.0	6.5	1.5	0.0	8.3
	>13 microns	22	11.6	0.8	1.5	9.7	3.5	46.7	0.0	5.4	3.3	0.0	8.5
	5.5-13 microns	23	5.9	1.2	11.2	21.9	20.0	24.2	1.0	15.6	0.9	0.0	12.9
	5.5-20 microns	24	3.8	1.1	10.3	19.9	13.0	82.3	0.0	17.1	7.6	0.0	17.8
	<2 microns	25	2.4	1.3	15.0	34.8	18.1	89.8	0.0	15.8	3.2	0.0	10.2
SCRB10	Bulk		13	<5	<5	15	26	43	-	-	-	-	-



Table 23B. Trace element concentrations in the size fractions.  
 (-: no data available); Bulk: Normandy Mining Ltd data.

	Size fraction	Sample n°	Mo	In	Sb	Bi	As	Te	W	Se	P	V	Cr
			ppm	ppm	ppm	ppm	ppm	ppm	ppm	ppm	ppm	ppm	ppm
SCRB103	Coarse residue	1	0.0	0.0	0.0	0.0	0.0	0.0	0.8	0.0	22.3	61.0	13.5
	5.5-13 µm heavier	2	0.0	0.0	0.0	0.0	0.0	0.0	0.0	0.0	24.4	61.9	8.9
	<2 µm	3	0.0	0.0	0.0	0.0	0.0	0.0	0.0	0.0	0.0	69.7	20.7
	<0.2 µm	4	1.0	0.0	0.0	0.0	1.4	0.0	0.0	0.0	79.9	87.9	35.3
	Bulk		0.3	<0.1	0.3	<0.2	-	-	-	-	-	-	-
SCRB102	Coarse residue	5	1.4	0.0	0.0	0.0	3.9	0.0	0.9	0.0	90.7	74.3	20.0
	>13 µm	6	0.0	0.0	0.0	0.0	3.2	0.0	0.0	0.0	125.4	60.2	16.6
	5.5-13 µm heavier	7	0.0	0.0	0.0	0.0	1.2	0.0	0.0	0.0	71.7	64.5	10.3
	5.5-13 µm lighter	8	0.0	0.0	0.0	0.0	2.1	0.0	0.0	0.0	76.4	105.4	23.3
	<5.5 µm	9	0.0	0.0	0.0	0.0	1.8	0.0	0.0	0.0	48.0	101.3	22.9
	<2 µm	10	0.0	0.0	0.0	0.0	2.6	0.0	0.0	0.0	69.6	95.1	28.4
	Bulk		0.6	<0.1	0.3	<0.2	-	-	-	-	-	-	-
SCRB07	Coarse residue	11	0.0	0.0	1.0	0.0	7.1	0.0	0.9	0.0	569.8	61.3	39.5
	>13 µm	12	0.0	0.0	0.0	0.0	4.9	0.0	0.0	0.0	461.1	52.6	41.9
	5.5-13 µm heavier	13	0.0	0.0	0.7	0.0	4.1	0.0	1.0	0.0	475.0	59.3	41.6
	5.5-13 µm lighter	14	0.0	0.0	0.0	0.0	7.2	0.0	0.9	0.0	1010.8	103.3	76.3
	<2 µm	15	0.0	0.0	9.8	0.0	12.9	0.0	0.0	0.0	1337.1	99.2	70.9
	Bulk		4.4	<0.1	1.4	<0.2	-	-	-	-	-	-	--
SCRB09	Coarse residue	16	0.7	0.0	6.0	0.0	1.9	0.0	0.0	0.0	123.2	17.7	4.8
	>13 µm	17	0.7	0.0	6.2	0.0	2.0	0.0	0.5	0.0	23.7	19.9	6.4
	5.5-13 µm	18	0.7	0.0	6.9	0.0	1.4	0.0	0.0	0.0	4.1	35.6	15.4
	<5.5 µm	19	1.3	0.0	9.2	0.0	2.2	0.0	0.0	0.0	0.0	57.7	30.3
	<2 µm	20	4.1	0.0	24.0	0.0	4.2	0.0	0.0	0.0	0.0	71.5	33.1
	Bulk		1.8	0.9	16.3	0.4	-	-	-	-	-	-	-
SCRB10	Coarse residue	21	0.0	0.0	2.4	34.8	1.7	0.0	0.0	0.0	36.4	22.1	7.5
	>13 microns	22	0.0	0.0	2.2	29.5	1.2	0.0	0.0	0.0	20.4	16.6	4.4
	5.5-13 microns	23	0.7	0.0	3.0	34.9	2.7	0.5	0.8	0.0	24.7	66.9	17.8
	5.5-20 microns	24	1.0	0.0	2.9	57.1	3.1	0.8	0.8	0.0	56.0	60.7	23.5
	<2 microns	25	2.7	0.0	3.3	71.6	3.8	1.9	0.0	0.0	121.8	85.2	35.5
	Bulk		0.5	0.7	5.0	47.3	-	-	-	-	-	-	-

## 8. DISCUSSION AND CONCLUSIONS ON ELEMENT-MINERAL ASSOCIATIONS IN THE SCUDDLES ZN-CU-DEPOSIT

### 8. 1. Element-mineral associations

The mineralogy and chemistry of the regolith materials from the Scuddles Pb-Zn-Cu deposit have been investigated to determine mineral-trace elements associations over the mineralisation and in the hanging wall. A combination of mineralogical and chemical microanalyses, with emphasis on *in situ* analyses, such as Laser Ablation Inductively Coupled Plasma Mass Spectrometry (LA-ICP-MS) has been used. The data provide new information about trace element occurrence and concentrations in clays, Fe and Mn oxides and resistates. The behaviour of some trace elements during mineral weathering reactions has also been characterised.

Tables 24 and 25 compile the trace element contents in a variety of minerals in regolith material developed directly over the Pb-Zn-Cu mineralisation, and further west in the lower and upper saprolite and from the surface horizon. The LA-ICP-MS data are often obtained on mixtures of minerals, and therefore the concentrations of the monomineralic phases are not always available, the isotopic concentrations of pure monophases are often lowered by the responses of the surrounding material.

At Scuddles, Cu, Zn and Pb are not specifically concentrated above the ore but more to the West. Bismuth, Mo, Sb and In proved to be much more useful pathfinders as they are concentrated in the top horizons over the mineralisation. The results show that the geochemical halos along sections 22240N and 21760N are strongly controlled by the mineralogy of the regolith material. Trace elements have either a single mineral host stable from the the saprock to the surface, or a succession of hosts stable in the different environments.

#### 8. 1. 1. *Hanging wall*

Lead, Cu, Mn, Zn and Co are concentrated in the lower saprolite developed on the hanging wall lavas, and their concentrations decrease towards the surface. Lead, Mn, Cu and Zn anomalies overlap in the hanging wall sequence. The data show that they share common hosts in the coinciding dispersion zones.

Manganese and Pb are concentrated in Mn oxide nodules scattered in the saprolite material. Copper and Zn are hosted in clays, Mn and Fe oxides. Interstratified clay minerals such as corrensite are significant constituents of the lower saprolite representing as much as 7% of the bulk material in some samples. These Mg-rich clays, which contain about 0.3% Cu and Zn, are responsible for the concentration of Zn and Cu under the Mg depletion line emphasized by Findlay (1998). Copper and Zn are preferentially captured by high-charge corrensite (chlorite-vermiculite interstratified mineral), indicating that vermiculite has a higher ability to integrate these cations than smectitic layers. Copper and Zn are relatively depleted in the upper saprolite as they are only partially retained in the weathering products of corrensite.

Zinc is also contained in more resistant minerals such as ilmenite-ecandrewsite and goethite which are present in the upper saprolite. Copper has also been captured in coronadite nodules.

Lead is much more concentrated than Cu and Zn up the profile along section 22240N as it is retained in plumbogummite, stable in near surface conditions.

Cobalt and Ni are immobilized in lithiophorite, possibly coronadite, and marginally by corrensite and smectites.

Bismuth, Sb, In and Mo are not significantly concentrated in the hanging wall regolith. However Mo is locally scavenged by coronadite and iron oxides. Antimony is present immediately west of the

mineralisation in weathered ilmenite and goethite. Indium and Bi have not been confidently detected. Arsenic is present in iron oxides and coronadite.

Phosphorous mainly occurs as plumbogummite and adsorbed on iron oxide surface. Vanadium, originally present in mica and ilmenite, is retained in coronadite and weathered ilmenite.

### **8. 1. 2. Over mineralisation**

There is an overall concentration of Sb, Bi, In and Mo immediately above the ore location. However, Sb, In and Mo on the one hand and Bi on the other hand display an antipathetic distribution suggesting that these trace elements have distinct and common mineralogical hosts.

The bleached upper saprolite material displays a strong Bi anomaly, whereas the reddish mottles are very concentrated in Sb, Mo and In. The LA-ICP-MS analyses have shown that Sb, Mo and In occur predominantly in iron oxides. On the contrary, Bi is not associated with iron oxides but is contained in Pb-Bi phases and rutile. Antimony, Mo and Bi are abundant in rutile present in the bleached and Fe-rich upper saprolite. This association is partially responsible for the overlapping concentration areas of these cations. The analysis of fresh sphalerite inclusions observed in quartz crystals shows that In is originally contained in the Zn sulphide.

Copper and Zn are moderately concentrated in Fe and Mn oxides (coronadite and lithiophorite) and in rare corrensite, in the lower saprolite. The regolith is poorly differentiated above mineralisation, contains abundant fresh chlorite and lacks clays able to capture traces such as corrensite and smectites. The upper saprolite, taken as a whole, is depleted in Cu and Zn. However the Fe oxides of the reddish mottles contain abundant Cu and Zn. Zinc and Cu are also hosted in sphalerite inclusions in quartz grains.

Lead is concentrated in the lower saprolite, in iron-oxides with a preference for hematite, and in tunnel Mn oxides (coronadite and hollandite). It is relatively less depleted than Cu and Zn in the upper saprolite where it is retained in Fe-oxides, plumbogummite, Pb-Bi phases, and sphalerite inclusions.

Arsenic is captured by iron oxides in the saprolite.

### **8. 1. 3. Conclusions**

At Scuddles, trace element dispersion is strongly controlled by the mineralogy of the regolith. Above the mineralisation, potential captors such as corrensite and smectites are not abundant, and as a result, Cu, Zn and Pb mobilised by the dissolution of sulphides, are not retained. They have been captured further west by abundant receptors such as Mg-clays and Mn oxides resulting in the concentration of Cu and Zn under the Mg depletion line observed by Findlay (1998).

Bismuth, Mo, Sb and In anomalies are residual at the scale of the whole regolith developed over the mineralisation. However, there are local variations controlled by the availability of suitable mineral scavengers such as Fe oxides. The variations indicate small range migration of these traces.

It has been shown that Bi, Mo and Sb anomalies detected by analysing the bulk samples have two origins. They are directly related to the mineralisation and are retained in Fe oxides, minor phases (Bi-Pb phases) and sulphide inclusions. They can also result from the relative accumulation of resistates such as rutile towards the surface of the regolith. Ashley et al (1988) reports that rutile is a characteristic mineral of the mineralised horizon and footwall at Scuddles, and therefore, these anomalies can be regarded as secondary or indirect indicators of mineralisation.

The data have shown that kaolinite is a barren clay which does not incorporate any base metals under the prevailing weathering conditions.

## **8. 2. Implications for exploration**

The mineralogical and geochemical investigation of the Scuddles regolith has provided new information about the location of trace elements. These data help to understand the geochemical dispersion at Scuddles, and to suggest guidelines to improve the detection of pathfinders.

The selection of the material containing the trace element hosts for chemical analysis will greatly improve anomalies and reveal some anomalies undetected in bulk samples. For example, bleached kaolinitic material should be rejected for sampling, whereas Fe-stained kaolinite will show enhanced anomalies. Iron oxides are choice sampling material able to retain In, Sb, Bi and Mo.

This work also demonstrates the important role played by clays with scavenging properties, such as smectites, vermiculites and interstratified minerals, in the dispersion of base metals in the regolith.

In addition to geochemical anomalies, much information is provided by a basic mineralogical investigation of the regolith material. There are numerous reliable mineralogical indicators of mineralisation and associated hydrothermal activity at Scuddles: sphalerite inclusions in quartz and gossan chips. The LA-ICP-MS analysis of gossan fragments gives Sb and Mo values multiplied by a factor of 18 and 13 respectively.

Table 24. Location and concentrations of selected trace elements in Scuddles lower saprolite.  
— : not measured or no qualitative data available.

Element	West of mineralisation		Over mineralisation	
	Mineralogy	ppm	Mineralogy	pmm
P	Plumbogummite Goethite	2800	Goethite-hematite	570
Ti	Ilmenite Mica	600	Rutile	
V	Coronadite Mica	2000 200	Coronadite Goethite-hematite	6000 220
Cr	Mica	175	—	—
Mn	Coronadite Lithiophorite	31000	Coronadite Goethite-hematite	36000 740
Co	Coronadite Chlorite/vermiculite	11100 80	Lithiophorite Goethite-hematite	21400 70
Ni	Chlorite/vermiculite Goethite	340 10	Lithiophorite Goethite-hematite	9900 130
Cu	Coronadite Goethite Chlorite/vermiculite Chlorite/smectite	21600 6300 3560 280	Goethite-hematite Coronadite Lithiophorite	35000 25600 27600
Zn	Chlorite/vermiculite Chlorite/smectite Goethite Coronadite	3300 930 870 550	Lithiophorite Goethite-hematite Coronadite	12000 4000 700
As	Goethite Coronadite	200 80	Goethite-hematite	1500
Se	—	—	Goethite-hematite	45
Nb	Ilmenite	540		
Mo	Coronadite Goethite	150 10	Goethite-hematite	90
Ag	Altered ilmenite	6500	—	—
Sb	Altered ilmenite Goethite	11 20	Goethite-hematite	40
Ba	Mica	650	Coronadite-hollandite	78900
Ce	Coronadite	6000	Coronadite	1000
Ta	Altered ilmenite	36	—	—
W	Altered ilmenite	9	—	—
Pb	Coronadite Plumbogummite Mica	31000  150	Coronadite Hematite-goethite	212000 4000

Table 25. Location and concentrations of selected trace elements in Scuddles upper saprolite.  
— : not measured or no qualitative data available.

Elements	West of mineralisation		Over mineralisation	
	Mineralogy	ppm	Mineralogy	pmm
P	Goethite-hematite	1600	Pumbogummite Goethite-hematite	420
Sc	—	—	Muscovite	68
Ti	Ilmenite		Rutile Goethite-hematite	1400
V	Weathered ilmenite	6000	Rutile Goethite-hematite	5800 1800
Cr	—	—	Spinel Goethite-hematite	— 1000
Mn	Coronadite Ecandrewsite	352000 21500	Sphalerite	—
Co	Lithiophorite Smectites	28000 50	Sphalerite	—
Ni	Lithiophorite Coronadite Smectites	1300 410 150	Spinel	—
Cu	Coronadite Smectites	25700 6700	Goethite-hematite Bi-Pb phase Sphalerite	4000 — —
Zn	Ecandrewsite Goethite Smectites Coronadite	61600 10000 1200 3000	Sphalerite Goethite-hematite	— 250
As	Goethite-hematite	140	Goethite-hematite	370
Nb	—	—	Rutile	70
Zr	—	—	—	—
Mo	—	—	Goethite-hematite	220
Ag	—	—	Associated with clays	1400
Sn	—	—	Cassiterite	
Sb	Anatase	79	Spinel Goethite-hematite	— 440
Ba	Coronadite-hollandite	21600	Bi-Pb phase	—
Ce	Coronadite	5600	Plumbogummite	24200
W	Anatase	100	Rutile	36
Pb	Coronadite Smectites	258000 7000	Goethite-hematite Bi-Pb phase Sphalerite	730 — —
Bi	—	—	Rutile Bi-Pb phase	310 —

## **9. ACKNOWLEDGEMENTS**

The Mineral Hosts for Gold and Trace Elements in the Regolith project results from a collaboration between Normandy Mining Ltd. and the Cooperative Research Centre for Landscape Evolution and Mineral Exploration (CRC LEME). The author and project leaders wish to thank Normandy Mining Ltd. for the funding of this study and for providing some samples and data.

Ravi Anand (CRC LEME/CSIRO project leader), Tony Eggleton (CRC LEME/ANU project leader), and Nigel Radford (Newmont Australia) initiated this project and are thanked for their support and critical comments on the manuscript.

The scanning electron microscopy analyses were carried out at the Electron Microscopy Unit at the Australian National University. Microprobe and LA-ICP-MS analyses were performed at the Research School of Earth Sciences at the Australian National University.

I would like to thank Steve Eggins (Research School of Earth Sciences, ANU) and Juan-Pablo Bernal (CRC LEME) who provided much useful background discussion and assistance with LA-ICP-MS applications.

Rob Hough provided critical review of the manuscript.

## 10. REFERENCES

- Ashley, P.M., Dudley, R.J., Lesh, R.H., Marr, J.M. and Ryall, A.W. 1988. The Scuddles Cu-Zn prospect, and Archean volcanogenic massive sulfide deposit, Golden Grove district, Western Australia. *Economic Geology*, 83, pp. 918-951.
- Axelsson, M.D. and Rodushkin, I. 2001. Determination of major and trace elements in sphalerite using laser ablation double focusing sector field ICP-MS. *Journal of Geochemical Exploration*, 72, 81-89.
- Baker, S.A., Bi, M., Aucelio, R.Q., Smith, B.W., and Winefordner, J.D. 1998. Analysis of soil and sediment samples by laser ablation inductively coupled plasma spectrometry, *Journal of Analytical Atomic Spectrometry*, 14, 19-26.
- Baxter, J.L. 1982. Stratigraphy and structural setting of the Warriedar Fold Belt. In J. L. Baxter, ed., *Archean geology of the southern Murchison: Perth, Geol. Soc. Australia, Excursion Guide*, 31-36.
- Durrant, S. 1999. Laser ablation inductively coupled plasma mass spectrometry: achievements, problems, prospects. *Journal of Analytical Atomic Spectrometry*, 14, 1385-1403.
- Findlay, S. 1998. Scuddles RAB Drilling Orientation Program 1998. Normandy Mining Ltd., Company report n° 66845.
- Foster, M.D. 1962. Interpretation of the composition and a classification of the chlorites. *Professional Papers U. S. geological Survey*, 414-A, 1-33.
- Hale, M., Thompson, M., and Wheatley, M.R. 1984. Laser ablation of stream-sediment pebble coatings for simultaneous multi-element analysis in geochemical exploration, *Journal of Geochemical Exploration*, 21, 361-371.
- Le Gleuher, M. 2003. Mineral hosts for gold and trace elements in the regolith, Boddington and Mt Percy gold deposits, Western Australia, Normandy Mining Ltd., CRC LEME Restrictd Report 196R, 94p.
- Longerich, H.P., Jackson, S.E. and Günter, D. 1996. Laser ablation inductively coupled plasma spectrometric transient signal data acquisition and analyte concentration calculation. *Journal of Analytical Atomic Spectrometry*, 11, pp. 899-904.
- Mill, J.H.A., Clifford, B.A., Dudley, R.J. and Ruxton, P.A. 1990. Scuddles Zinc-Copper deposit at Golden Grove. In *Geology of the Mineral Deposits of Australia and Papua New Guinea* (F. E. Hughes, ed.), 583-590.
- Moore, D.M., and Reynolds, R.C.Jr. 1997. X-ray diffraction and the identification and analysis of clay minerals. Oxford: Oxford University Press., second edition, 378p.
- Motelica-Heino, M., Le Coustemer, P., Thomassin, J.H., Gauthier, A. and Donard, O.F.X. 1998. Macro and microchemistry of trace metals in vitrified domestic wastes by laser ablation ICP-MS and scanning electron microprobe X-ray energy dispersive spectroscopy. *Talanta*, 407-422.
- Pearce, N J.G., Perkins, W.T., Westgate, J.A., Gorton, M.P., Jackson, S.E., Neal, C.R. and Chenery, S. P. 1996. A compilation of new and published major and trace element data for NIST SRM 610 and NIST SRM 612 glass reference materials. *Geostandards Newsletter*, 21, 1, 115-144.
- Radford, N.W. and Burton, P.E. 1999. The geochemistry of transported overburden: the time factor. An example from the Fender deposit, Big Bell, Western Australia. *Journal of Geochemical Exploration*, 66, 71-83.



Smith, R.E. and Perdrix, J.L. 1983. Pisolitic laterite geochemistry in the Golden Grove Massive Sulphide District, Western Australia. *Journal of Geochemical Exploration*, 18, 131-164.

Taylor, J.C. and Clapp, R.A. 1992. New features and advanced applications of SIROQUANT: A personal computer XRD full profile quantitative analysis software package. *Advances in X-ray analysis*, 35, 49-55.

## 11. APPENDICES

### APPENDIX 1

Particle-size separation: clean protocol for ICP—MS analyses.

No dispersing agent was used to avoid the introduction of pollutant. Flocculating sample were disregarded. All glass wares *etc...* were washed with decon<sup>®</sup>90 and rinsed with deionized water (2 last rinses).

Depending on the clay content, 50 to 150 g of powdery sample were placed in a beaker. The sample was ultrasonically desegregated in deionized water at an approximate ratio of 2:1 water to sample.

The sample was allowed to settle undisturbed for 5mn to remove the coarse particle fraction. The supernatant was decanted into a 1000 ml-settling tube and the coarse fraction is dried in a drying oven at 40°C. This operation was repeated until the settling tube was full.

The supernatant was allowed to settle for about 60 mn (1hr, 20°C). The top 10 cm, which mainly contain particles with a diameter <5.5µm, were pipetted and placed in another settling tube. This stage was repeated up to 12 times depending on the opacity of the suspension.

A part of the suspension with <5.5 µm particles was allowed to settle (8hr, 20°C) to separate the particles <2 µm (up to 5 times). The top 10 cm were pipetted into a centrifuge bottle. The rest of the 0-5.5 µm fraction was centrifuged and dried.

The <2 µm fraction was centrifuged (approximately 1/2hr, 2400 rpm) and dried. The supernatant concentrated in the <0.2 µm fraction was also dried.

The suspension with >5.5 µm particles was filtered with a nylon 13 µm-mesh sieving cloth. The >13µm fraction was dried at 40°C.

The <13 µm fraction containing particles with a diameter comprised mainly between 5.5 µm and 13 µm was further separated into two fractions: a "heavier" <13 µm fraction and a "lighter" 13 µm fraction by allowing the suspension to settle about 1/2hr and dried at 40°C.

When possible enough material was collected in order to carry out ICP-MS and X-ray analyses.

#### *Sample digestion*

Samples were dissolved in a mixture of HF-HNO<sub>3</sub> (~1 ml of each) in teflon containers in ceramic jackets under low pressure within a microwave oven. They were evaporated with extra HNO<sub>3</sub> 6N, dried down in two steps and taken in HNO<sub>3</sub> 2%. Organic matter and oxides were dissolved with HClO<sub>4</sub> and HCL 6N.

Samples were analysed with an Elan 6000 spectrometer, equipped with an AS90 autosampler. An external certified sample was analysed (SRM 2704 – Buffalo River Sediment) and internal standards were automatically added to each sample using a FIAS system 200.

## APPENDIX 2.

Trace elements concentrations (ppm), silica and alumina contents (%) for the reference synthetic glasses NIST SRM 610 and NIST SRM 612. (From Pearce *et al*, 1996).

	NIST SRN 610		NIST SRM 612	
Element ppm	Average	std dev	average	std dev
Mg	465.3	26.6	78.00	34.78
P	342.5	53.1	55.16	22.71
K	463.1	8.1	65.51	1.33
Sc	439.3	10.9	41.05	4.09
Ti	432.8	12.1	48.51	2.76
V	440.2	36.4	38.21	2.64
Cr	388.0	15.2	42.46	13.95
Mn	436.4	21.4	38.50	1.06
Fe	453.1	17.9	55.57	15.78
Co	400.9	22.6	35.09	2.33
Ni	439.1	15.8	37.77	4.11
Cu	432.9	16.9	36.82	2.89
Zn	429.3	16.4	36.64	2.52
As	317.6	13.9	37.33	6.56
Se	112.0	2.8		
Rb	430.2	7.0	31.61	0.56
Zr	439.9	7.8	35.99	1.25
Nb	381.8		38.06	0.86
Mo	396.1	38.9	38.30	1.65
Ag	240.5	19.7	22.06	3.24
Cd	260.9	4.5	28.02	0.54
In	439.8	35.5	42.80	4.98
Sn	390.0	19.8	37.67	2.04
Sb	388.3	5.1	38.44	2.26
Ba	415.9	21.5	38.52	1.9
La	436.6	39.6	35.49	2.16
Ce	443.3	15.0	38.24	1.71
Pr	431.2	33.3	37.06	0.97
Ta	361.0	71.6	39.77	2.15
W	434.5	23.3	39.55	0.78
Au	22.9	3.7	5.03	0.05
Pb	419.1	9.4	38.74	1.67
Bi	373.8	28.7	29.84	5.98
Th	463.1	11.9	37.31	0.72
U	462.9	6.2	36.88	1.13
SiO <sub>2</sub> wt. %	72 0		72.00	
Al <sub>2</sub> O <sub>3</sub> wt. %	1.9		1.9 0	

## APPENDIX 3

### Determination of trace elements in regolith material by Laser Ablation Inductively Coupled Plasma Mass Spectrometry (LA-ICP-MS)

#### *Samples*

The analyses have been conducted on two types of samples:

Epoxy-embedded grains: SCRB10 (44-45 m), SCRB05 (34-35 m) and SCRB07 (54-55 m);

Thin sections: SCRB102 (69-70 m), SCRB103 (59-60 m), SCRB07 (54-55 m), SCRB10 (14-15m) and SCRB (9-10 m).

#### *Data acquisition and reduction*

In order to identify the mineralogy of the ablated sample and to enable the calculation of an internal standard, the isotopes of five major elements  $^{24}\text{Mg}$ ,  $^{27}\text{Al}$ ,  $^{29}\text{Si}$ ,  $^{39}\text{K}$  and  $^{57}\text{Fe}$  were analysed. The following isotopes were also measured:  $^{31}\text{P}$ ,  $^{45}\text{Sc}$ ,  $^{47}\text{Ti}$ ,  $^{51}\text{V}$ ,  $^{53}\text{Cr}$ ,  $^{55}\text{Mn}$ ,  $^{59}\text{Co}$ ,  $^{60}\text{Ni}$ ,  $^{63}\text{Cu}$ ,  $^{65}\text{Cu}$ ,  $^{66}\text{Zn}$ ,  $^{68}\text{Zn}$ ,  $^{75}\text{As}$ ,  $^{82}\text{Se}$ ,  $^{95}\text{Mo}$ ,  $^{115}\text{In}$ ,  $^{121}\text{Sb}$ ,  $^{137}\text{Ba}$ ,  $^{139}\text{La}$ ,  $^{140}\text{Ce}$ ,  $^{141}\text{Pr}$ ,  $^{184}\text{W}$ ,  $^{208}\text{Pb}$ ,  $^{209}\text{Bi}$ .

From the first serie of data sites were selected for the measurement of gold and silver in particular. In order to maximise the detection of gold and silver in the clays and iron oxides, a large probe (50  $\mu\text{m}$ ) has been used. In addition to  $^{197}\text{Au}$ , the following isotopes were measured:  $^{27}\text{Al}$ ,  $^{29}\text{Si}$ ,  $^{49}\text{Ti}$ ,  $^{55}\text{Mn}$ ,  $^{57}\text{Fe}$ ,  $^{95}\text{Mo}$ ,  $^{98}\text{Mo}$ ,  $^{107}\text{Ag}$ ,  $^{109}\text{Ag}$ ,  $^{115}\text{In}$ ,  $^{184}\text{W}$ , and  $^{209}\text{Bi}$ . Isotopes  $^{91}\text{Zr}$ ,  $^{93}\text{Nb}$ ,  $^{181}\text{Ta}$  were also analysed to check on potential oxide interferences with silver and gold:  $^{91}\text{Zr } ^{16}\text{O} = ^{107}\text{Ag}$ ,  $^{93}\text{Nb } ^{16}\text{O} = ^{109}\text{Ag}$ ,  $^{181}\text{Ta } ^{16}\text{O} = ^{197}\text{Au}$ . In some cases (Ag and Mo), two isotopes were measured.

The ablation pits were systematically observed with the SEM to check their morphology, and to confirm the expected mineralogy of the site.

The calibration of the analytical results was carried out using the NIST SRM 610 and NIST SRM 612 glass reference standards (Appendix 2). The NIST SRM 616 (0.18% Au) was also randomly used to check the gold concentration of the NIST 612. The calculation of the isotopic concentrations were performed using alumina as internal standard. Alumina concentrations are stoichiometric values normalised to 100% wt or microprobe data acquired on monomineralic phase. When the signal had to be decomposed into slices representing “purer” phases the most suitable internal standard was chosen for each slice.

The qualitative data presented in this report are mostly concentrations of traces contained in volumes of composite material and not in pure phases.